AD-A058 706 ARMY ENGINEER WATERWAYS EXPERIMENT STATION VICKSBURG MISS F/G 13/2
AN ESTIMATE OF CHANNEL ROUGHNESS OF INTEROCEANIC CANALS.(U)
JUL 78 G H KEULEGAN

UNCLASSIFIED WES-TR-H-78-13 NL

1 OF 2

AD A058706

LEVEL II

12

TECHNICAL REPORT H-78-13

AN ESTIMATE OF CHANNEL ROUGHNESS OF INTEROCEANIC CANALS

by

Garbis H. Keulegan

Hydraulics Laboratory
U. S. Army Engineer Waterways Experiment Station
P. O. Box 631, Vicksburg, Miss. 39180

July 1978
Final Report

Prepared for U. S. Army Engineer District, Jacksonville
Jacksonville, Florida 32201

Destroy this report when no longer needed. Do not return it to the originator.

Unclassified

SECURITY CLASSIFICATION OF THIS PAGE (When Data Entered)

(12)

REPORT DOCUMENTATION PAGE

READ INSTRUCTIONS BEFORE COMPLETING FORM

1. REPORT NUMBER: Technical Report H-78-13	2. GOVT ACCESSION NO.
3. RECIPIENT'S CATALOG NUMBER	
4. TITLE (and Subtitle): AN ESTIMATE OF CHANNEL ROUGHNESS OF INTER-OCEANIC CANALS	5. TYPE OF REPORT & PERIOD COVERED: Final report.
6. PERFORMING ORG. REPORT NUMBER	
7. AUTHOR(s): Garbis H. Keulegan	8. CONTRACT OR GRANT NUMBER(s): 32p.
9. PERFORMING ORGANIZATION NAME AND ADDRESS: U. S. Army Engineer Waterways Experiment Station, Hydraulics Laboratory, P. O. Box 631, Vicksburg, Mississippi 39180	10. PROGRAM ELEMENT, PROJECT, TASK AREA & WORK UNIT NUMBERS
11. CONTROLLING OFFICE NAME AND ADDRESS: U. S. Army Engineer District, Jacksonville, P. O. Box 4970, Jacksonville, Florida 32201	12. REPORT DATE: July 1978
	13. NUMBER OF PAGES: 124
14. MONITORING AGENCY NAME & ADDRESS (if different from Controlling Office): WES-TR-H-78-13	15. SECURITY CLASS. (of this report): Unclassified
	15a. DECLASSIFICATION/DOWNGRADING SCHEDULE

16. DISTRIBUTION STATEMENT (of this Report)

Approved for public release; distribution unlimited.

17. DISTRIBUTION STATEMENT (of the abstract entered in Block 20, if different from Report)

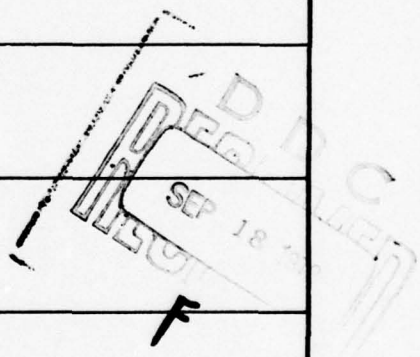

18. SUPPLEMENTARY NOTES

19. KEY WORDS (Continue on reverse side if necessary and identify by block number)

Canal construction	Hydraulic roughness
Canals	Interoceanic canals
Excavated channels	

20. ABSTRACT (Continue on reverse side if necessary and identify by block number)

The hydraulic roughness of the interoceanic canals created by either nuclear or conventional construction is considered. In the canals of nuclear excavation, the part of resistance due to the ejecta is estimated on the basis of distribution of size of ejecta material; and the part due to the expansions and contractions in the canal created by the explosives is attributed to the isostatic losses from free turbulence. For the conventional canals charged

CONT'

(Continued)

DD FORM 1 JAN 73 1473 EDITION OF 1 NOV 65 IS OBSOLETE

Unclassified

SECURITY CLASSIFICATION OF THIS PAGE (When Data Entered)

20 ABSTRACT (Continued).

cont'

with very fine sediment, the friction of the granular surfaces is assumed to be that in a hydrodynamically smooth surface. In the presence of bed features, the added form resistance is estimated from the findings of Alam and Kennedy concerning alluvial rivers. A detailed study of resistance noted in Fort Collins tests shows that there is a difference in the frictional processes between the laboratory flumes and the natural rivers, suggesting that for resistance estimates reliance should be placed on river calibration.

PREFACE

As a part of the investigation of a possible Sea Level Canal connecting the Atlantic and Pacific Oceans, the U. S. Army Engineer District, Jacksonville, requested the U. S. Army Engineer Waterways Experiment Station (WES) to investigate roughness that would result in the canal.

This report was prepared by Dr. G. H. Keulegan with the assistance of CPT M. J. Mathews, formerly with the Mathematical Hydraulics Division of the Hydraulics Laboratory, WES.

The work on this study was commenced in 1969 and was followed somewhat intermittently since then. The study was under the general supervision of Mr. E. P. Fortson (retired), former Chief of Hydraulics Laboratory, and Mr. H. B. Simmons, present Chief; Mr. F. A. Herrmann, Jr., former Chief of Estuaries Division, and Mr. R. A. Sager, present Chief.

Directors of WES during the course of this investigation and the preparation and publication of this report were COL J. R. Oswalt, Jr., CE, COL L. A. Brown, CE, BG E. D. Peixotto, CE, COL G. H. Hilt, CE, and COL John L. Cannon, CE. Technical Directors were Messrs. J. B. Tiffany and F. R. Brown.

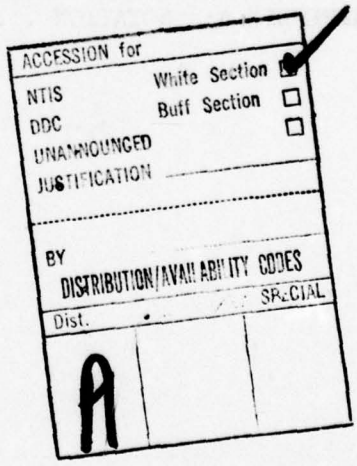

CONTENTS

CONVERSION FACTORS, U. S. CUSTOMARY TO METRIC (SI) UNITS OF MEASUREMENT

U. S. customary units of measurement used in this report can be converted to metric (SI) units as follows:

Multiply	By	To Obtain
cubic feet	0.02831685	cubic metres
degrees (angle)	0.01745329	radians
feet	0.3048	metres
feet per second	0.3048	metres per second
feet per second per second	0.3048	metres per second per second
inches	25.4	millimetres
miles (U. S. statute)	1.609344	kilometres
pounds (mass) per second per foot	0.4535924	kilograms per second per foot
square feet	0.09290304	square metres
square feet per second	0.09290304	square metres per second

AN ESTIMATE OF CHANNEL ROUGHNESS OF INTEROCEANIC CANALS

PART I: RESISTANCE OF NONALLUVIAL CHANNELS

Introduction

1. The present study deals with the expected values of the roughness of the interoceanic canals created by either nuclear or conventional construction methods. Nuclear-cratered channels pose two problems. The first refers to the roughness under the hypothetical assumption that the crater channels are of a uniform cross section throughout. Knowing the distribution of rock sizes in the ejecta and in the fallback, the roughness is to be inferred in terms of Manning's n. Eventually, a relation of rock size and Manning's n can be established by relying upon the concept of equivalent sand roughness. Next, with this information as a basis, the effective Manning's n of crater channels is derived subject to the known distribution of rock sizes and uniform cross section. The second problem deals with the increase of channel resistance resulting from the expansions and contractions of a nuclear-blasted channel. Part of the answer to this question comes from the experiments conducted at the U. S. Army Engineer Waterways Experiment Station (WES). Difficulties, however, arise in the attempt to apply laboratory results to prototype situations. The ordinary model rules for the transfer of roughness do not apply since the alternating expansions and contractions bring about losses that are not related to wall skin friction but are caused by internal turbulent friction. The proper transfer relation is established by developing the theory of losses encountered in the mixing of a current moving over adjacent stagnant or static waters.

2. In canals created by conventional methods the bottom is composed of Atlantic muck. Eden, formerly of the U. S. Army Engineer District, Jacksonville (SAJ), has informed us that the muck has the following grain size distribution: 100 percent less than 0.1 mm, 65 percent less than 0.01 mm, and 35 percent less than 0.002 mm. This extremely fine composition poses the difficult problem of deciding

exactly what the equivalent roughness would be. In ordinary alluvial streams, with bed materials of a mean grain size on the order of a millimeter or a tenth of a millimeter, the resistance is related to the presence of ripples or dunes. For flows with a Froude number less than 0.5, and if the velocity, grain-size distribution, channel dimensions, and channel slope are known, the corresponding resistance can be roughly established. The question of bed feature formation with very fine sand has rarely been investigated. If it is found that the effect of ripples, if present, is of no consequence, the channel boundaries may be regarded as hydrodynamically smooth and having small friction.

3. The importance of the problem dictates that an effort be made to determine the condition or the likelihood of the formation of bed feature with fine particles and the resultant resistance. Two approaches are open for the examination of friction. First, various theories on the resistance of alluvial streams with bed materials of moderate sizes are considered. Selecting from these the one most convenient for the purpose, relations are projected to canals with fine bed material. Secondly, an attempt is made to determine the resistance of individual ripples or dunes assuming that the relevant current velocity is the velocity at the apices of the ripples or dunes. The resistance coefficients are established for each form by referring to laboratory results which have noted the dimensions of these forms in addition to the stresses at the walls and the bottom. If there is additional information on the sizes of these bed features in fine sediment channels, the resistance coefficient, being a dimensionless quantity, could be applied directly.

Estimates of Roughness of Crater Surfaces

An exposé of open channel formulae

4. An earlier study on the laws of turbulent flow in open channels[1] led to the relation

$$\frac{U}{U_*} = 6.25 + 5.75 \log \frac{R}{k_s} \qquad (1.1)$$

$$U_* = \sqrt{gRS} \tag{1.2}$$

where

U = channel mean flow velocity*

U_* = shear velocity

g = gravitational acceleration constant

R = hydraulic radius

S = the energy gradient

In the event that the depth is uniform and the variation of velocity head with distance is negligible, S merely represents the slope of the water surface; k_s = equivalent sand roughness height. Equation 1.1 represents the logarithmic law of mean velocity. This is also nearly equivalent to

$$\frac{U}{U_*} = 8.12 \left(\frac{R}{k_s}\right)^{1/6} \tag{1.3}$$

provided that

$$\frac{1}{500} < \frac{k_s}{R} < \frac{1}{15} \tag{1.4}$$

which is a form of Manning's law. The ordinary form of this law when lengths are measured in feet** is

$$U = \frac{1.476}{n} R^{1/6} \sqrt{RS} \tag{1.5}$$

which may be written also as

$$U = \frac{0.260}{n} \sqrt{gRS}\, R^{1/6} \tag{1.6}$$

where R is expressed in feet. Accordingly

$$\frac{U}{U_*} = \frac{0.260}{n} R^{1/6} \tag{1.7}$$

---

* For convenience, symbols and unusual abbreviations are listed and defined in the Notation (Appendix A).

** A table of factors for converting U. S. customary units of measurement to metric (SI) units is presented on page 3.

Hence comparing Equation 1.7 with Equation 1.3 gives

$$n = 0.0324 k_s^{1/6} \tag{1.8}$$

a relation between Manning's n and the equivalent sand roughness k_s, the latter expressed in feet.

Equivalent sand roughness
and asperity concentration

5. The very fruitful idea of equivalent sand roughness is due to Schlichting.[2] The practical implication of the idea is as follows. One may consider two channels or two conduits having the same form and hydraulic radius. The walls of one channel are covered with asperities of height k and the other with closely packed sand of height k_s. If the flows in the two channels under the same pressure difference are equal, then k_s is the equivalent sand roughness of the asperities k of the first channel. Schlichting conceived an ingenious apparatus that eliminated the use of towing tanks to investigate the resistance of battleship armor design. The apparatus consisted of a wide rectangular channel, three sides of which were smooth surfaces while the fourth side consisted of a rough plate. The rough plate could be covered with any type of asperities and concentration values. The asperities concentration is defined by Schlichting as follows. If A_r is the total value of the projected area of all the asperities found on an area A, upon a a plane parallel to the direction of flow, then A_r/A is to be taken as the concentration of the asperities. If the projection of a single asperity is a_r and there are N number of them on an area A, then $A_r = a_r N$. For a layer of spheres of diameter 2a, spheres squarely compacted, taking $N = 1$, $A = 4a^2$, $A_r = \pi a^2$, and $A_r/A = 0.783$. Schlichting recognized that the relation between k and k_s is of the form

$$\frac{k_s}{k} = \lambda\left(\frac{A_r}{A}\right) \tag{1.9}$$

the function relation being different for different forms of the asperities. For example, Figure 1 shows the manner of dependence for spheres

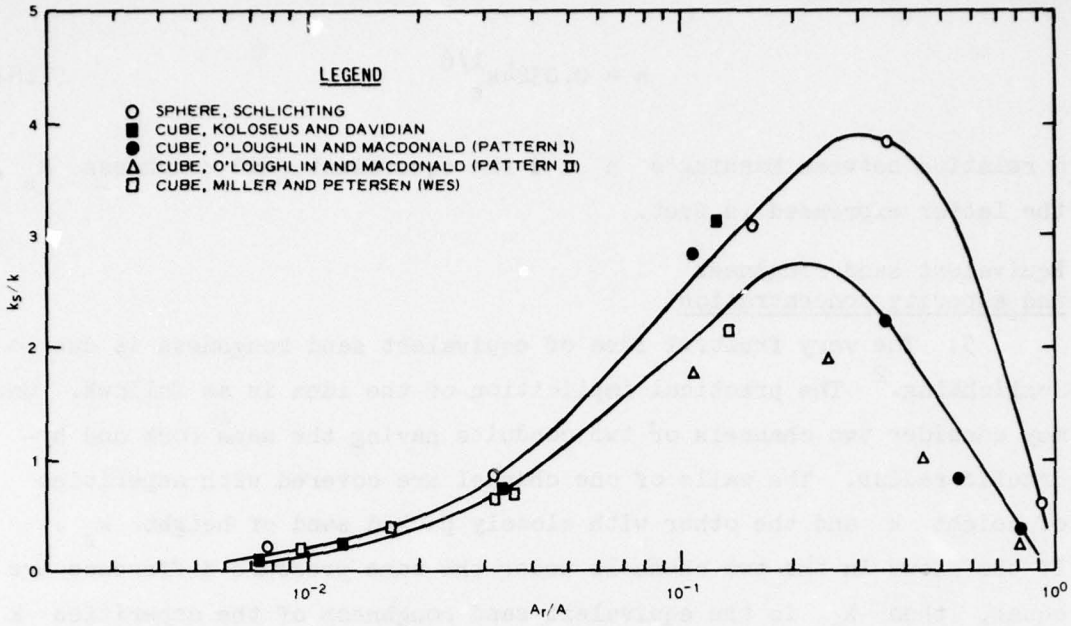

Figure 1. Effect of asperities concentration on resistance

as found by Schlichting. Also shown in this figure are the resistance characteristics of cubes. Part of the data of the cubes was taken from Iowa tests[3,4] and the remaining part from WES tests. The investigators of the latter tests, Miller and Petersen, do not give the quantities A_r/A and k_s/k in their report, but they do give the sizes of the cubes and the spacing of the cubes.[5] Among other things they give the depth of the water y_m, hydraulic radius r, and Manning's n. The values of A_r/A depend upon the values of k and the spacing. The expression

$$5.75 \log \frac{R}{k_s} = \frac{0.260}{n} R^{1/6} - 6.25$$

which results upon elimination of U/U_* from Equations 1.1 and 1.7 enables us to determine k_s from the known values of R and n. Forming k_s/k and y_m/k, the limiting values of k_s/k for greater water depths are determined from a plot as in Figure 2. Referring again to Figure 1 it is to be inferred that for small values of A_r/A the

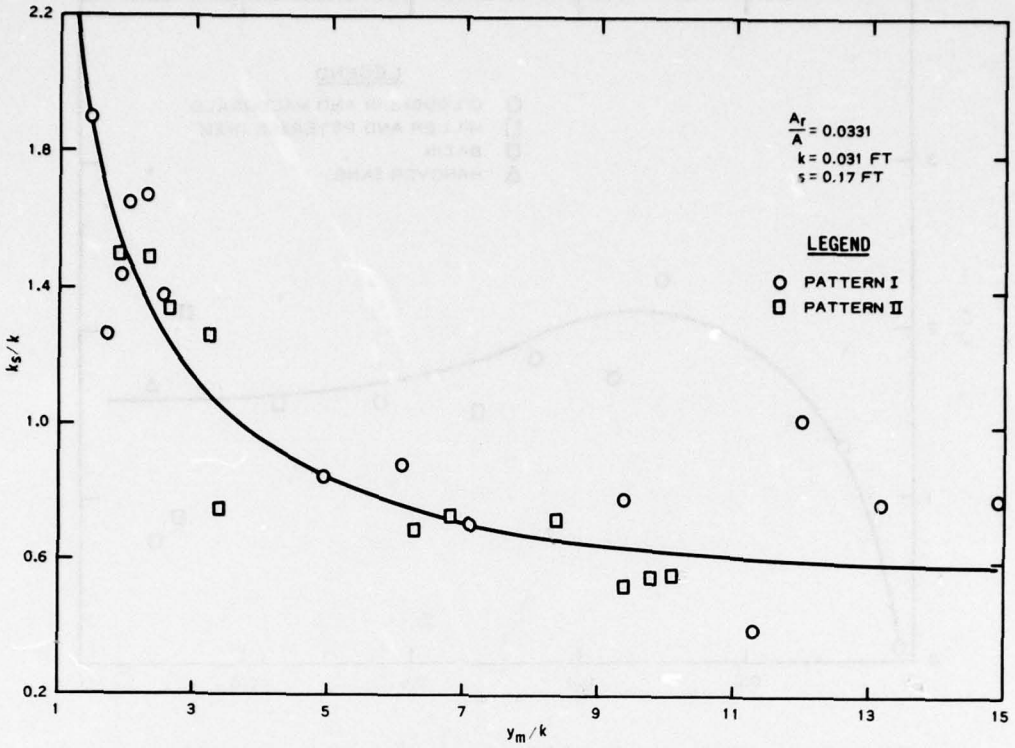

Figure 2. Dependence of effective roughness on water depth in channel

ratio k_s/k increases with A_r/A . The ratio k_s/k attains its greatest value at about $A_r/A = 0.4$. Beyond that there is a decrease with increasing A_r/A .

Equivalent sand roughness
of rocks and pebbles

6. For gravelly and rocky channels, data similar to those shown in Figure 1 are needed. This information is shown in Figure 3 for sand,[4] limestone rock,[6] and Hanover sand.[2] Schlichting's experiments were performed on Hanover sand similar in compactness to that of Nikuradze.

7. The value of k_s/k found by Schlichting is 1.6 which suggests that all sands are not alike with respect to their resistance characteristics. The full curve shows mainly the effect of concentration on the value of k_s/k . Thus for rocks and pebbles with concentrations A_r/A

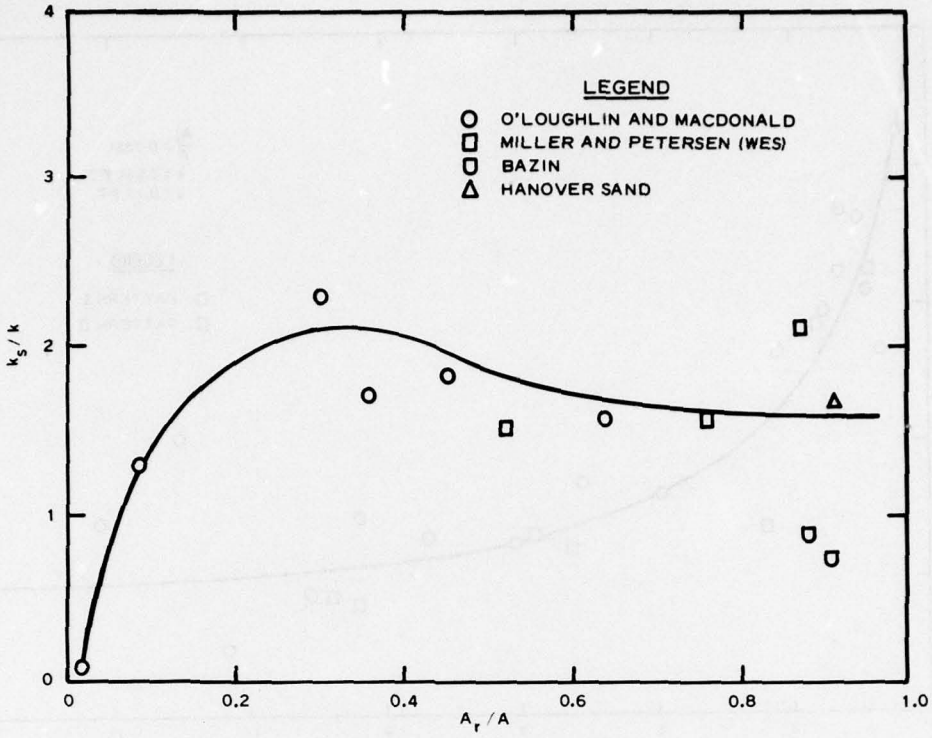

Figure 3. Effect of pebble concentration on resistance

greater than 0.5, k_s/k is nearly constant. When A_r/A is greater than 0.5 we shall regard the rocks as closely packed and assume that k_s/k is 1.75, i.e., the equivalent grain size is 1.75 times the grain size of rocks.

The Manning's n of
rocks of a specified size

8. Since k_s/k equals 1.75 for closely packed rocks, Equation 1.8 becomes

$$n = 0.0324(1.75k)^{1/6}$$

or

$$n = 0.0355k^{1/6} \qquad (1.10)$$

where k is the grain size of rocks expressed in feet. This relation is shown in Figure 4. The upper curve is for the range $0.1 < k < 10$; the lower curve is for the range $0.001 < k < 0.1$. Thus a

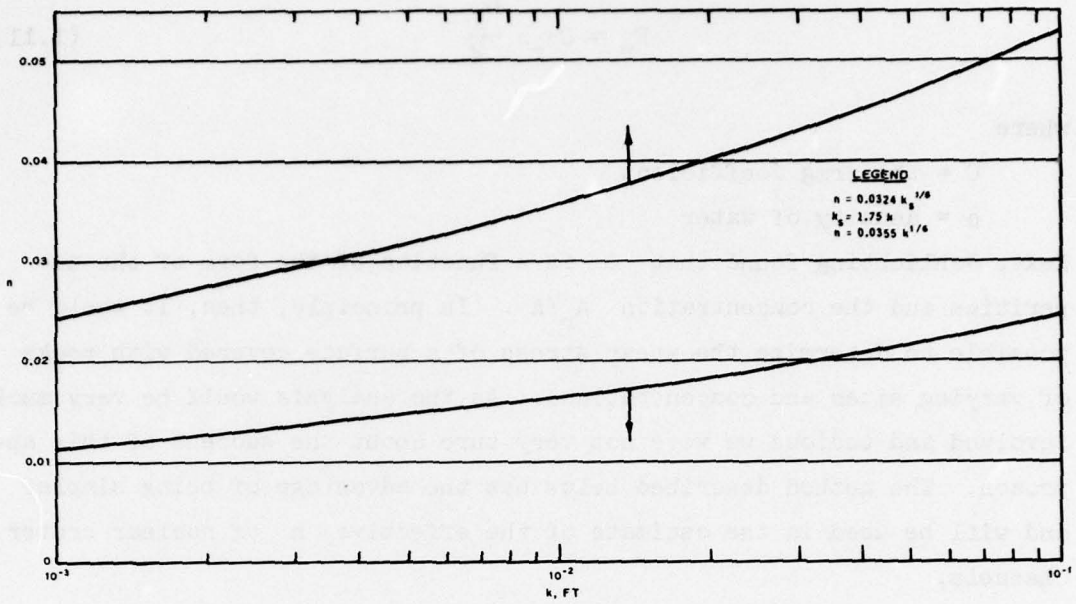

Figure 4. Relation between Manning's n and rock size k ; $A_r/A > 0.6$

concrete surface yielding $n = 0.01$ may be regarded as a surface covered with asperities of grain size equal to 0.001 ft.

Method of establishing
the effective n of ejecta
and fallback of nuclear craters

9. When the asperities of a channel are uniform, the Manning's n of the channel is readily obtained. In the case of ejecta and fallback of crater channels, the rock sizes are highly variable and the determination of n is not so simple. In his experiments with pyramidal asperities affixed to the sides of a square closed conduit, Fage[7] found that the shear stress of the walls is related to the resistive force of the pyramids. He determined the resistive force on the pyramids by measuring the pressure on the faces of the pyramids. Sadron[8] conceived that if U_k is the velocity at the apices of the asperities and a_r is the projected area of the asperities in a plane normal to the direction of flow, the resistive force F_r is

$$F_r = Ca_r\rho \frac{U_k^2}{2} \tag{1.11}$$

where

C = the drag coefficient

ρ = density of water

Next, Schlichting found that C is a function of the form of the asperities and the concentration A_r/A. In principle, then, it would be possible to determine the shear stress of a surface covered with rocks of varying sizes and concentrations. As the analysis would be very much involved and tedious we were not very sure about the success of this approach. The method described below has the advantage of being simpler and will be used in the estimate of the effective n of nuclear crater channels.

Effective n of normalized channels

10. Rocks of the surface of a crater channel are conceptually sorted according to their sizes and are rearranged on the same surface with the provision that the surface width everywhere is the same. This is the normalized channel and the arrangement is shown in Figure 5. The

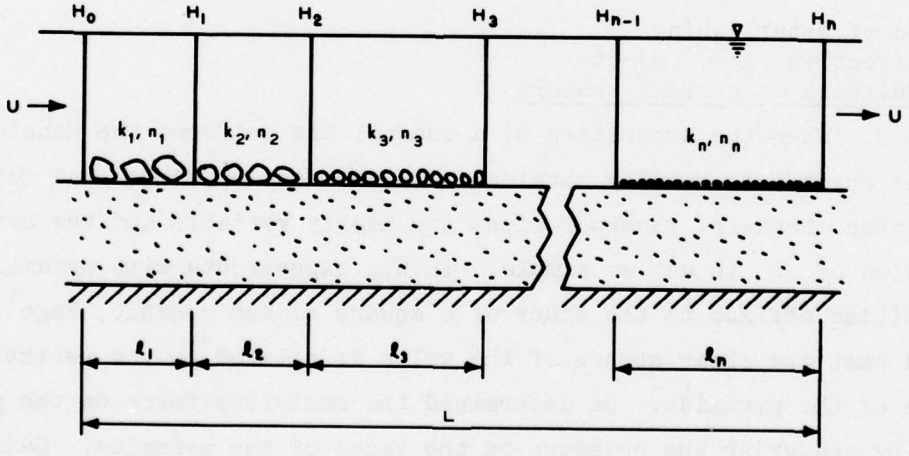

Figure 5. Sorted rocks of a crater channel

lengths of the rectangular areas occupied by rocks of sizes k_1, k_2, $k_3 \ldots k_n$ are l_1, l_2, $l_3 \ldots, l_n$, respectively. Let the total length

be L. Manning's n corresponding to the several rocks in the separate areas is $n_1, n_2, n_3, \ldots, n_n$, respectively; these values are determined by noting the rock sizes. In effect we now have a channel of width B and of length L. Imagine that a discharge Q is related to the depth of waters $H_0, H_1, H_2, H_3, \ldots, H_n$. H_0 and H_n are values at the ends, and H_1, say, is the depth at the separation between the rocks k_1 and k_2. Assume that water is large and hydraulic radius is nearly constant throughout. Applying Manning's formula

$$H_0 - H_1 = l_i n_1^2 N \qquad N = U^2/2.18R^{4/3}$$

$$H_1 - H_2 = l_2 n_2^2 N$$

$$H_{n-1} - H_n = l_n n_n^2 N$$

adding

$$H_0 - H_n = \left(\sum_{i=1}^{n} l_i n_i \right) N$$

Introducing the effective n_e of the normalized channel

$$H_0 - H_n = L n_e^2 N$$

Hence

$$n_e^2 = \sum_{i=1}^{n} n_i^2 \frac{l_i}{L} \tag{1.12}$$

This constitutes the basis of estimating the effective Manning's n of the crater channels. It is assumed that by rearranging the surface rocks in the above manner, the resistance of the channel thus formed would be practically the same as in the original or the initial channel, and that as the rocks get smaller in size, their number increases.

Effective n of basalt craters
and of craters in glassy rhyolite

11. The effective Manning's n of craters in basalt and in

glassy rhyolite was determined on the basis of data of size distribution furnished by the engineers of U. S. Army Engineer Nuclear Cratering Group. This information is contained in Figures 6 and 7 and also in Table 1. The procedure followed will be illustrated for the case of the basalt crater. It is imagined that the partitioning of the rocks is in 10 percent intervals as shown in Table 2.

Table 1

Grain-Size Distribution of Nuclear Channel Materials

Percent Finer by Weight	Basalt	Rhyolite d, ft	Rhyolite Adjusted
100	6.0	5.0	5.0
90	3.7	1.5	2.0
90	3.0	0.55	1.0
70	2.3	0.27	0.50
60	1.8	0.13	0.30
50	1.4	0.070	0.19
40	0.90	0.038	0.12
30	0.58	0.022	0.080
20	0.30	--	0.050
10	0.10	--	0.036
0	--	--	--

Table 2

Parts	Steps	d, ft	d^3	N_i	$N_i d^2$	l_i/L
(1)	(2)	(3)	(4)	(5)	(6)	(7)
1	100 to 90	4.20	74.0	1	17.6	0.055
2	90 to 80	3.20	32.7	2.26	23.2	0.073
3	80 to 70	2.60	17.1	4.3	29.0	0.091
4	70 to 60	2.00	8.0	9.2	37.0	0.117
5	60 to 50	1.60	4.09	18.1	46.3	0.181
6	50 to 40	1.10	1.37	54.0	65.2	0.205
7	40 to 30	0.74	0.40	185	100.0	0.315
8	30 to 20	0.43	0.08	920		
9	20 to 10	0.20	0.008	9200		
(7, 8, 9)					318.0	1.000

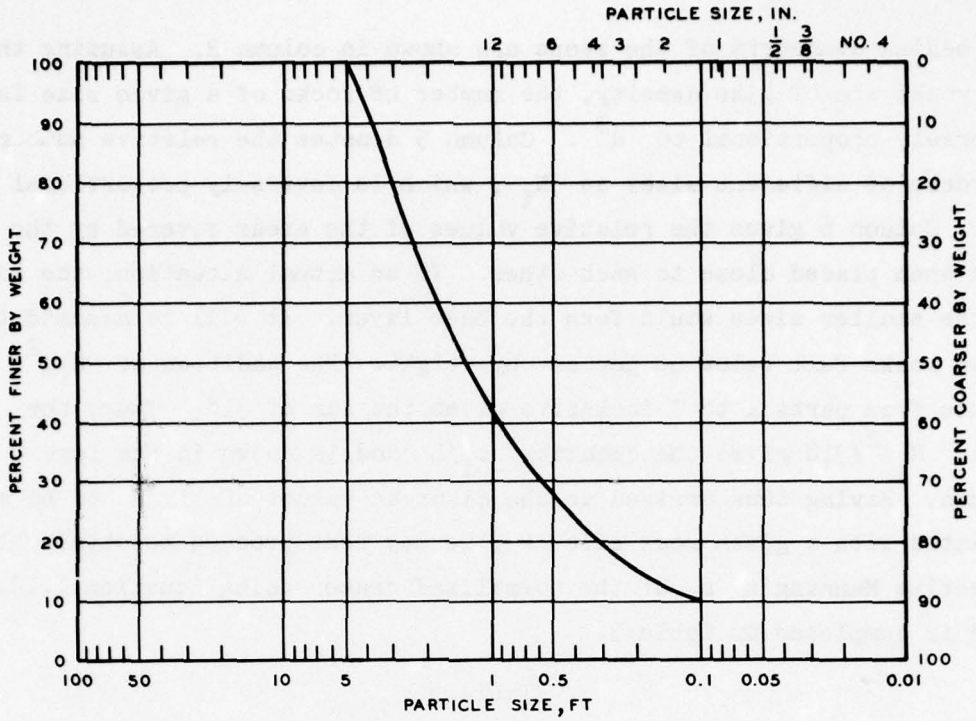

Figure 6. Average ejecta and fallback size distribution from basalt craters

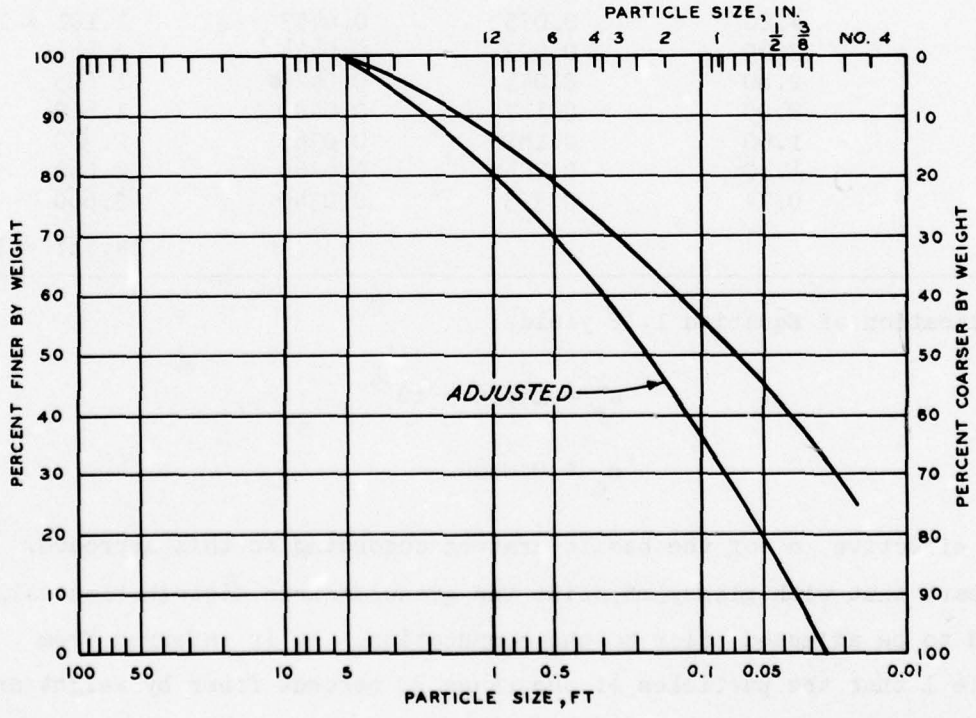

Figure 7. Average ejecta and fallback size distribution from a crater in glassy rhyolite

The median diameters of the steps are shown in column 3. Assuming that the rocks are of like density, the number of rocks of a given size is inversely proportional to d^3. Column 5 denotes the relative number of rocks of different sizes as N_i, which is inversely proportional to d^3. Column 6 gives the relative values of the areas covered by the rock when placed close to each other. In an actual situation, the rocks of the smaller sizes would form the base layer. It will be assumed that these rocks fall below 30 percent by weight. The addition of $N_i d^2$ values from parts 1 to 7 inclusive gives the sum of 318. Thus, the ratio $N_i d^2/318$ gives the quantity l_i/L and is shown in the last column. Having thus arrived at the discrete values of l_i/L to be associated with a given rock size k, we may next proceed to obtain the effective Manning's n of the normalized crater using Equation 1.12. This is completed in Table 3.

Table 3

Parts	k, ft	l_i/L	n	$l_i n^2/L$
(1)	(2)	(3)	(4)	(5)
1	4.20	0.055	0.0453	1.101×10^{-4}
2	3.20	0.073	0.0434	1.482
3	2.60	0.041	0.0420	1.605
4	2.00	0.117	0.0400	1.869
5	1.60	0.181	0.0385	2.380
6	1.10	0.205	0.0360	2.660
7	0.74	0.315	0.0340	3.660
				14.757×10^{-4}

Application of Equation 1.12 yields:

$$n_e^2 = 14.76 \times 10^{-4}$$

$$n_e = 0.0384$$

the effective n of the basalt craters according to this approach. It appears that with glassy rhyolite the granulometric distribution values need to be adjusted prior to the computation. It is inferred from Table 1 that the particles of the range 30 percent finer by weight are

too small. Discarding these, the new adjusted distribution values would be as shown in the last column of Table 1. Repeating the calculations as for basalt and using the adjusted distribution, the effective resistance coefficient for glassy rhyolite is:

$$n_e = 0.0275$$

12. The effective Manning coefficients for the surface of nuclear-cratered channels derived by the method described above are the minimum ones. In the actual channels, the larger rocks are not closely packed but are randomly spaced, and the effective k_s would be greater than the k_s of the closely packed rocks. Again, whether the rocks are closely packed or are randomly distributed, the rocks of smaller sizes would be sheltered by the larger ones. The consequence of the latter would be a reduction of the areas of smaller rocks exposed to the action of the flowing water. As a consequence of these two conditions, the effective Manning coefficient of an actual cratered channel surface would be a factor larger than the minimum value computed by the above method. A modified form of Equation 1.12 is:

$$n_e^2 = m^2 \sum_{i=1}^{n} n_i^2 \frac{l_i}{L} \qquad (1.13)$$

where m is a constant close to unity.

13. Since the theoretical evaluation of m is not practical it is necessary to resort to experimental evidence. In recent experiments on the flow of water over graded beds,[9] three sizes of gravel were employed with gradations as shown in Table 4. In forming the bed, first the larger rocks were randomly placed and successively the small sizes were added. At the ends the beds were of two layers. We have theoretically determined the effective n_e for these gravel surfaces by the above methods and also from the flow measurements. The steps in the determination of n_e for the gravels of gradation 1 are shown in Tables 5 and 6. Here, also, the gravels 30 percent finer by weight are assumed to be in the underlayer. The theoretically computed coefficient

Table 4

Gradation of Gravels in the WES Experiments[6]

Percent Finer by Weight	Gradation, d, ft		
	1	2	3
100	0.124	0.0624	0.0312
90	0.101	0.0525	0.0231
80	0.004	0.044	0.0175
70	0.071	0.037	0.0141
60	0.061	0.031	0.0122
50	0.048	0.026	0.0103
40	0.040	0.022	0.0082
30	0.032	0.019	0.0075
20	0.027	0.016	0.0055
10	0.022	0.011	0.0043
0	0.019	0.008	0.0039

Table 5

Percent Finer by Weight	d, ft	d^3	N_i	d^2	$N_i d^2$	l_i/L
100-90	11.25×10^{-2}	1420×10^{-6}	1.00	126×10^{-4}	126×10^{-4}	0.079
90-80	9.25	791	1.79	85.5	153	0.092
80-70	7.75	465	3.05	60.0	183	0.109
70-60	6.20	238	5.96	38.4	228	0.136
60-50	5.45	162	8.76	29.7	260	0.155
50-40	4.40	85	16.70	19.4	325	0.194
40-30	3.60	46.6	30.5	13.0	396	0.237
30-20	2.95	25.7	55.2	8.7	462	
20-10	2.45	14.7	96.8	6.0	580	
10-0	2.10	9.26	153	48	730	

Table 6

Parts	k, ft	l_i/L	n	n^2	$n^2 l_i/L$
1	0.1125	0.077	0.0250	6.26×10^{-4}	0.482×10^{-4}
2	0.0925	0.092	0.0240	5.78	0.532
3	0.0775	0.109	0.0233	5.44	0.594
4	0.0620	0.136	0.0225	5.05	0.688
5	0.0545	0.155	0.0220	4.85	0.752
6	0.0440	0.194	0.0215	4.62	0.896
7	0.0360	0.237	0.0205	4.20	1.000
					$4.9[illegible] \times 10^{-4}$

$n^2 = 4.946 \times 10^{-4}$; $n = 0.0222$

n_e equals 0.0222 for the gravel surface of gradation 1 and 0.0199 and 0.0171 for gradations 2 and 3, respectively. In Reference 9 the values of the ratio U/U_* and the depths for each test are recorded. Using these values, we have determined by Equation 1.7 the n for every test run. There is considerable disparity in the values of n from the tests with a given distribution of rocks, but by averaging the observed values, these are $n_e = 0.0280$, 0.0243, and 0.0213 for surfaces of gradations 1, 2, and 3, respectively. Comparing these with the theoretical values shown and using m for the ratio of the observed to the computed, we have $m = 1.25$, 1.22, and 1.24 for the gravels of gradations 1, 2, and 3, respectively. Hence, Equation 1.13 can be modified as:

$$n_e = 1.24\left(\sum_{i=1}^{n} n_i^2 \frac{l_i}{L}\right)^{1/2} \tag{1.14}$$

Applying this, a better value of resistance coefficient for the basalt craters is

$$n_e = 1.24(0.0384) = 0.0476$$

and for glassy rhyolite:

$$n_e = 1.24(0.0275) = 0.0342$$

14. An alternate procedure in the last problem would be to consider the effective k_s of a given gradation of rocks. In the WES test, Brown[9] has determined the k_s for each run. There are large disparities between the individual values from the tests and a bed of a given gradation of rocks. If averages are taken, k_s is equal to 0.233, 0.0968, and 0.0613 ft. One should inquire as to the ratio of k_s in the average value of rock sizes for a given gradation. The average value of the rock sizes $\bar{d}$ may be determined as

$$\bar{d} = \Sigma \frac{d\Delta A}{A}$$

or

$$\bar{d} = \Sigma \frac{dl_i}{L} \tag{1.15}$$

as it is best to do the averaging on the basis of areas covered by the

rocks. One finds the mean values equal to 0.0598, 0.0310, and 0.0125 ft for rocks of the gradations 1, 2, and 3. Thus

$$\frac{k_s}{\bar{d}} = 3.89 \quad \text{for gradation 1}$$
$$= 3.13 \quad \text{for gradation 2}$$
$$= 4.90 \quad \text{for gradation 3}$$

As an average, then,

$$k_s = 3.97\ \bar{d} \tag{1.16}$$

Resorting to the values of d and l_i/L shown in Table 2, $\bar{d} = 1.687$ ft for the basalt rocks. Hence, using Equation 1.16, $k_s = 6.69$ ft and turning to Equation 1.8, the channel effective n is

$$n_e = 0.0445$$

which agrees fairly well with the calculation by Equation 1.14. In the same manner, one finds for the rhyolite channel

$$n_e = 0.0324$$

Loss of Energy in an Isostatic Area

Losses in isostatic flow areas

15. The term isostatic refers to areas of the flow where a mean movement out of the area is absent, although there are local movements from point to point. In these areas, pressures are uniform and the movements are essentially cyclic induced by the tangential stresses of the main flow turbulence. This situation arises when a current is deflected or a current moving in a constant direction experiences a sudden expansion. In such areas there is loss of energy in the main current, due partly to the maintenance of the eddying motion and to the turbulent dissipation in the waters adjacent to the isostatic area.

Energy loss in Tollmien free jet

16. When a current meets and runs over a body of still water, a zone of turbulent waters is created as shown in Figure 8. The zone is limited between two straight lines oy_1 and oy_2 showing that the width of the turbulent zone increases linearly with distance measured from the point where the current meets the still water. At any point on

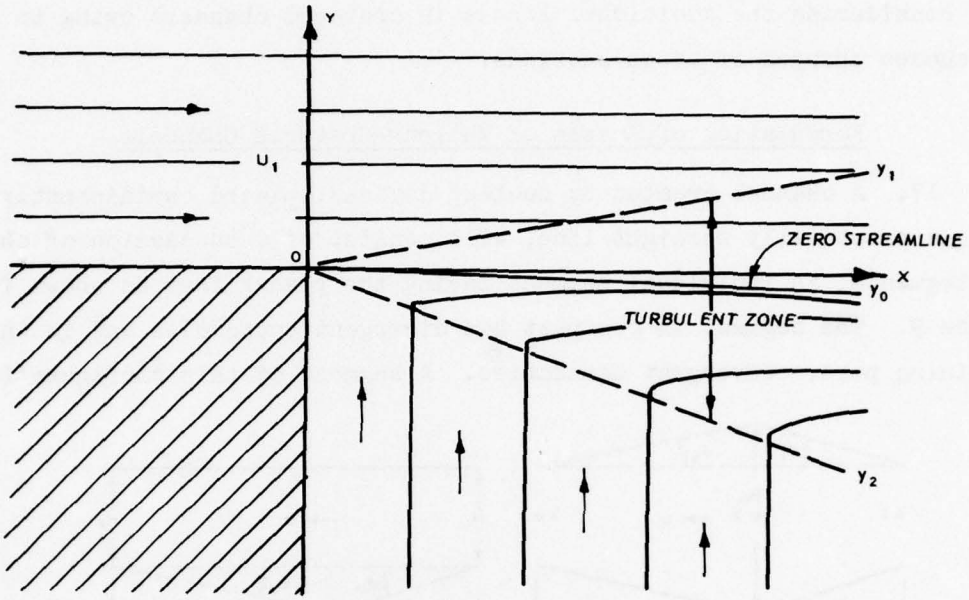

Figure 8. Free turbulence between current and still water (semijet)

the line oy_1, the longitudinal velocity equals the initial velocity u_1, of the current. At any point on the line oy_2, the longitudinal velocity vanishes but there is a lateral movement. The line oy_0 is the zero streamline with an angle of inclination α with the horizontal. The water below oy_0 is in the isostatic area. The theory of this type of mixing has been developed by Tollmien[10] and it can be shown that $\tan \alpha = 0.19$. A single streamline in this area closes at infinity and the flow below oy_0 is virtually cyclic. Energy lost from the main current is expended in maintaining the cyclic motion below oy_0 and in the turbulence of the zone above oy_2. Analysis shows that the jet dissipation (loss of energy per unit time) amounts to

$$E_L = 0.0468\ \rho\ \frac{U_1^3}{2} A_x \qquad (1.17)$$

where A_x is the area of contact between the isostatic zone of cyclic motion and the main current. The losses encountered in miter bends and in sudden expansions are nearly in accordance with Equation 1.17 as shown by Sager and others.[11] Thus this should prove to be of value when considering the additional losses in cratered channels owing to the sudden changes of cross sections.

Formulation of Losses of Nuclear-Cratered Channels

17. A channel created by nuclear devices, placed equidistantly along a practically straight line, will consist of a succession of channel segments, an individual segment having the planar form as shown in Figure 9. The segment in one part has divergent boundaries and in the remaining part, convergent boundaries. A segment of this configuration

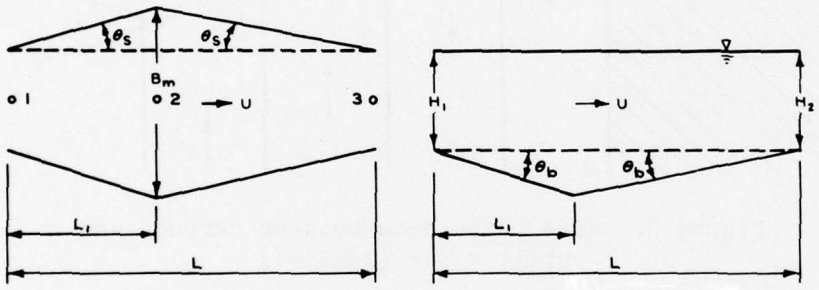

LEGEND

R = AVERAGE HYDRAULIC RADIUS
X = AVERAGE WETTED PERIMETER
U = AVERAGE CURRENT VELOCITY

Figure 9. Notation diagram of cratered segments

will be referred to as a cratered segment. Despite the fact that the devices creating the channel are arranged equidistantly, the resulting crater segments may not always have equal divergent and the convergent parts. Let L be the total length of the cratered segment and L_1 be the length of the divergent part. If the flow were reversed, the length of divergent part would be $L - L_1$. Taking the point of view adapted in

the previous sections, it is assumed that a flow separation occurs in the divergent part of the cratered segment. This is part of an isostatic area, and in this area, the loss of energy per unit time is:

$$E_1 = C \frac{\rho}{2} U^3 A_1 \tag{1.18}$$

where

E_1 = jet dissipation due to free turbulence in a nuclear segment

C = an experimentally determined constant depending on the form of the segment

U = the mean velocity averaged along the segment length L

A_1 = the total area of the separation surface

In addition, there is the rate of loss in the segment induced by the solid boundaries

$$E_2 = \frac{\lambda_1}{2} \rho U^3 (A - A_1) \tag{1.19}$$

where

λ_1 = the coefficient of friction due to the boundary asperities

A = the wetted wall surface

If n_1 is Manning's n for the surface, from Equation 1.7

$$\lambda_1 = \frac{29.16}{R^{1/3}} n_1^2 \tag{1.20}$$

where R is the mean hydraulic radius of the cratered segment.

18. Let Q be the discharge and ΔH the fall of the energy line along the segment. Hence,

$$\rho g \Delta H Q = E_1 + E_2$$

or

$$g \Delta H \rho Q = \lambda_1 \frac{\rho}{2} U^3 (A - A_1) + C \frac{\rho}{2} U^3 A_1 \tag{1.21}$$

Introducing the average wetted perimeter χ

$$Q = \chi RU, \quad A = L\chi, \quad A_1 = \ell_1 \chi$$

Substituting these in the above and dividing by ρQL one has

$$g \frac{\Delta H}{L} = \left[\lambda_1 \left(1 - \frac{\ell_1}{L} \right) + C \frac{\ell_1}{L} \right] \frac{U^2}{2R} \tag{1.22}$$

This may be written, introducing λ_2, the effective resistance coefficient of the cratered segment, as

$$g \frac{\Delta H}{L} = \lambda_2 \frac{U^2}{2R} \tag{1.23}$$

where

$$\lambda_2 = \lambda_1 \left(1 - \frac{\ell_1}{L} \right) + C \frac{\ell_1}{L} \tag{1.24}$$

One may also write this as

$$\lambda_2 = \lambda_1 \left(1 - \frac{\ell_1}{L} \right) + N \tag{1.25}$$

where

$$N = C \frac{\ell_1}{L} \tag{1.26}$$

19. Equation 1.25 above refers to a single cratered segment. In the derivation, use was made of the average value of the mean currents in various channel cross sections. This is permissible if it is assumed that the variation of the cross sections and of the hydraulic radii between extremes is linear with distance. Now, if it is further assumed that the quantities ℓ_1/L and C are practically constant over the channel length, Equation 1.21 may be assumed to apply to a long cratered channel consisting of many cratered segments, and $\Delta H/L$ would denote the gradient of energy line of the long channel. The interpretation of

Equation 1.23 is that once the average quantities ℓ_1/L and N are known, the effective λ_2 or the Manning's n_2 of the channel can be determined. For determination of these quantities in special cases, reference will be made to the WES channel experiments.[11]

Results from WES Channel Experiments

20. The nature of the increased losses due to the divergence and convergence in a cratered channel was examined in three channels, all having the same length, the same average cross section of 1.206 sq ft, and the same average hydraulic radius of 0.0378 ft. The surface asperities of all the channels were the same. One of the channels was of uniform cross section throughout. The other two channels consisted of cratered segments with form specifications indicated by the coordinator of the WES channel experiments, Major Robert G. Bening, U. S. Army Engineer Nuclear Cratering Group, Livermore, California. The experiments showed that the losses of the two cratered channels were practically of like value,

$$\frac{\Delta H}{L} = 4.65 \times 10^{-4} Q^2$$

and for the channel of uniform cross section

$$\frac{\Delta H}{L} = 1.36 \times 10^{-4} Q^2$$

Using Manning's formula for both channels

$$\frac{\Delta H}{L} = \frac{n^2}{2.22} \frac{U^2}{R^{4/3}}$$

and

$$g \frac{\Delta H}{L} = \frac{\lambda_2}{2} \frac{U^2}{R} \quad \text{for the cratered channel} \qquad (1.23 \text{ bis})$$

and

$$\lambda_1 R^{1/3} = 29.16\, n_1^2 \quad \text{for the smooth channel} \qquad (1.20\ \text{bis})$$

one finds that for the uniform channel

$$\lambda_1 = 48.1 \times 10^{-4}$$

and

$$n_1 = 0.0108$$

For the cratered channels

$$\lambda_2 = 164.5 \times 10^{-4}$$

and

$$n_2 = 0.0201$$

Accordingly, the expansions and the contractions do increase the Manning's n to twice the value of the uniform channel.

21. The area of the separation of the flow in the cratered channel was examined visually through the introduction of dye in one of the cratered channels for the two directions of flow, regular and reversed, and for two discharges. Only the surface dimensions of the separations could be noted with certainty. Let ℓ_{lm} denote the length of the separated area in the direction of flow, Δ denote the maximum width of this same area, and B_m denote the maximum width of the segment (see Figure 10). The observed values of ℓ_{lm}/L show some variations: for one discharge the average values were 0.698 and 0.678 with reversed flow; for another discharge the corresponding values were 0.638 and 0.687. Also, there were small variations in the values of $2\Delta/B_m$ from segment to segment: for one discharge the average values were 0.263 and 0.288; for the other discharge the corresponding values were 0.285 and 0.354. These show the extent of the separations. The same dye technique could

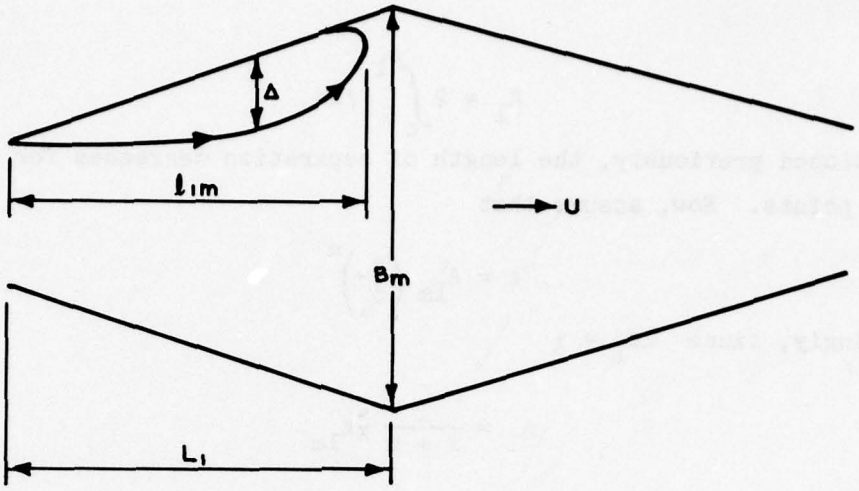

Figure 10. Notation diagram of surface separations in cratered segments

not be extended to points below the surface. The impressions gathered indicated that the separation became smaller with increased depth. As the extent of the separations should depend on the inclinations of the boundaries, the depth dependence should be noted for the channels of the investigation. The inclination θ varies with depth. Values for the different crater segments do vary somewhat. Without making a distinction between the inclinations in the divergent and convergent parts, the mean of θ_s at the surface is 9.95 degrees and θ_b at the bottom 6.62 degrees for the two channels.

Establishment of Cratered Channel Formula

22. Determinations of the quantities ℓ_1/L and N of Equation 1.25 will be made on the basis of the results obtained in the WES cratered channel experiments. The quantity ℓ_1 can be related to the length ℓ_{1m} of the separation area observed at the surface in the following manner. One may consider the wetted perimeter of a cross section in the general area of the separation (Figure 10). Let s be the arc length measured from the lowest point in the section along the rigid boundary. Place $2s_1 = \chi$. Let ℓ be the length of the separated area at the level of s. Thus, A_1, the total area of the separating surface, is

$$A_1 = 2\int_0^{s_1} \ell ds$$

As mentioned previously, the length of separation decreases for the deeper points. Now, assume that

$$\ell = \ell_{1m}\left(\frac{s}{s_1}\right)^m$$

Accordingly, since $2s_1 = \chi$

$$A_1 = \frac{1}{1+m}\chi\ell_{1m}$$

Recalling the definition, $A_1 = \chi\ell_1$, it is seen that

$$\ell_1 = \frac{\ell_{1m}}{1+m}$$

and

$$\frac{\ell_1}{L} = \frac{1}{1+m}\frac{\ell_{1m}}{L}$$

23. The experimental results (shown in Tables 4 and 5) show that the average value of ℓ_{1m}/L from four sets of separate observations is 0.668. If one places coefficient $m = 1.5$, then

$$\frac{\ell_1}{L} = \frac{0.668}{2.5} = 0.268$$

Equation 1.25 then becomes

$$\lambda_2 = 0.732\lambda_1 + N$$

In the WES channel tests with the channel of uniform cross section

$$\lambda_1 = 48.1 \times 10^{-4}$$

and in the cratered channels

$$\lambda_2 = 164.5 \times 10^{-4}$$

With these values it is found that

$$N = 129.3 \times 10^{-4} \tag{1.27}$$

with $m = 3.0$

$$\frac{\ell_1}{L} = 0.223$$

$$\lambda_2 = 0.777\lambda_1 + N$$

and

$$N = 127.3 \times 10^{-4} \tag{1.28}$$

Again, if $m = 1.0$,

$$\frac{\ell}{L} = 0.334$$

$$\lambda_2 = 0.666\lambda_1 + N$$

and

$$N = 132.3 \times 10^{-4} \tag{1.29}$$

24. In the above there are three expressions to evaluate the effective resistance coefficients of a cratered channel. It is difficult to make a selection. Before a selection is made, however, it is necessary to ascertain if these expressions could be valid, at least approximately. The criterion is that the losses thereby indicated are of the order met within the turbulent isostatic zone of a semijet. It will be recalled that the latter loss is given by

$$E_1 = C\rho \frac{U_1^3}{2} A_1$$

$$C = 0.0468 \tag{1.17 bis}$$

With the case of the cratered segments, correspondingly, the expression is

$$E_1 = C \frac{\rho}{2} U^3 A_1 \qquad (1.18 \text{ bis})$$

and

$$C = N \frac{L}{\ell_1} \qquad (1.26 \text{ bis})$$

Introducing values of N and L/ℓ_1 from Equations 1.27, 1.28, and 1.29 gives

$$m = 3, \quad C = 0.0572$$

$$m = 3/2, \quad C = 0.0483$$

$$m = 1, \quad C = 0.0393$$

which show, indeed, that the losses thus calculated for a cratered segment are of the same order of magnitude as for a semijet. We shall adopt the expression of loss corresponding to $m = 3/2$. Accordingly, the expression

$$\lambda_2 = 0.732\lambda_1 + 129.3 \times 10^{-4} \qquad (1.30)$$

is adopted for the effective coefficient of friction of a cratered channel segment of the general form tested in the model channels at WES.

Cratered Channel Loss Formula in Terms of Manning's n

25. The cratered channel loss expression

$$\lambda_2 = 0.732\lambda_1 + 0.0129 \qquad (1.31)$$

involving the roughness coefficients may be changed into one involving the Manning's coefficients n_2 and n_1. Using the form in Equation 1.20, measuring R in feet,

$$\lambda_1 = \frac{29.16}{R^{1/3}} n_1^2$$

$$n_2^2 \times 10^4 = 0.732 n_1^2 \times 10^4 + 4.43 R^{1/3} \qquad (1.32)$$

where

n_2 = the effective Manning's n of the cratered channel

n_1 = the Manning's n if the channel did not have expansions and contractions

R = the average value of the hydraulic radii

The above expression indicates that the increase of the effective Manning's n of a cratered channel over that of a uniform channel would be more pronounced with smaller surface asperities and with greater hydraulic radii.

26. It is envisaged that the formula given could not be applied to all cases of cratered channels but only to those having form characteristics similar to the channels studied at WES. As a criterion of form, one may take the angle of divergence θ of the channel lines at the water surface and those at the bed bottom. Let θ_s refer to the surface expansions or contractions and θ_b to the bottom expansions or contractions. Taking average values of these quantities expressed as radians from all the cratered segments in channel 2 and in channel 3: $\theta_s = 9.95$ degrees and $\theta_b = 6.62$ degrees . Note than θ_b is smaller than θ_s . This may be the reason that the separation areas in the expanding sections are greater and more significant at the water surface.

27. An alternate approach to the problem is one proposed by Mr. J. H. Douma of the Office, Chief of Engineers, U. S. Army. The losses are visualized as arising from expansion. The idea was followed previously by Sager and others[11] with the result that

$$n_2^2 \times 10^4 = n_1^2 \times 10^4 + 3.99 R^{1/3} \qquad (1.33)$$

One may call this the Douma formula. The difference between the main formula (Equation 1.32) and the Douma formula (Equation 1.33) is small. Indeed, theoretically, Equation 1.33 represents the limiting form of Equation 1.32. The Douma formula could have been obtained directly from Equation 1.24 if one had supposed that in this equation ℓ_1/L vanishes and C becomes infinite. Interpreting physically, one would have

assumed that the separation areas responsible for added losses are infinitely small and the dissipation rate infinite. This is a difficulty avoided in the derivation of Equation 1.32, which is suitable for the estimate of the effective resistance of cratered channels.

Effective Resistance of Nuclear-Cratered Section

28. In August 1968 the Nuclear Cratering Group, Corps of Engineers, furnished data on dimensions of a long section of a hypothetical nuclear-cratered channel. These data will be utilized to illustrate the manner of determining the effective resistance using Equation 1.32. The size distribution is given in Table 7, the material of the section being basalt, rhyolite, or clay shale.

Table 7

Nuclear Excavation Data

Explosive Location	Explosive Spacing ft	Channel Depth ft	Channel Width ft	Channel Area in Cross Section sq ft	Hydraulic Radius ft	Channel Length ft
1	565	336	1193	227,928	165	0
2	652	418	1436	336,969	201	565
3	739	312	1188	216,573	160	1,217
4	652	386	1407	312,625	193	1,956
5	652	374	1307	222,002	182	2,608
6	823	461	1627	426,417	226	3,260
7	907	330	1300	253,142	172	4,083
8	823	364	1402	299,075	187	4,990
9	739	420	1507	362,169	208	5,813
10	739	340	1271	251,012	172	6,562
11	823	440	1566	392,895	217	7,291
12	823	293	1188	207,155	156	8,114
13	652	461	1627	426,417	226	8,937
14	565	374	1307	276,664	182	9,589
1		335	1193	227,928	165	10,154

29. Let L be the length of a segment, R and A the average hydraulic radius and the average cross section, respectively, of the segment, Q the discharge, and ΔH the fall of the water surface between the ends of the segment. Now

$$\Delta H = n^2 NL$$

$$N = 0.458 \frac{Q^2}{A^2 R^{4/3}}$$

where n is the Manning's coefficient of the segment. Dropping the subscript 2, Equation 1.32 becomes

$$n^2 \times 10^4 = 0.732 n_1^2 \times 10^4 + 4.43 R^{1/3}$$

The fall of the water surface in the individual segments, in the order of the segments, is

$$H_1 - H_2 = L_1 n_1^2 N_1$$

$$H^2 - H_3 = L_2 n_2^2 N_2$$

$$H_n - H_{n+1} = L_n n_n^2 N_n$$

Similarly, introducing the effective Manning's n for the entire section of length L_T,

$$H_{n+1} - H_1 = L_T n_e^2 \bar{N}$$

where $\bar{N}$ is computed as

$$\bar{N} = 0.458 \frac{Q^2}{\bar{A}^2 \bar{R}^{4/3}}$$

where $\bar{A}$ and $\bar{R}$ are the average cross section and the average hydraulic radius, respectively, of the entire channel. Since the energy loss in the entire channel equals the sum of the losses in the segments:

$$L_T n_e^2 \bar{N} = \sum_{i=1}^{n} L_i n_i^2 N_i$$

and hence

$$n_e^2 = \sum_{i=1}^{n} n_i^2 \left(\frac{\bar{A}}{\bar{A}_i}\right)^2 \left(\frac{\bar{R}}{\bar{R}_i}\right)^{4/3} \frac{L_i}{L_t} \qquad (1.34)$$

If R_1 and R_3 are the hydraulic radii at the ends of a segment and R_2 the hydraulic radius at the cross section of the largest area, and L_1 and L_2 are the lengths of converging and diverging parts, then the average hydraulic radius of a segment i is

$$\bar{R}_i = \left(\frac{R_1 + R_2}{2}\right) \frac{L_1}{L} + \left(\frac{R_2 + R_3}{2}\right) \frac{L_2}{L}$$

Similarly the average cross section of a segment i is

$$\bar{A}_i = \left(\frac{A_1 + A_2}{2}\right) \frac{L_1}{L} + \left(\frac{A_2 + A_3}{2}\right) \frac{L_2}{L}$$

The average hydraulic radius $\bar{R}$ and the average cross section $\bar{A}$ of the entire section are evaluated as:

$$\bar{R} = \sum_{i=1}^{n} \bar{R}_i \frac{L_i}{L_T}$$

and

$$\bar{A} = \sum_{i=1}^{n} \bar{A}_i \frac{L_i}{L_T}$$

Equation 1.34 requires that for the evaluation of the effective n_e of the entire channel the quantity

$$\left(\frac{\bar{A}}{\bar{A}_i}\right)^2 \left(\frac{\bar{R}}{\bar{R}_i}\right)^{4/3} \left(\frac{L_i}{L_T}\right)$$

relating to a segment of position i be determined. For the hypothetical channel of the dimensions shown in Table 7, the steps of the computations are shown in Table 8.

30. To complete the computation of n_e through Equation 1.34, the n_2 for each segment must also be known. As will be recalled, this is done using Equation 1.32. For a basalt hypothetical channel,

Table 8

Steps in the Evaluation of n_e

Segment	R_1	R_2	R_3	L_1	L_2	L_i	R_i
1	165	201	160	565	652	1217	178.8
2	160	193	182	739	652	1391	181.8
3	182	226	172	652	823	1475	201.2
4	172	208	172	730	739	2469	190.0
5	172	217	155	739	823	1562	190.0
6	155	226	165	823	1217	2040	190.0

Segment	A_1	A_2	A_3	L_1	L_2	L_i	$\bar{A}_i$
1	227.9×10^3	337.0×10^3	216.6×10^3	565	652	1217	279.4×10^3
2	216.6	312.6	222.0	739	652	1391	265.9
3	222.2	426.5	253.1	652	823	1475	332.9
4	253.1	362.2	251.0	1730	739	2469	307.4
5	251.0	392.9	207.2	739	1823	1562	310.4
6	207.2	426.4	227.9	823	1217	2040	310.2

Segment	L_i	$\frac{L_i}{L_T}$	$\bar{R}_i$	$\bar{R}_i \frac{L_i}{L_T}$	$\bar{A}_i$	$\bar{A}_i \frac{L_i}{L_T}$	Average
1	1217	0.1198	178.8	21.42	279.4×10^3	33.47×10^3	
2	1391	0.1370	181.8	24.91	265.9	36.43	$\bar{R} = 189.1$
3	1475	0.1453	201.2	29.23	332.9	48.37	$\bar{A} = 302.2 \times 10^3$
4	2649	0.2431	190.0	46.19	307.4	74.73	$L_T = 10{,}154$
5	1562	0.1543	190.0	29.31	310.4	47.89	
6	2040	0.2008	190.0	38.00	310.2	62.29	

Segment	$\frac{\bar{R}}{\bar{R}_i}$	$\frac{\bar{A}}{\bar{A}_i}$	$\left(\frac{\bar{R}}{\bar{R}_i}\right)^{4/3}$	$\left(\frac{\bar{A}}{\bar{A}_i}\right)^2$	$\frac{L_i}{L_T}$	$\left(\frac{\bar{R}}{\bar{R}_i}\right)^{4/3}\left(\frac{\bar{A}}{\bar{A}_i}\right)^{2}\frac{L_i}{L_T}$	$R_i^{1/3}$
1	1.057	1.085	1.079	1.173	0.1198	0.1523	5.63
2	1.039	1.140	1.053	1.296	0.1370	0.1874	5.67
3	0.939	0.911	0.920	0.954	0.1453	0.1109	5.86
4	0.995	0.986	0.993	0.993	0.2431	0.2346	5.75
5	0.995	0.977	0.993	0.988	0.1543	0.1463	5.75
6	0.995	0.974	0.993	0.987	0.2008	0.1892	5.75

$n_1 = 0.0476$. This would be the appropriate Manning's n had the channel been of uniform cross section throughout. Then the appropriate values n_2 on the basis of Equation 1.32 are given in the fourth column of Table 9. The sum of the entries in the last column give $n_e^2 \times 10^4$; thus the effective Manning's n of the hypothetical channel of the

Table 9

Coefficient of Basalt Section

Segment	$\bar{R}_i^{1/3}$	$4.43\bar{R}_i^{1/3}$	(a) $n_2^2 \times 10^4$	(b) $\left(\frac{\bar{R}}{R_i}\right)^{4/3}\left(\frac{\bar{A}}{A_i}\right)^2 \frac{L_i}{L_T}$	(a) · (b)
1	5.63	24.94	47.69	0.1523	7.263
2	5.67	25.12	47.87	0.1874	8.970
3	5.86	25.96	48.21	0.1109	5.335
4	5.75	25.47	48.22	0.2346	11.313
5	5.75	25.47	48.22	0.1463	7.044
6	5.75	25.47	48.22	0.1892	9.123
				Sum	58.02

$n_e^2 \times 10^4 = 58.02$ $\quad n_e = 0.0762$

dimensions shown in Table 7 is $n_e = 0.0762$. Making similar computations for channels of rhyolite or clay shale, the results are shown below.

Material	n_1	n_e
Basalt	0.0476	0.0762
Rhyolite	0.0332	0.0609
Clay shale	0.010	0.0514

An obvious deduction from this summary is that divergence and convergence in segments considerably increase the resistance factor of the channnels.

Estimate of Roughness of Channels with a Muck Bottom

31. According to Mr. Eden, formerly of SAJ, the distribution of grain size of the Atlantic muck is 100 percent less than 0.1 mm, 65 percent less than 0.01 mm, and 35 percent less than 0.002 mm (see Figure 24). The estimate of roughness having a material this fine raises some difficult questions. If it is assumed that no ripples or dunes are present, the boundary surface could be hydrodynamically smooth. In order that this be the case, the criterion

$$\frac{U_* d}{\nu} < 3.3 \qquad (1.35)$$

need be satisfied. Here U_* is the shear velocity $\sqrt{\tau_o/\rho}$, τ_o the wall stress, ρ the density of water, ν the kinematic viscosity, and d the grain diameter. With this condition satisfied, the mean current U prevailing in a trapezoidal channel would be

$$\frac{U}{U_*} = 3.25 + 5.75 \log \frac{RU_*}{\nu} \tag{1.36}$$

One may approximate this by a power expression of the form

$$\frac{U}{U_*} = K\left(\frac{RU_*}{\nu}\right)^{1/6} \tag{1.37}$$

The coefficient K, a dimensionless number, may be determined by equating the right-hand sides of Equations 1.36 and 1.37, for a selected value of U_*R/ν. The values of K obtained in this manner are shown in Table 10. Comparing Equation 1.37 with Manning's law, Equation 1.3, the effective sand roughness appropriate for hydrodynamical smooth surface is

Table 10

$\frac{U_*R}{\nu}$	$\frac{UR}{\nu}$	K	K_1	K_2
1×10^2	1.48×10^3	6.85	0.0382	0.0504
1×10^3	2.05×10^4	6.50	0.0405	0.0532
1×10^4	2.65×10^5	5.75	0.0456	0.0601
1×10^5	3.20×10^6	4.70	0.0560	0.0700
1×10^6	3.75×10^7	3.77	0.0697	0.0843
1×10^7	4.35×10^8	2.97	0.0884	0.1032

$$k_s = \left(\frac{8.12}{K}\right)^6 \frac{\nu}{U_*} \tag{1.38}$$

Using Equation 1.8

$$n = K_1 R^{1/6} \left(\frac{U_*R}{\nu}\right)^{-1.6} \tag{1.39}$$

where

$$K_1 = \frac{0.0324 \times 8.12}{K} \tag{1.39}$$

This establishes the Manning's n for the hydrodynamically smooth surfaces. The dependence of the coefficient K on the flow Reynolds number based on shear velocity is shown in Table 10.

32. The effective sand roughness depends on the channel roughness boundary stress. The determination of this quantity in a smooth channel is somewhat uncertain if the flow of the channel is unsteady. In simple terms, the equation of motion of this flow would be

$$\frac{\partial U}{\partial t} + g \frac{\partial h}{\partial x} = \frac{-U_*^2}{R}$$

Now, if the resistance term (the right-hand side) is large in comparison with the acceleration term, the boundary stress is determined by the slope of the water surface. Thus, if L is the length of the inter-oceanic channel, R is the hydraulic radius, and H is the semirange of the Pacific tide, then the limiting value of U_* for steady flow is

$$U_* = \sqrt{\frac{gRH}{L}}$$

This could be true only when the tidal period extends into days. Since the acceleration term in general is not negligible with respect to the resistance term, one may represent this by writing

$$U_* = m\sqrt{\frac{gRH}{L}} \tag{1.40}$$

where m is a fractional number. Taking L as 50 miles, R = 50.6 ft which is the hydraulic radius of a trapezoidal channel with dimensions of 600 ft surface width and 60 ft depth with an embankment slope of 1 on 1.5, one may evaluate Manning's coefficient n for a set of values of m and the energy loss H using Equation 1.39 with U_* from Equation 1.40 and assuming that $\nu = 1 \times 10^{-5}$ ft^2/sec. The result is the following set of values for n .

m	H, ft 10	2.5	0.62
1	0.0129	0.0133	0.0136
1/2	0.0133	0.0136	0.0139
1/4	0.0136	0.0139	0.0156
1/8	0.0139	0.0156	0.0160

These results indicate that in the part of a canal with a muck boundary the effective Manning coefficient varies slightly over a tidal cycle.

33. An alternate treatment of this problem would be to express the effective n in terms of mean current instead of mean shear velocity. From Equation 1.37

$$U_* = K^{-6/7} \left(\frac{UR}{\nu}\right)^{-1/7} U \tag{1.41}$$

Inserting this in Equation 1.38

$$\frac{k_s}{R} = \left(\frac{8.12}{K}\right)^6 K^{6/7} \left(\frac{UR}{\nu}\right)^{-6/7} \tag{1.42}$$

and introducing in Equation 1.8

$$n = K_2 \left(\frac{UR}{\nu}\right)^{-1/7} R^{1/6} \tag{1.43}$$

where $K_2 = 0.2631K^{-6/7}$

The dependence of K_2 on the Reynolds number UR/ν is shown in Table 10. The variation of K_2 with Reynolds number is appreciable. In a given channel the Manning's n decreases when the velocity of current is increased. Considering again the same channel as described in the preceding paragraph, R = 50.6 ft and $\nu = 1 \times 10^{-5}$ ft^2/sec, the following set of n values is calculated for various current velocities.

U, ft/sec	n	U, ft/sec	n
0.5	0.0154	6.0	0.0136
1.0	0.0152	8.0	0.0131
2.0	0.0146	10.0	0.0130
4.0	0.0139		

34. It is also necessary to establish the limiting value of the

current above which the channel walls cease to be hydrodynamically smooth. To determine the limiting velocity, the value of U_* from Equation 1.41 is introduced into Equation 1.35. Thus, the criterion for hydrodynamic smoothness of a channel is

$$\frac{UR}{\nu} \leq 4.02K\left(\frac{R}{d}\right)^{7/6} \tag{1.44}$$

where d is the grain size d_{65}, which for the Atlantic muck is 0.01 mm on 3.28×10^{-5} ft. Inserting this in the above, taking $R = 50.6$ ft, $\nu = 1 \times 10^{-5}$ ft^2/sec and obtaining the value of K from Table 10 as 3, the maximum value of the current above which the channel ceases to be hydrodynamically smooth is 41.5 ft/sec. Thus, the channel may be considered to be hydrodynamically smooth under all flow rates. On this basis, the average value of the Manning's n of a channel in Atlantic muck with no ripples or dunes during a tidal cycle as deduced from the results of the preceding paragraphs would be about 0.014. This also applies to clay shale with the grain-size distribution shown in Figure 11.

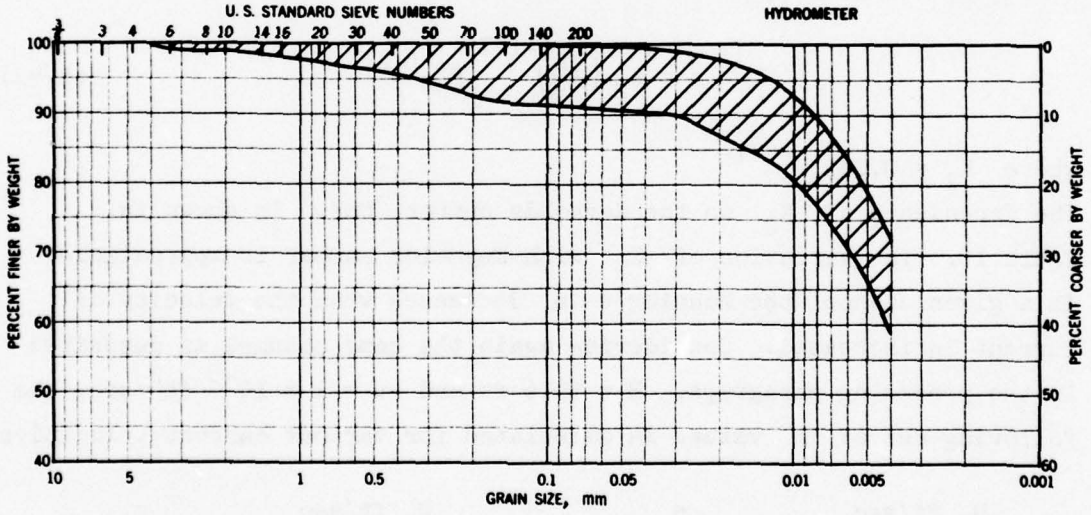

Figure 11. Grain-size distribution range; weathered Bearpaw shale (5 samples), Pre-GONDOLA site

PART II: MECHANICS OF BED FEATURES IN ALLUVIAL CHANNELS

Entrainment of Sand

35. In alluvial channels, where the bed is composed of loose sand, the resistance encountered for a given flow is much higher than what may be inferred from the drag on the individual grains. This increase has been attributed to the form resistance of the bed features. The low Manning n values derived in previous paragraphs for channels in Atlantic muck were derived under the assumption that no bed features were present. In natural alluvial streams characterized by bed features, the grain size is about 0.1 mm. It is not clear if bed features should be expected with grain sizes as small as in Atlantic muck or clay shale of the same size; this point should be examined. The answer may possibly be obtained from the complex hydraulics of movable-bed material. The literature in this field of hydraulics is extensive. Nevertheless, it may suffice to focus attention only on the form resistance of bed features of natural channels, laying stress on laboratory studies, and to develop proper formulations to fine alluvial materials.

36. The bed surface would be plane for currents less than some critical velocity. For currents slightly above critical, the first features observed are ripples. Ripples are triangular corrugations of small height and length, the upstream faces being flatter than the downstream faces. At a higher current velocity, these irregularities grow in height and in length to form features ordinarily called dunes. Both ripples and dunes move downstream. These two features are responsible for the increase of resistance in an alluvial channel. The presence of ripples causes no agitation of waters at the surface, while dunes generate surface disturbances in the form of waves. This latter condition has been utilized by some investigators to formulate theoretical relations between the sand waves and the surface waves. As the velocity is increased, a point is reached where the dunes are erased and the bed becomes flat. This transition ordinarily occurs at a Froude number less than unity for ordinary sands of about 1 mm. As the Froude

number increases above unity, one may observe a sequentially plane bed with a smooth water surface and antidunes. Antidunes are standing waves of sand that are accompanied by corresponding standing surface waves; both the antidunes and the surface waves move upstream, grow in height, and then break.

Initiation of sediment motion

37. One may proceed with dimensional analysis to establish expressions for the initial entrainment of sand. The quantities involved are: U_r, the velocity of current at the apices of sands; d, the grain size; ρ, the density of water; ρ_s, the density of sand; ν, the kinematic viscosity of water; and g, the constant of gravity. Assume that the initial motion of sand is an upward displacement due to the lift arising from the pressures around the sand surface of the value

$$F_r = C_1 \rho U_r^2 d^2 \tag{2.1}$$

The constant C_1 in general is a function of placement, of the shape of sands, and Reynolds number $U_r d/\nu$. The uplifting force has to overcome the weight of sand in water.

$$W_g = \frac{\pi}{6} (\rho_s - \rho) g d^3 \tag{2.2}$$

Equating these two forces

$$\frac{\rho U_r^2}{(\rho_s - \rho) g d} = \phi_1 \frac{U_r d}{\nu} \tag{2.3}$$

concealing in the functional the constants relating to placement and shape of sands. In regular channels, the velocities may be inferred from the shear velocity U_*, $U_* = \sqrt{\tau/\rho}$, where τ is the shear acting on the channel floor bearing on the sands. Whether the flow be laminar or turbulent

$$U = U_* \phi_2 \frac{U_* y}{\nu}$$

where U is the velocity at the point of distance y from the channel floor. Thus

$$U_r = U_* \phi_2 \frac{U_* d}{\nu}$$

and introducing this in Equation 2.3, the result is

$$\frac{\tau}{(\rho_s - \rho) g d} = \phi \frac{U_* d}{\nu} \qquad (2.4)$$

This initially was given by Shields. Shields has shown the validity of this expression using the data of his experiments with grains of varying densities together with the data from Casey, Krammer, WES, and Gilbert.[12] The solid curve shown in Figure 12 and referred to as Shields' curve is a good representation from Vanoni.[13] The curve was drawn by Rouse[14]

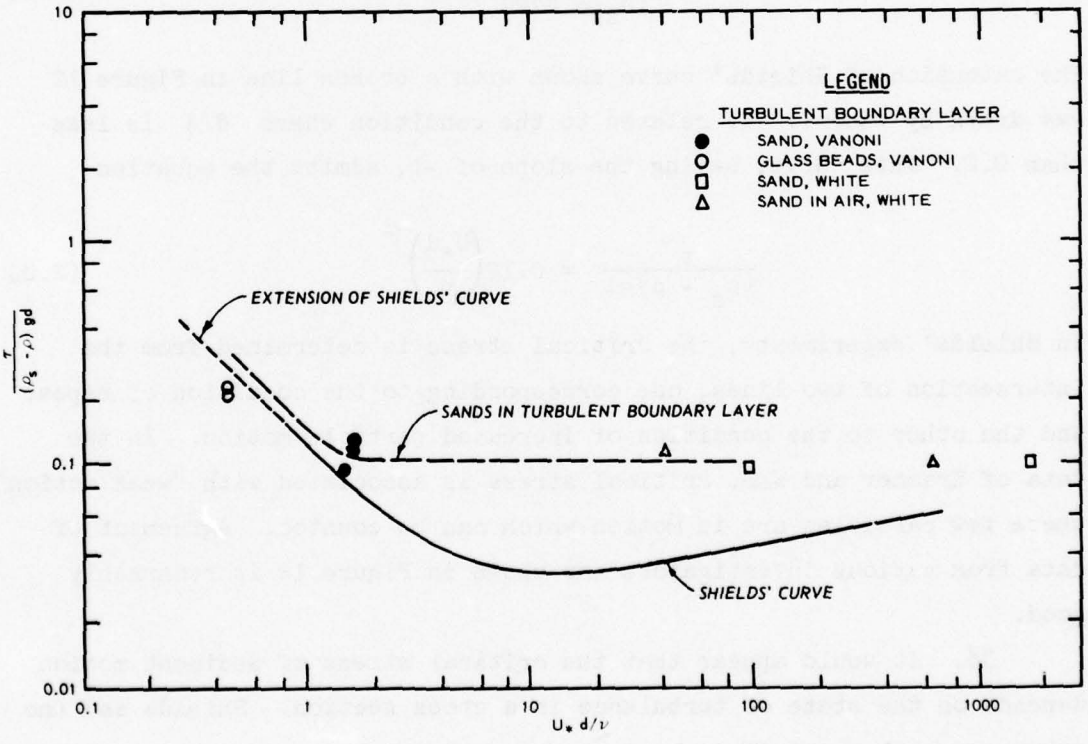

Figure 12. Criteria of sand entrainment in terms of shear stress

and covers the range of U_*d/ν from 2 to 500. Since the boundary layer thickness δ can be expressed by

$$\frac{U_*\delta}{\nu} = 11.6 \tag{2.5}$$

then the range of d/δ covered by the curve is from 0.2 to 50. The minimum value of Shields' stress parameter is

$$\frac{\tau}{(\rho_s - \rho)gd} = 0.035 \tag{2.6}$$

and this at a point $U_*d/\nu = 10$ and where the sand diameter equals the laminar boundary layer thickness. For grains increasing in diameter, the parameter approaches asymtotically to the maximum value

$$\frac{\tau}{(\rho_s - \rho)gd} = 0.06 \tag{2.7}$$

The extension of Shields' curve shown with a broken line in Figure 12 was drawn by Vanoni. It relates to the condition where d/δ is less than 0.2. This curve, having the slope of -1, admits the equation

$$\frac{\tau}{(\rho_s - \rho)gd} = 0.12\left(\frac{U_*d}{\nu}\right)^{-1} \tag{2.8}$$

In Shields' experiments, the critical stress is determined from the intersection of two lines, one corresponding to the condition of repose and the other to the condition of increased particle motion. In the data of Krammer and WES, critical stress is associated with "weak motion" where few particles are in motion which can be counted. Agreement of data from various investigators not shown in Figure 12 is remarkably good.

38. It would appear that the critical stress of sediment motion depends on the state of turbulence in a cross section. Shields and the other researchers studied channels where the turbulence of the cross section is fully developed. In contrast with this, White[15] examined the critical stresses for several sediments in the laminar and

turbulent boundary layers associated with the flow created in a nozzle. Contrary to Shields' results, the critical stress parameter for the turbulent boundary layer was independent of U_*d/ν and had the uniform value of about 0.10. This is twice as large as that read from Shields' curve, and the enlarged value is attributed to the turbulent velocity fluctuations which at the bed may amount to as much as half the value of the local mean velocity. The stress parameter for the laminar boundary layer, U_*d/ν less than 3.5, was also uniform having the value of 0.18. This matter was reexamined by Vanoni[13] also in a channel of developing boundary layer, using fine sediments, sand, and glass beads. The results for the turbulent boundary layer are shown in Figure 12. Vanoni data are in good agreement with the extrapolated Shields' curve. This may mean that for U_*d/ν less than 2, results regarding the critical stress are independent of flow conditions. Further researches concerning the point are necessary.

39. For some problems such as the stability of rocks of river embankments, it would be most helpful to turn to the relation, Equation 2.3, with the function f determined as a function of U_rd/ν. This becomes necessary in those conditions where in principle U_r cannot be inferred either from the mean channel current velocity $\overline{U}$ or from the stress τ on the rigid boundaries. In the presence of eddies, for example, U_r takes on new values and one must now account for the increases realized.

Valembois grain parameter

40. Valembois introduces the dimensonless number G which is the ratio of $(U_*d/\nu)^2$ and $\tau_c/(\rho_s - \rho)gd$

$$G = \frac{(\rho_s - \rho)gd^3}{\rho\nu^2}$$

This is termed the grain parameter, which has a special significance for the transport of sediments.[16] The Shields' relation, putting

$$\frac{U_*d}{\nu} = R_*$$

now may be written as

$$G = \phi_1(R_*)R_*^2$$

or simply

$$G = \phi_2(R_*)$$

However, as suggested by Bonnefille,[17] it would be more appropriate to represent the grain parameter by a new symbol d_*

$$d_* = G^{1/3} = \left[\frac{(\rho_s - \rho)g}{\rho\nu^2}\right]^{1/3} d \qquad (2.9)$$

where d now enters as a first power. Hence the condition for entrainment could be expressed by the relation

$$d_* = \phi_3(R_*) \qquad (2.10)$$

Bonnefille noted that different formulae proposed by various investigators could be reduced into the above form. Plotting results from various authors, this yields a well-defined curve (Figure 13) with a discontinuity of slope at $R_* = 12$. At this value, the thickness of the boundary layer and the diameter of grains are of equal value and there is a separation between two different hydraulic regimes. For $R_* < 12$

$$d_* = 2.5R_*^{4/5} \qquad (2.11)$$

For $R_* > 12$, the experimental points align themselves about a curve with the equation

$$d_* = 3.8R_*^{5/8} \qquad (2.12)$$

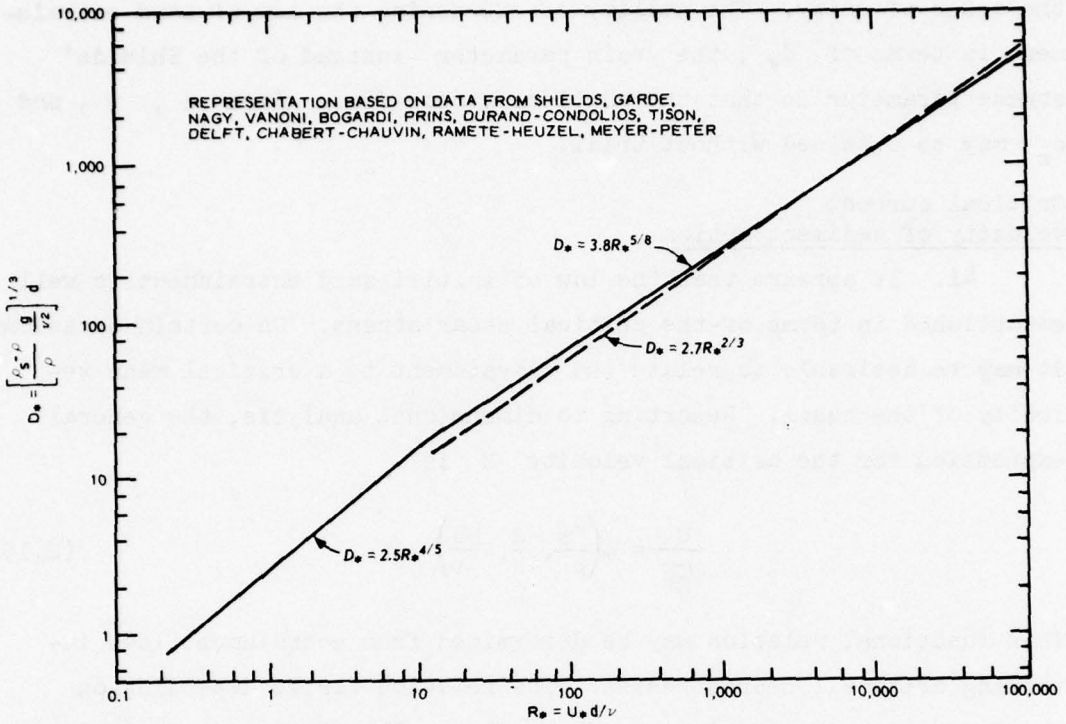

Figure 13. Criteria of sand entrainment in terms of sand parameter

but it may be said that the law

$$d_* = 2.7R_*^{2/3} \tag{2.13}$$

represents the phenomena also equally well. These expressions cover a range of R_* equal to 0.2 up to 10,000, and of d_* from 0.8 up to 6,000, involving grain sizes from 0.04 mm to 7.5 cm. From Equation 2.3, introducing R_* and d_*, we obtain

$$d_* = 2.56R_*^{2/3}$$

which is in agreement with Equation 2.11, and from Equation 2.8,

$$d_* = 2.08R_* \tag{2.14}$$

which does not vary appreciably from Equation 2.13, the law for R_* of the order of unity. The utility of expressing the law of sand entrainment in terms of d_*, the grain parameter, instead of the Shields' stress parameter is that the critical stress for a given d, ν, and ρ_s may be obtained without trial.

Critical current
velocity of sediment motion

41. It appears that the law of initial sand entrainment is well established in terms of the critical shear stress. On certain occasions it may be desirable to relate the entrainment to a critical mean velocity of the canal. Resorting to dimensional analysis, the general expression for the critical velocity U is

$$\frac{U}{\sqrt{gH}} = \phi\left(\frac{\rho_s}{\rho}, \frac{d}{H}, \frac{Ud}{\nu}\right) \tag{2.15}$$

This functional relation may be determined from entrainment laws involving critical shear stresses. The relation varies depending on the hydraulic characteristics of the flow. The flow may be hydrodynamically smooth at the transition stage, or turbulent at the initiation of sand movement. It must be assumed that the Karman constant k equals 0.4 at the start of motion. When the grain diameter is much smaller than the viscous sublayer thickness, $U_*d/\nu < 3.3$

$$U_* = 0.193\left(\frac{UH}{\nu}\right)^{-1.7} U \tag{1.41 bis}$$

Equation 2.8 may be written as

$$U_*^3 = 0.12\nu\left(\frac{\rho_s}{\rho} - 1\right)g$$

Eliminating the shear velocity U_* between these latter two equations, one has

$$\frac{U}{\sqrt{gH}} = 3.00\left(\frac{\rho_s}{\rho} - 1\right)^{7/18}\left(\frac{\nu}{g^{1/2}H^{3/2}}\right)^{4/18} \tag{2.16}$$

which is the critical velocity for the initial motion of granular material with diameters smaller than the sublayer thickness. Note that the criterion is independent of the size of the sediment particles when the grain size is small in comparison with the viscous sublayer thickness. Referring once more to Shields' curve in Figure 12, it is seen that the stress parameter is minimum around $R_* = 10$. At such regimes the sediments project from the laminar sublayer and the shear velocity may be approximated by

$$U_* = 0.123 \left(\frac{H}{d}\right)^{-1/6} U$$

This is really more valid for flow regime with $R_* = 60$, and the coefficient of the formula needs to be modified slightly in order that the formula apply to the transition from smoothness to complete roughness. At the moment we shall ignore the necessary corrections. For the region in the neighborhood of $R_* = 10$, Shields' curve gives

$$U_*^2 = 0.030\left(\frac{\rho_s}{\rho} - 1\right) gd \tag{2.17}$$

Eliminating U_* between these last two equations, one has

$$\frac{U}{\sqrt{gH}} = 1.41\sqrt{\frac{\rho_s}{\rho} - 1}\left(\frac{H}{d}\right)^{-1/3}$$

For ordinary sand $\rho_s = 2.65$ and the relation becomes

$$\frac{U}{\sqrt{gH}} = 1.81\left(\frac{d}{H}\right)^{1/3} \tag{2.18}$$

Had we used Equation 2.7 applicable for gravels one would have obtained

$$\frac{U}{\sqrt{gH}} = 1.98\left(\frac{\rho_s}{\rho} - 1\right)^{1/2}\left(\frac{H}{d}\right)^{-1/3} \tag{2.19}$$

For ordinary gravels $\rho_s = 2.65$ and this relation becomes

$$\frac{U}{\sqrt{gH}} = 2.54\left(\frac{d}{H}\right)^{1/3} \tag{2.20}$$

The Fort Collins data on the initial motions of the sands[18] are shown in Table 11. The same table shows the values of the parameters in Equation 2.18. The ratios of these parameters are plotted against U_*d/ν in Figure 14 and indicate that the value of the ratio of the Froude number to $(d/h)^{1/3}$ tends to 1.75 in agreement with Equation 2.18 where the ratio in question has the value 1.81. This agreement, if not fortuitous, is rather surprising. Equation 2.18 relates to uniform sand, whereas the Collins data are for graded sand with σ practically close to 1.75.

Table 11

Fort Collins Data of Initial Motion of Sediments

No.	d_{50} ft	σ	H ft	U_* ft/sec	ν ft^2/sec	F	U ft/sec	$\frac{F}{(\frac{d}{H})^{1/3}}$	$\frac{U_*d}{\nu}$
1	0.628×10^{-3}	1.80	0.44	0.045	1.15×10^{-5}	0.22	0.83	1.75	2.46
2	0.886	1.71	0.96	0.047	1.25	0.14	0.79	1.45	3.61
3	0.920	1.58	1.01	0.058	1.30	0.15	0.90	1.55	4.10
4	1.48	2.70	0.48	0.050	1.42	0.18	0.72	1.33	5.12
5	1.54	1.85	0.78	0.109	1.31	0.23	1.13	1.85	12.8
6	3.05	1.40	1.02	0.092	1.09	0.24	1.41	1.67	26.1
7	1.76	1.34	0.60	0.061	1.16	0.22	0.96	1.53	14.2
8	1.08	1.60	0.50	0.063	1.08	0.28	1.14	2.16	6.42
9	1.08	1.90	0.50	0.066	1.13	0.27	1.28	2.09	6.38
10	1.04	1.60	0.51	0.048	1.41	0.22	0.90	1.74	4.44
								Mean = 1.71	

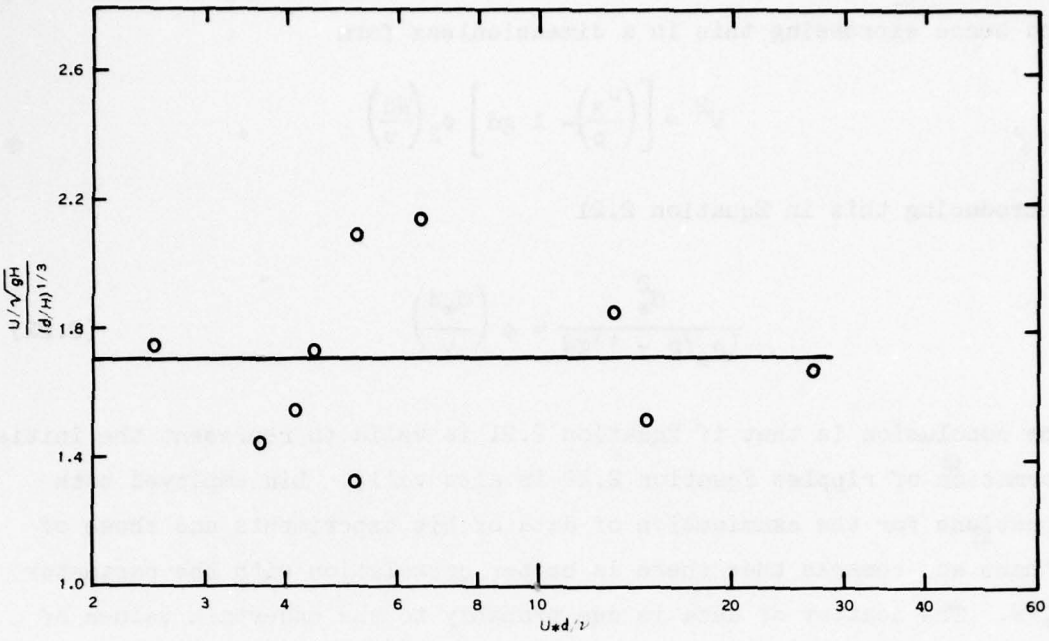

Figure 14. Fort Collins data on critical velocity for sand entrainment

Criterion of Formation of Bed Features

42. Since various bed features affect the flow resistance in an alluvial channel in a decisive manner, it is important that a criterion for their formation be derived. The problem was approached first by Liu.[19] Noting that at the instant of ripple formation, the water surface in the channel is smooth and without waves, an instability of flow near the bottom was considered to be the cause of the ripples. The analysis proceeds analogously as with the instability of an interface between two liquids of different density. The conclusion is that

$$\frac{U_*}{W} = \phi_0\left(\frac{U_* d}{\nu}\right) \tag{2.21}$$

where W is the fall velocity. Now, obviously,

$$W = \phi_1(\rho_s - \rho,\ g,\ d,\ \nu)$$

and hence expressing this in a dimensionless form

$$W^2 = \left[\left(\frac{\rho_s}{\rho}\right) - 1\ gd\right] \phi_2\left(\frac{Wd}{\nu}\right)$$

Introducing this in Equation 2.21

$$\frac{U_*^2}{(\rho_s/\rho - 1)gd} = \phi\left(\frac{U_* d}{\nu}\right) \qquad (2.22)$$

The conclusion is that if Equation 2.21 is valid to represent the initial formation of ripples Equation 2.22 is also valid. Liu employed both equations for the examination of data of his experiments and those of others and remarks that there is better correlation with the parameter U_*/W. The scatter of data is due probably to the uncertain values of U_*, which would be twice as large in Equation 2.22. We shall pursue our examination of the criterion of formation of bed features, applying Equation 2.22 to the Fort Collins data.[18]

43. The method followed to determine the shear velocities U_* associated with the initiation of the various bed feature formations is as follows. For a specified sand, the shear velocities U_* and the corresponding sediment transport quantity q_t are read from the data tables given in Reference 18 and are plotted one against the other on semilogarithmic coordinate paper, as shown in Figure 15. The points belonging to different bed features are differently indicated. Fortunately, the laws giving the dependence of q_t on U_* are different for the different bed features, and this allows us to single out the start of the various bed features. The open squares show the values of U_* corresponding to the initial motion of sediments. The intersection of the straight line passing through the solid squares, the marks for ripples, with the $q_t = 1 \times 10^{-5}$ axis is taken at the start of ripples. Thus, for sand $d_{50} = 1.47 \times 10^{-3}$ ft and for viscosity $\nu = 1.25 \times 10^{-5}$ ft^2/sec, $U_* = 0.075$ ft/sec is the shear velocity at the start of ripple formation, $U_* = 0.112$ ft/sec at the start of dune formation, and $U_* = 0.22$ ft/sec for transition. This and the corresponding data for the remaining

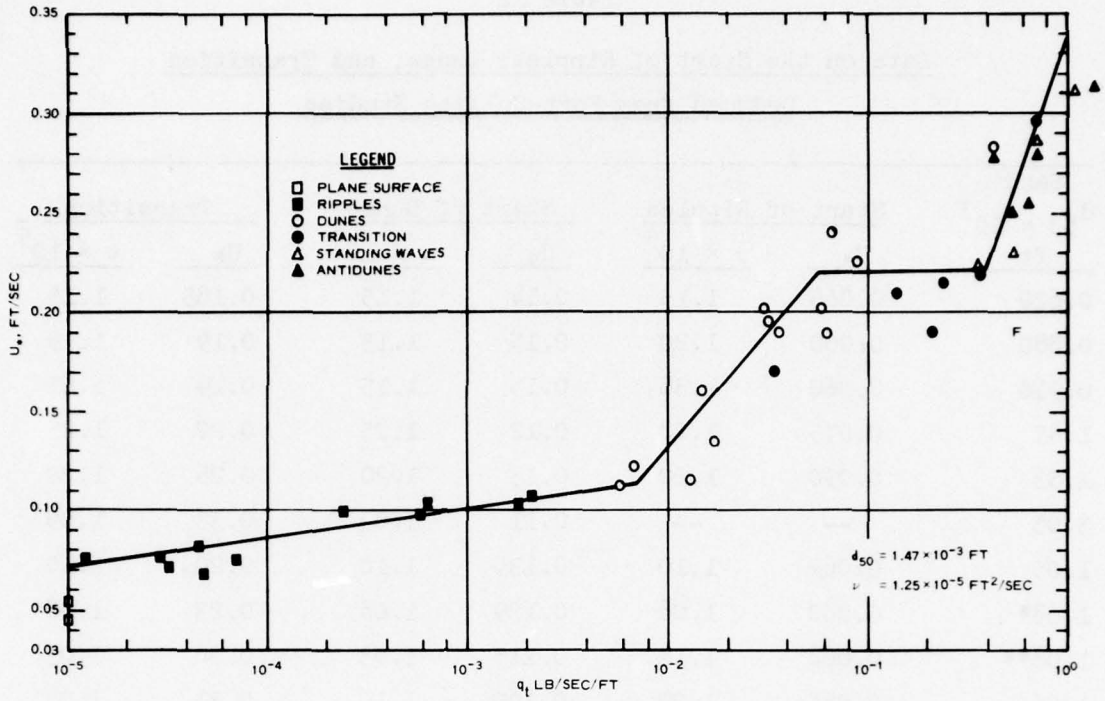

Figure 15. Shear velocity versus sand transport in Fort Collins 8-ft flume

sands are given in Table 12. In the Fort Collins tests, the shear stress is determined as $\tau = \rho gHS$. This means that sidewall frictions are neglected and corrections are needed to obtain the stress of the bottom.

Sidewall corrections

44. The Fort Collins tests were carried out in two different flumes. In one, with the channel width of 8 ft, the maximum value of the ratio of water depth to channel width was about 0.25. The corrections in the determination of the channel bottom shear stresses would be small. In the other, with the channel width of 2 ft, the maximum value of the ratio of water depth to channel width was about 0.50. For the latter, sidewall corrections could be considerable. Ordinarily, two methods are used to correct for wall friction: one is the Johnson method, and the derivations are based on the assumption of a logarithmic velocity distribution of smooth walls; the other is the Einstein method

Table 12

Data on the Start of Ripples, Dunes, and Transition
Deduced from Fort Collins Studies

Sand $d_{50} \times 10^3$ ft	Start of Ripples		Start of Dunes		Transition	
	U_*	$\nu \times 10^5$	U_*	$\nu \times 10^5$	U_*	$\nu \times 10^5$
0.622	0.065	1.15	0.14	1.15	0.185	1.15
0.880	0.060	1.20	0.15	1.13	0.19	1.15
0.910	0.060	1.38	0.15	1.15	0.19	1.21
1.47	0.075	1.28	0.12	1.25	0.22	1.25
1.53	0.090	1.20	0.13	1.20	0.26	1.20
3.05	--	--	0.11	1.09	0.33	1.09
1.05	0.062	1.10	0.135	1.10	0.20	1.10
1.08*	0.080	1.08	0.129	1.08	0.23	1.08
1.08**	0.068	1.12	0.115	1.03	0.20	1.03
1.76	0.065	1.20	0.100	1.10	0.31	1.08

$$U_* = \sqrt{gHS}$$

* Uniform.
** Graded.

and assumes a Manning's form of velocity distribution. Here the method of Einstein will be used, but first it is desirable to establish the desired formula using the Johnson approach. The channel cross section A_o may be divided into two parts, A_w and A_b : the first is the domain of influence of the frictional action of the two walls and the second, the domain of influence of the frictional action of the bottom. Assume that at the points of the lines separating the two areas the stresses vanish. This assumption is correct as an approximation. To be absolutely valid, the velocity rates normal to the lines of separation should vanish, which is not always the case. The second approximation is that the average values of the velocities in the two regions A_w and A_b are equal to each other. This is also only approximately correct, as the mean velocity in A_w is smaller than that in A_b . Subject to this

assumption, resolution of forces in a channel section gives the relations

$$A_o \rho g S = \tau_o p$$

$$A_b \rho g S = \tau_b p_b$$

$$A_w \rho g S = \tau_w p_w$$

where

S = slope of energy gradient

ρ = density of water

τ_o = average shear stress of all the rigid boundaries

τ_b = average shear stress of the bottom

τ_w = average shear stress of the two walls

The channel wetted perimeter is p_o ; p_b and p_w are the wetted lines of the sides and of the bottom, respectively. Let B be the channel width and H the depth; thus

$$p_o = B + 2H, \; p_b = B, \; p_w = 2H$$

As

$$A_o = A_b + A_w$$

then

$$\tau_o p_o \approx \tau_w p_w + \tau_b p_b$$

or

$$\frac{\tau_b}{\tau_o} \approx \frac{p_o}{p_b} - \frac{\tau_w}{\tau_o} \frac{p_w}{p_b} \tag{2.23}$$

Introducing the definitions of the coefficient of resistance λ

$$\tau_o = \lambda_o \frac{\rho}{2} U^2$$

$$\tau_b = \lambda_b \frac{\rho}{2} U^2$$

$$\tau_w = \lambda_w \frac{\rho}{2} U^2$$

where U is the mean velocity of the overall cross section A_o, or the subsections A_b and A_w, Equation 2.23 becomes

$$\frac{\tau_b}{\tau_o} = \frac{p_o}{p_b} - \frac{\lambda_w}{\lambda_o} \frac{p_w}{p_b} \tag{2.24}$$

or

$$\frac{\tau_b}{\tau_o} = 1 + \frac{2H}{B} - \frac{2H}{B} \frac{\lambda_w}{\lambda_o}$$

Thus, the ratio of the effective shear stress on the bottom to the stress of the entire channel may be obtained if the ratio λ_o/λ_w is known. The shear stresses in terms of the hydraulic radii are

$$\tau_o = \rho R_o g S$$

$$\tau_b = \rho R_b g S$$

$$\tau_w = \rho R_w g S$$

Comparing these with the expressions of the stresses in terms of the current, given above, we have

$$\frac{R_w}{R_o} = \frac{\lambda_w}{\lambda_o} \quad \text{and} \quad \frac{R_b}{R_o} = \frac{\lambda_b}{\lambda_o} \tag{2.25}$$

The coefficient of resistance λ in terms of Manning's n is

$$\lambda = \frac{2n^2 g}{2.208 R^{1/3}}$$

where R is measured in feet and g is 32.2 feet per second per second. Hence

$$\lambda = 29.1 n^2 R^{-1/3}$$

specializing

$$\lambda_w = 29.1 n_w^2 R_w^{-1/3}$$

Substituting from Equation 2.25 for R_w and solving for λ_w

$$\lambda_w = 12.5 n_w^{3/2} \left(\frac{\lambda_o}{R_o}\right)^{1/4}$$

and then

$$\frac{\lambda_w}{\lambda_o} = 12.5 n_w^{3/2} \lambda_o^{-3/4} R_o^{-1/4} \tag{2.26}$$

In channels where the sidewalls are constructed from glass or aluminum an appropriate value n_w is 0.01. For such channels, using Equation 2.26 in connection with Equation 2.24

$$\frac{\tau_b}{\tau_o} = 1 + \frac{2H}{B} - \left(0.0125 \lambda_o^{-3/4} R_o^{-1/4}\right) \frac{2H}{B} \tag{2.27}$$

Introducing the Darcy-Weisbach coefficient f_o, $f_o = 4\lambda_o$

$$\frac{\tau_b}{\tau_o} = 1 + \frac{2H}{B} - \left(0.0353 f_o^{-3/4} R_o^{-1/4}\right) \frac{2H}{B} \tag{2.28}$$

In the data of the Fort Collins tests[18] the stresses τ and ρ are computed as

$$\tau = \rho g H S \quad \text{and} \quad f = \frac{8gHS}{U^2}$$

However, in terms of τ and f, since $R_o = \left(1 + \frac{2H}{B}\right)^{-1} H$

$$\tau_o = \left(1 + \frac{2H}{B}\right)^{-1} \tau \quad \text{and} \quad f_o = \left(1 + \frac{2H}{B}\right)^{-1} f$$

Introducing these in Equation 2.28

$$\tau_b = \left(1 - 0.0353 f^{-3/4} H^{-1/4} \frac{2H}{B}\right) \tau \qquad (2.29)$$

The values of H, B, f, and τ are read from the data tables of the Fort Collins tests.[18] More generally it may be desirable to resort to Manning's n_o of the composite channel, n_w of the walls, and n_b of the bottom. From the analysis and omitting the details of the derivations

$$\frac{R_w}{R_o} = \left(\frac{n_w}{n_o}\right)^{3/2} , \quad \frac{R_b}{R_o} = \left(\frac{n_b}{n_o}\right)^{3/2}$$

$$\frac{\tau_b}{\tau_o} = \left(\frac{R_b}{R_o}\right) = 1 + \frac{2H}{B} - \frac{2H}{B}\left(\frac{n_w}{n_o}\right)^{3/2} \qquad (2.24 \text{ bis})$$

Usually it is the custom when analyzing the characteristics of bed features observed in the laboratory composite channel, to replace the channel with an infinitely wide channel of energy gradient S_o, current velocity U, and depth R_b. It is equally serviceable to choose the wide channel with the energy gradient $S_b (= S_o R_o / R_b)$, current velocity U, and the depth H. In the studies of the bed features subsequently adopted the latter selection will be followed.

First appearances of ripples and dunes according to the Fort Collins data

45. The formula of correction Equation 2.29 was applied to the data shown in Table 12. In general, during the regimes of ripples or dunes, according to these computations bottom shear stress τ_b is smaller than τ, the channel shear stress evaluated by neglecting the resistance of walls by 7 percent in the 8-ft-wide channel. The corresponding reduction in the 2-ft-wide channel is about 25 percent. Data of Table 13 incorporate these corrections and then represent the shear velocity proper of the channel bed; the plotting in Figure 16 is

Table 13

Criteria of Appearance of Ripples, Dunes, and Transition with Sidewall Corrections

$F_*^2 = U_*^2/(\rho_s/\rho - 1)gd$ $\qquad$ $R_* = U_*d/\nu$

Sand	Start of Ripples		Start of Dunes		Transition	
$d_{50} \times 10^3$	F_*^2	R_*	F_*^2	R_*	F_*^2	R_*
0.62	0.120	3.4	0.552	5.9	0.842	9.63
0.88	0.073	4.2	0.460	11.3	0.705	14.0
0.91	0.070	4.4	0.435	11.5	0.670	13.8
1.47	0.067	8.6	0.173	13.5	0.566	25.0
1.53	0.093	11.0	0.192	16.0	0.760	32.2
3.05	--	--	0.065	29.8	0.612	89.0
1.05	0.059	5.4	0.268	11.4	0.590	17.4
1.08*	0.096	7.4	0.234	11.5	0.782	21.6
1.08**	0.051	6.0	0.186	10.7	0.590	18.8
1.76	0.038	8.9	0.097	10.6	0.880	46.9

* Uniform.
** Graded.

from this table. Despite the scatter of the plotted points, straight lines should suffice to represent them as a first approximation. The line for the ripple formation cuts the Shields' curve at a point

$$\frac{U_*^2}{(s - 1)gd} = 0.032, \quad \frac{U_*d}{\nu} = 12.0$$

and accordingly

$$\frac{(\rho_s/\rho - 1)gd^3}{\nu^2} = \frac{(12.0)^2}{0.032} = 4500$$

or

$$d_* = \left[\frac{(\rho_s/\rho - 1)g}{\nu^2}\right]^{1/3} d = 16.5 \qquad (2.30)$$

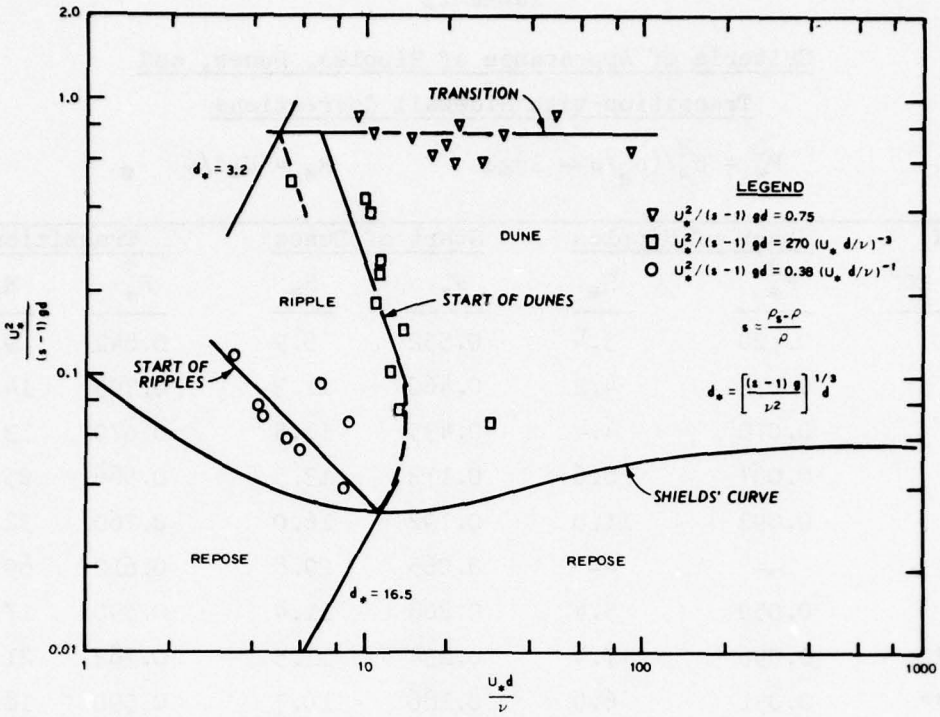

Figure 16. Domains of the bed features in the Fort Collins tests

which is the criterion of the limiting grain size for the ripple formation. For quartz sand, this limiting value is 0.65 mm on the basis that the viscosity of water is $\nu = 1.0 \times 10^{-5}$ ft^2/sec. With the sands having grain sizes larger than this, no ripple would be formed. For coal particles, $\rho_s/\rho = 1.30$, the corresponding limiting value is 1.14 mm. Reductions shown in Figure 16 are mostly from Fort Collins data for sands with sizes smaller than 0.64 mm, excepting one $d_{50} = 0.93$ mm. In the tests with this latter sand no ripples were formed; the surfaces remained smooth with sand transportation present. Thus information regarding the formation of bed features that might be abstracted from Figure 16 need be confined to sands with grain sizes smaller than the criterion $d_* < 16.5$. The straight line drawn through the points that mark the beginning of ripples has the slope of -1. Accordingly, the channel bottom shear velocity at the start of the ripple formation is expressed by equation of the line of the start of ripples

$$U_* = 0.72[(s - 1)g\nu]^{1/3} \tag{2.31}$$

The slope of the straight line drawn through the points that mark the beginning of the formation of dunes is equal to -3. Therefore, channel bottom shear velocity at the start of the dunes is

$$U_* = 3.06\left[(s - 1)gd\right]^{1/5}\left(\frac{\nu}{d}\right)^{3/5} \tag{2.32}$$

The expression of the criteria for the start of the ripple formation is independent of the size of the grains. In contrast with this, the criteria for the start of the dune formation does depend on the size of grains. Because of the scatter of points, the true form of the criteria by the present method cannot be obtained. The transition from dunes to flat bed occurs at the shear velocity.

$$U_* = 0.86\sqrt{(s - 1)gd} \tag{2.33}$$

Note that the shear stress is independent of viscosity. The intersection of the curves marking the start of the formation of dunes and transition yields the critical of value of d_* for the condition that ripples are followed by transitions. To obtain the intersection, we consider the short dashed line passing through the point corresponding to $d_m = 0.19$ mm. This line has the same slope as the full line giving the start of the dune formation for most of the observed data. The intersection yields

$$\frac{U_*^2}{(s - 1)gd} = 0.75; \quad \frac{U_* d}{\nu} = 4.9$$

$$\frac{(s - 1)gd^3}{\nu^2} = \frac{24.5}{0.75} = 32.8 \tag{2.34}$$

or

$$d_* = 3.2$$

This is the critical value for the condition that ripple is followed by transition without the intermediate dune formation.

46. The field of validity of the above relations is the region between the lines $d_* = 3.2$ and $d_* = 16.5$ in Figure 16 and this is the field proper for sand of size less than the critical, with its dimensionless value as $d_* = 16.5$. The line $d_* = 5.0$ goes with the sand of $d_{50} = 0.19$ mm of the Fort Collins studies, the smallest sand used in these studies. The marked data deviations noted are not entirely due to observational errors but are brought about by the granulometric dissimilar size distribution. For example, the sand in the series referred to as of median size of 47 mm was produced from 45-mm sand. Coarser sand was retained and the fines were washed away in overflow. Although as a result the change in gradation was small, from $\sigma = 1.60$ to $\sigma = 0.54$, with the fines removed the starting of the ripples was markedly delayed. Precise determination of the criteria of the appearances of bed features cannot be made, apparently, if the effects of gradation are ignored.

The Chatou studies on the
appearance of bed features

47. In the above, the question of the appearance of bed features for sands with sizes smaller than the critical, $d_* < 16.5$, was considered. Projection from this to the cases where the sand grain size is greater than the critical is not allowed. Fortunately, for the desired information one may now turn to the Chatou studies carried out by Chabert and Chauvin.[20] The experiments were made in an inclined flume with glass walls 21 m long, 80 cm wide, and 70 cm deep with a movable bed of 15-cm thickness. Eleven different materials were considered with densities ranging from 1.075 to 2.62 and with particles with sizes ranging from 0.17 mm to 3.0 mm. Seven of the materials had sizes greater than 0.55 mm and with these, ripple formation was not observed. The authors' description of the behavior of these materials under the action of increasing tractive force is paraphrased as follows. Following the initial entrainment of the sediment, material is transported without undulations. The flats are the only possible forms of

the bed. If a small swelling is artificially produced, it is soon wiped out. Very long flat plateau waves are noted which eventually evolve into dunes of large height, closely spaced, and often covered with smaller dunes. Omitting the experimental points of the observations, the appearance of bed forms is very neatly represented by the curves in Figure 17. Delineations are indicated separating the various

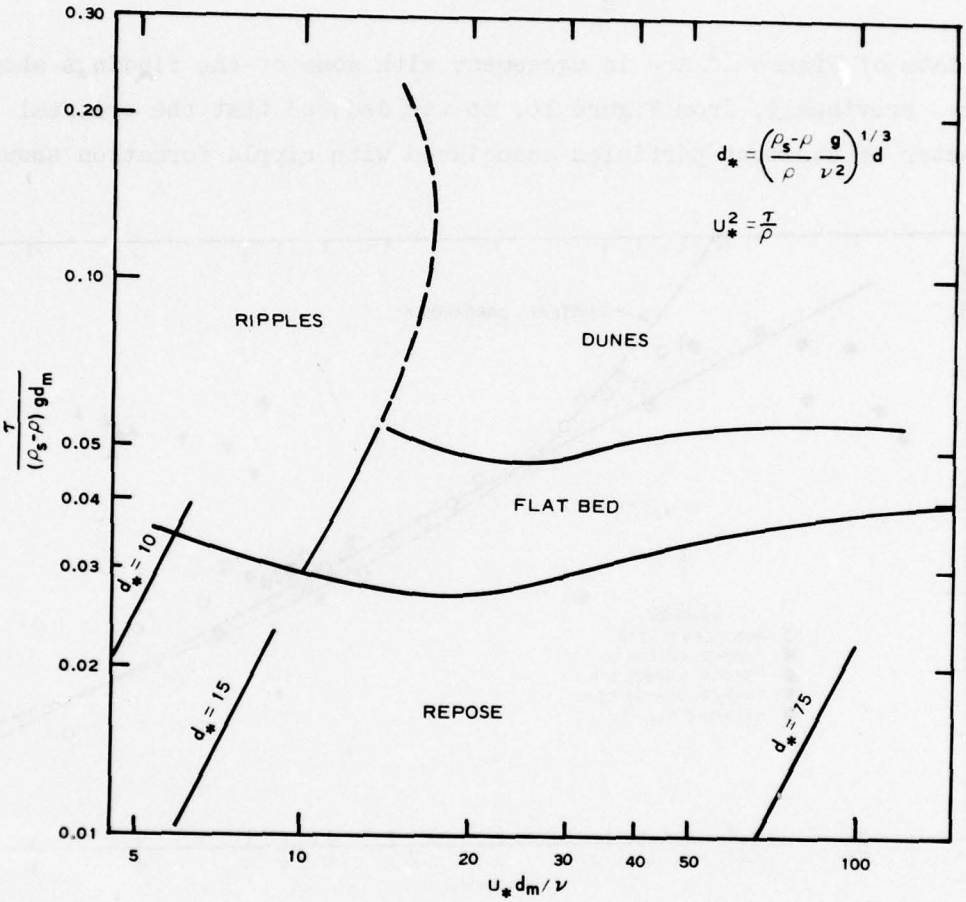

Figure 17. Domains of ripples and dunes as shown by Chabert and Chauvin

regimes from each other. The curve for the entrainment of the particles is somewhat displaced downward from the curve of Shields. The area to the left of the line $d_* = 15$ represents the domain of the ripples. According to that, the particles with the dimensionless diameter

$d_* > 15$ will not engender ripples but flats. This is shown in the figure. The curve that separates the domain of dunes from the domain of flat bottoms to the right of the line $d_* = 15$ shows that dunes will appear at the instant that the bottom shear velocity reaches the average value of:

$$\frac{U_*^2}{(\rho_s/\rho - 1)gd} = 0.055 \qquad (2.35)$$

The data of Figure 18 are in agreement with some of the findings shown here. Previously, from Figure 16, it was deduced that the critical diameter of sediment particles associated with ripple formation should

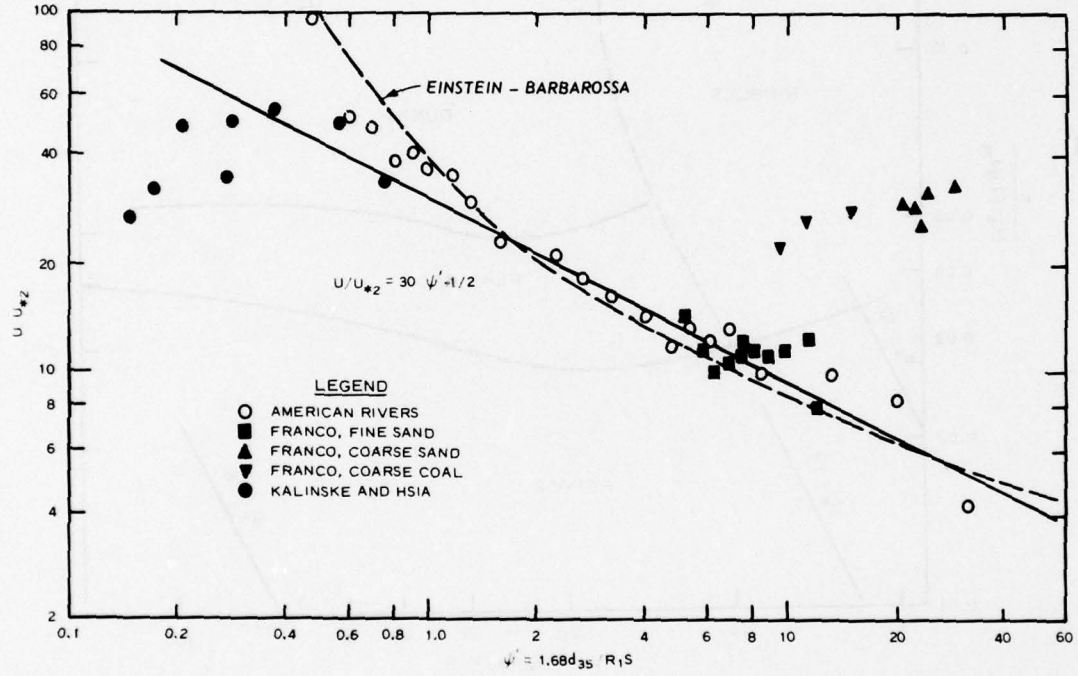

Figure 18. Friction loss due to channel bed features in alluvial streams

be $d_* = 16.5$. This compares well with the criterion $d_* = 15.2$ of figure established more definitely. In the Fort Collins study, no ripples were formed with sand of 0.93 mm and of dimensionless size $d_* = 23.2$. According to Table 13 and Figure 16, when dunes first

appeared the shear velocity for this sand was

$$\frac{U_*^2}{(\rho_s/\rho - 1)gd} = 0.065$$

a value which is in close agreement with the one shown above.

Resistance of Alluvial Channels

Einstein-Barbarossa analysis of alluvial channel resistance

48. It is postulated in this analysis that the total resistance τ of an alluvial channel may be broken into two parts τ_1 and τ_2, the first being due to friction of granular surface and the second to the form resistance of the ripples and dunes.[21] Therefore

$$\tau = \tau_1 + \tau_2 \tag{2.36}$$

Dissipation of energy associated with these two frictional stresses occurs in two areas, A_1 and A_2. These areas are not separate but are interlocked and have the same wetted perimeter p as the entire cross section A. Correspondingly, R_1 will be the hydraulic radius associated with the granular resistance and R_2 that associated with the form resistance; that is

$$R_1 = A_1/p$$

$$R_2 = A_2/p$$

Denoting the hydraulic radius of the entire channel R and as $A_1 + A_2 = A$,

$$R = R_1 + R_2 \tag{2.37}$$

The current mean velocity in relation to the granular surface resistance is

$$\frac{U}{U_{*1}} = 5.75 \log \left(12.21 \frac{R_1}{\Delta}\right) \tag{2.38}$$

$$U_{*1} = \sqrt{\tau_1/\rho} = \sqrt{gR_1S} \tag{2.39}$$

where

S = slope of the energy line

Δ = an effective roughness height related to the height of the actual asperities k

Where the bed material is not uniform k is taken to equal d_{65}, the grain size 65 percent finer by weight. Einstein's sediment transport theory assumes that only the stress action on the grains is responsible for the movement of bed material and the subsequent formation of bed features. The stress parameter pertinent in the transportation is the ratio of submerged weight of a particle to the shear stress action on it.

$$\psi' = \frac{(\rho_s - \rho)gd^3}{\rho g R_1 S d^2} = \frac{(s-1)d}{R_1 S} \tag{2.40}$$

For quartz sand s = 2.65 and if the bed material is not uniform in size, d is taken to equal d_{35}. With

$$U_{*2} = \sqrt{\tau_2/\rho} = \sqrt{gR_2S} \tag{2.41}$$

the form resistance of bed is assumed to depend on ψ' and thus

$$\frac{U}{U_{*2}} \approx \phi \left(\frac{1.68 d_{35}}{R_1 S}\right) \tag{2.42}$$

The form of the latter function was determined by Einstein and Barbarossa on the basis of observation from a few American alluvial rivers with grain sizes ranging from 0.19 mm to 4.30 mm. Average values of these determinations are shown by circles in Figure 18. The curve in dashes has been referred to as the Einstein-Barbarossa bar curve. We have drawn the straight line in full in the figure as an approximate

representation to the observed values. This has the equation

$$\frac{U}{U_{*2}} = 30\left(\frac{\rho_s - \rho}{\rho}\frac{k_s}{R_1 S}\right)^{-1/2} \qquad (2.43)$$

which will be used subsequently.

49. Expressing the quantity Δ appearing in Equation 2.38 as

$$\Delta = mk \qquad (2.44)$$

the proportionality factor will depend on the circumstances whether the channel is hydrodynamically smooth or rough in transition. When $U_{*1}k/\nu$ is less than 3.5, the channel is hydrodynamically smooth and

$$m = \frac{3.3\nu}{U_{*1}k} \quad \text{or} \quad \Delta = \frac{3.3\nu}{U_{*1}} \qquad (2.45)$$

when $U_{*1}k/\nu$ is greater than 60 or 70, the channel is rough and

$$m = 1 \quad \text{or} \quad \Delta = k \qquad (2.46)$$

$$3.5 < \frac{U_{*1}k}{\nu} < 60$$

m will be a numeric as shown in Table 14. The determination of R_1 may be carried out in the following manner. Equation 2.38 may be written as

$$\frac{U}{\sqrt{g\Delta S}} = 5.75\left(\frac{R_1}{\Delta}\right)^{1/2} \log\left(12.21\,\frac{R_1}{\Delta}\right) \qquad (2.47)$$

which determines $U/\sqrt{g\Delta S}$ as function of R_1/Δ. In Table 15 the tabular relation between these two quantities is given. The determination of R_1 when U, R, k, and S are given is made by trial. Assume a value of R_1 somewhat smaller than R. Evaluate U_{*1} using Equation 2.39. Establish n to obtain Δ. Compute $U/\sqrt{g\Delta S}$ and find the corresponding value R_1/Δ using the entries of Table 15. From this

Table 14

Correction Factor m in the Logarithmic Resistance Function

$U_{*1}k/\nu$	m	$U_{*1}k/\nu$	m
3.48	1.00	11.60	0.62
4.64	0.86	22.04	0.73
5.80	0.72	33.64	0.85
6.96	0.68	45.24	0.91
8.12	0.64	56.84	0.95
9.28	0.63	68.44	0.97
10.44	0.62	80.04	1.00

Table 15

Relation Between Current Velocity and Relative Hydraulic Radius

$U/\sqrt{gS\Delta}$	R_1/Δ	$U/\sqrt{gS\Delta}$	R_1/Δ
113.4	50	422.4	400
175.5	100	467.8	500
229.9	150	544.2	600
275.2	200	598.4	700
355.1	300	649.0	800

R_1/Δ compute R_1. If the computed R_1 is different from the initial selected value repeat the process starting with a new R_1, which is the average of R_1 initially selected and of R_1 obtained after the first trial.

Comparison with laboratory tests

50. We shall make use of bed-load movement research at WES to obtain an insight into the limitations of the Einstein-Barbarossa analysis. Some aspects of this study have been reported by Franco.[22] Working with water depths of approximately 1/2 ft or 3/4 ft and with current velocities of about 1 ft/sec, the effect of temperature on

channel roughness is investigated. The materials used were fine sand of median diameter 0.23 mm, coarse sand of median diameter 4.6 mm, and coal of median diameter 2.2 mm. The data of resistance of the tests, with sidewall effects removed, were necessitated to evaluate U/U_{*2} in the manner suggested by the Einstein-Barbarossa analysis; results are shown in Figure 18. The results from the fine sand are in good agreement with the curve for the alluvial rivers, whereas the results for the coarse sand and for the coal fall well above the curve, indicating less resistance. With the fine sand tests, ripples were present; with the tests using coarser particles, sand or coal, the channel bottom was flat. To examine if these conditions are in accordance with the criteria developed previously, the dimensionless grain sizes d_* are calculated in Table 16 for the tests with coarse sand and coal. For the coarse sand,

Table 16

Dimensionless Diameters of Franco Test Sands

$$F_*^2 = U_*^2/(s-1)gd;\ R_* = U_*d/\nu;\ d_* = \left[\frac{(s-1)g}{\nu^2}\right]^{1/3} d$$

Run	ν ft^2/sec	F_*^2	R_*	d_*	Bed Feature
	Coarse Sand: $d_{50} = 15.4 \times 10^{-3}$ ft, $s - 1 = 1.68$				
36	0.93×10^{-5}	0.0381	0.310	99.0	Flat bed
39	0.93×10^{-5}	0.0493	0.333	99.0	and
41	0.93×10^{-5}	0.0474	0.327	99.0	transport
37	1.67×10^{-5}	0.0414	0.170	88.0	of
38	1.67×10^{-5}	0.0488	0.185	88.0	sediment
42	1.67×10^{-5}	0.0474	0.202	88.0	
	Coal: $d_{50} = 7.8 \times 10^{-3}$ ft, $s - 1 = 0.30$				
23	0.93×10^{-5}	0.0600	56.3	37.6	Flat bed
25	0.93×10^{-5}	0.0751	65.0	37.6	and
27	0.93×10^{-5}	0.0393	47.4	37.6	transport
29	0.93×10^{-5}	0.0870	70.8	37.6	of
22	1.67×10^{-5}	0.0512	29.0	26.0	sediment
24	1.67×10^{-5}	0.0546	29.9	26.0	
26	1.67×10^{-5}	0.0421	26.2	26.0	
28	1.67×10^{-5}	0.0782	35.8	26.0	

the dimensionless grain sizes are 99.0 and 88.0 for two kinematic viscosities; for the coal, these sizes are 37.6 and 26.0. These values are all larger than the critical $d_* = 15.6$, and therefore ripples should never be formed. Examining the table it is seen that the maximum stress parameter for the two kinematic viscosities noted in the entries for coal is about $F_*^2 = 0.087$; that for the two kinematic viscosities for coarse sand is about $F_*^2 = 0.049$. One expects that the appearance of the dunes for these larger particles will be for a higher stress parameter than this. The Chatou data, as it will be remembered, places the criteria at $F_*^2 = 0.055$. The determination from the Fort Collins data gave $F_*^2 = 0.065$ for $d_{50} = 0.93$ mm. Tentatively, one may place the criterion for the appearance of dunes with larger particles, $d_* > 15$, as $F_*^2 = 0.69$, the average of the above three; that is 0.087, 0.055, and 0.065.

51. The comparison of laboratory data with field data in relation to ψ' and U/U_{*2} was previously made by Vanoni and Brooks[23] using their own laboratory tests and also those of Barton and Liu. In the latter case, there was good agreement with the Einstein-Barbarossa bar resistance curve. In their own tests, however, although the agreement was satisfactory for large values of ψ', considerable deviation was observed with points of small ψ', suggesting that with increasing velocity the "flume rivers" get smooth faster than natural rivers. The studies of Smith[24] reveal that relative depth R_1/Δ is another parameter to consider in the relation

$$\frac{U}{U_{*2}} = \phi\left(\psi', \frac{R_1}{\Delta}\right)$$

Although Smith's modifications produce improvements, in our subsequent application the simplicity of the Einstein-Barbarossa procedure will be preferred.

Equivalent sand
roughness in WES tests

52. As mentioned previously, in the WES tests with coarse sand and coal particles ripple formation was absent. Subsequent to entrainment, the surfaces of the beds were smooth. With coal particles, for

example, the bed was flat with waves across the width of channel 8 to 10 ft apart. Although there was movement of bed material, the resistance to flow was very small. Since there was movement of bed material, the question would arise if this fact would have an effect on the effective or equivalent sand roughness of the bed material. After a careful study Vanoni and Nomicos[25] indicate that Karman's constant would decrease if the material is suspended. As particle suspensions were avoided, in the WES tests it is assumed that for these cases the Karman constant has the usual value and the sand equivalent roughness may be computed by

$$\frac{U_1}{U_{*1}} = 5.75 \log \frac{12.8R}{k_s}$$

provided that the particle sizes are larger than the laminar boundary layer thickness. For the coarser sand, the ratio k/δ varies from 15 to 30 and with the coal particles, from 3 to 6. Computing k_s on this basis the values of k_s/k are shown in Figure 19. The size k and

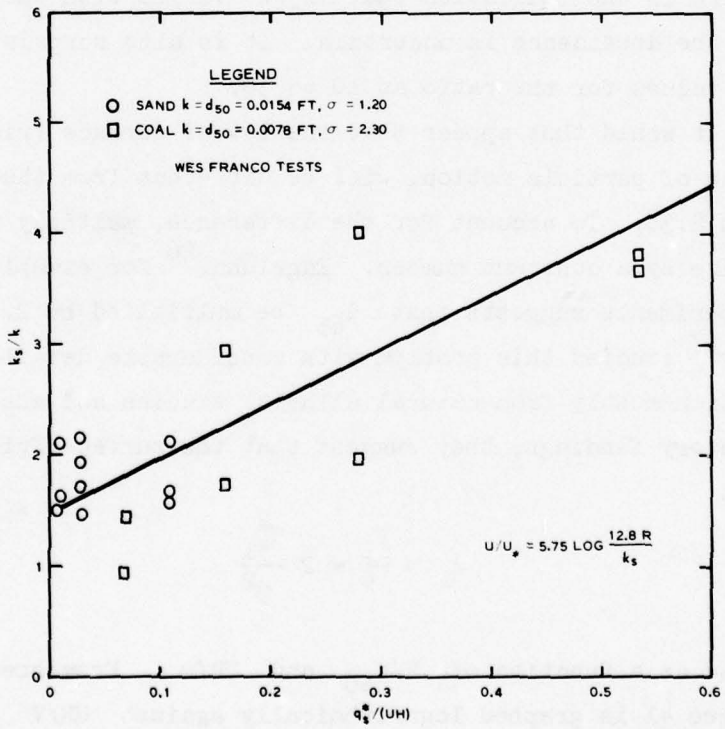

Figure 19. Dependence of effective sand roughness on sand transport rate over flats

the gradation number σ of the particles are also shown in the figure. The gradation number is computed by

$$\sigma = \frac{1}{2}\left(\frac{d_{50}}{d_{16}} + \frac{d_{84}}{d_{50}}\right)$$

The ratio k_s/k is plotted against q_s^*/UH, where q_s^* is volume rate of flow of particles expressed as cubic feet per hour per foot of channel width. Here, U is the mean current velocity in feet per second and H, depth in feet. Although there is some scatter in the points, perhaps the line as drawn is acceptable. On this basis, one may venture to state that the equivalent sand roughness of particles when in motion is increased. This matter was further examined in the corresponding data of Fort Collins studies for plane surfaces, including also the cases of initial entrainment. For these later ones, q_s^* is nil. Results of the determinations are shown in Figure 20. Although, in general there is the indication that k_s/k varies with the sediment discharge, the dependence is uncertain. It is also surprising to find such large values for the ratio as 10 to 30.

53. It would thus appear that the law of surface friction, in the presence of particle motion, will be different from the law given by Equation 2.38. To account for the difference, multiply the actual asperity size by a constant number. Engelund,[26] for example, guided by his own experiments suggests that d_{65} be multiplied by 2. Lovera and Kennedy[27] studied this problem with considerable detail. Relying on information mostly from natural alluvial studies and also partly from laboratory findings, they suggest that the surface friction coefficient

$$\lambda_1 = \frac{f_1}{4} = 2\,\frac{U_{*1}^2}{U^2} \qquad (2.48)$$

be expressed as a function of R/d_{50} and UR/ν. From one of their figures where 4λ is graphed logarithmically against UR/V for constant values of R/d_{50}, one may derive the relation

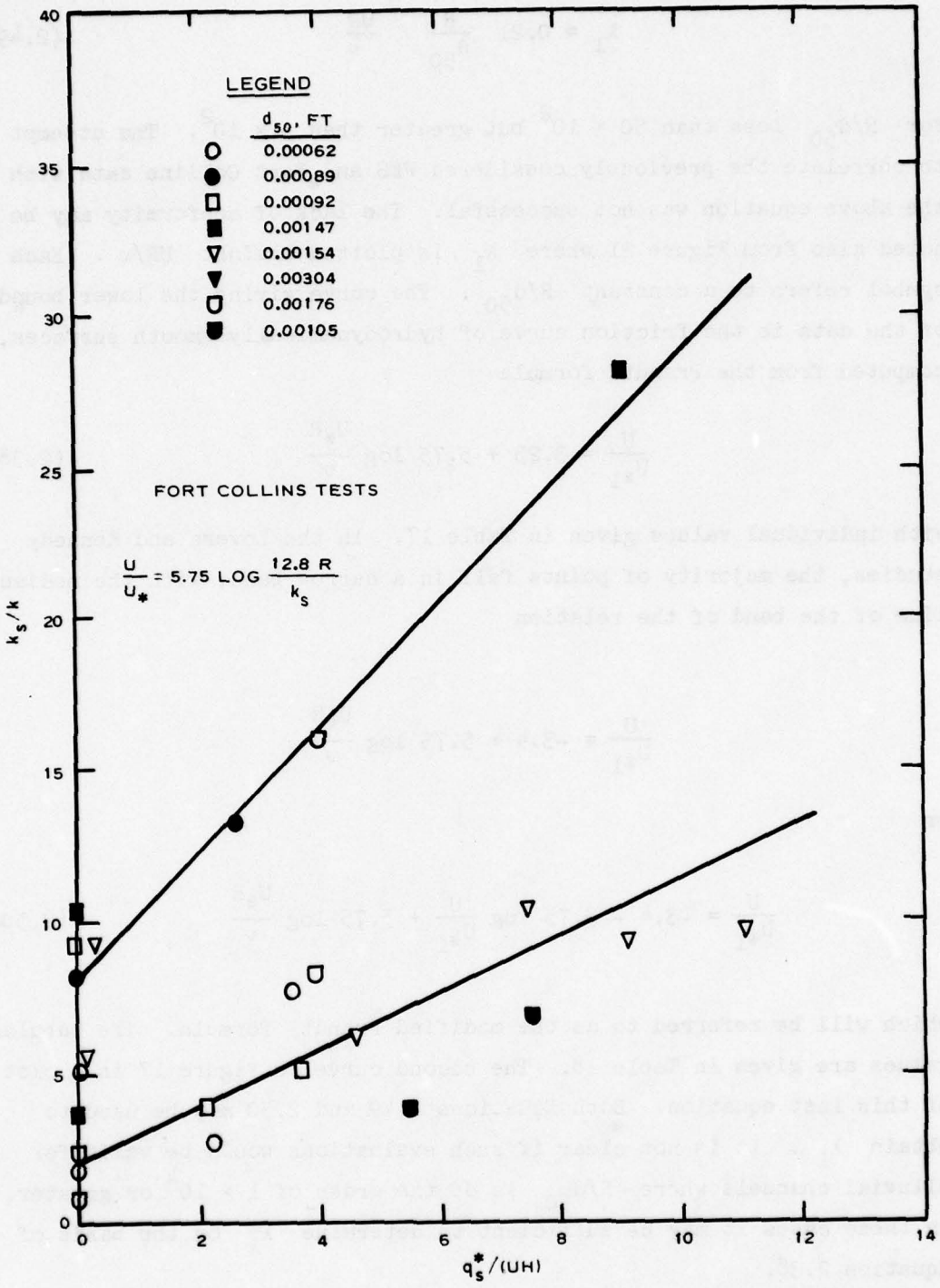

Figure 20. Dependence of effective sand roughness on sand transport rate over flats

$$\lambda_1 = 0.21 \left(\frac{R}{d_{50}}\right)^{-2} \frac{UR}{\nu} \qquad (2.49)$$

for R/d_{50} less than 50×10^2 but greater than 5×10^2. The attempt to correlate the previously considered WES and Fort Collins data with the above equation was not successful. The lack of conformity may be noted also from Figure 21 where λ_1 is plotted against UR/ν. Each symbol refers to a constant R/d_{50}. The curve giving the lower bound of the data is the friction curve of hydrodynamically smooth surfaces, computed from the Prandtl formula

$$\frac{U}{U_{*1}} = 3.25 + 5.75 \log \frac{U_* R}{\nu} \qquad (2.38)$$

with individual values given in Table 17. In the Lovera and Kennedy studies, the majority of points fall in a narrow band, with the median line of the band of the relation

$$\frac{U}{U_{*1}} = -3.4 + 5.75 \log \frac{U_* R}{\nu}$$

or

$$\frac{U}{U_{*1}} = -3.4 - 5.75 \log \frac{U}{U_{*1}} + 5.75 \log \frac{U_* R}{\nu} \qquad (2.50)$$

which will be referred to as the modified Prandtl formula. The tabular values are given in Table 18. The second curve in Figure 17 is a plot of this last equation. Both Equations 2.49 and 2.50 may be used to obtain λ_1. It is not clear if such evaluations would be valid for alluvial channels where R/d_{50} is of the order of 1×10^4 or greater. In these cases it may be sufficient to determine λ_1 on the basis of Equation 2.38.

Table 17

Coefficient of Surface Friction for Hydrodynamically Smooth Surfaces

U/U_{*1}	$\lambda_1 \times 10^3$	UR/ν	U/U_{*1}	$\lambda_1 \times 10^3$	UR/ν
14	11.2	1.05×10^3	28	2.54	5.22×10^5
16	7.78	2.40	30	2.20	1.28×10^6
18	6.16	6.57	32	1.96	3.72
20	5.00	1.63×10^4	34	1.63	7.50
22	4.14	4.00	36	1.55	1.73×10^7
24	3.46	9.77	38	1.38	4.23
26	2.94	2.30×10^5	40	1.25	9.95

Table 18

Coefficient of Surface Friction for Plane Surfaces of Alluvial Channels

U/U_{*1}	$\lambda_1 \times 10^3$	UR/ν	U/U_{*1}	$\lambda_1 \times 10^3$	UR/ν
12	13.8	5.76×10^3	20	5.00	2.40×10^5
14	10.2	1.48×10^4	21	4.52	3.63
15	8.88	2.24	22	4.12	5.63
16	7.80	3.81	24	3.46	1.41×10^6
17	6.90	5.89	26	2.90	3.39
18	6.16	9.34	28	2.54	8.13
19	5.54	1.55×10^5	30	2.20	1.82×10^7

Alam and Kennedy analysis of alluvial channel resistance

54. In this analysis[28] the surface energy gradient $S_o (=S_b)$ is divided into two parts S_1 and S_2 instead of dividing the hydraulic radius R into two parts. This is in accordance with an earlier proposal by Meyer-Peter[29] which was adopted also by Taylor and Brooks in a later investigation.[30] Here, S_1 is the slope that would be required had the bed been flat and the grain size fixed, while keeping the discharge the same; and S_2 is the additional slope as a consequence of the bed features present. Similarly

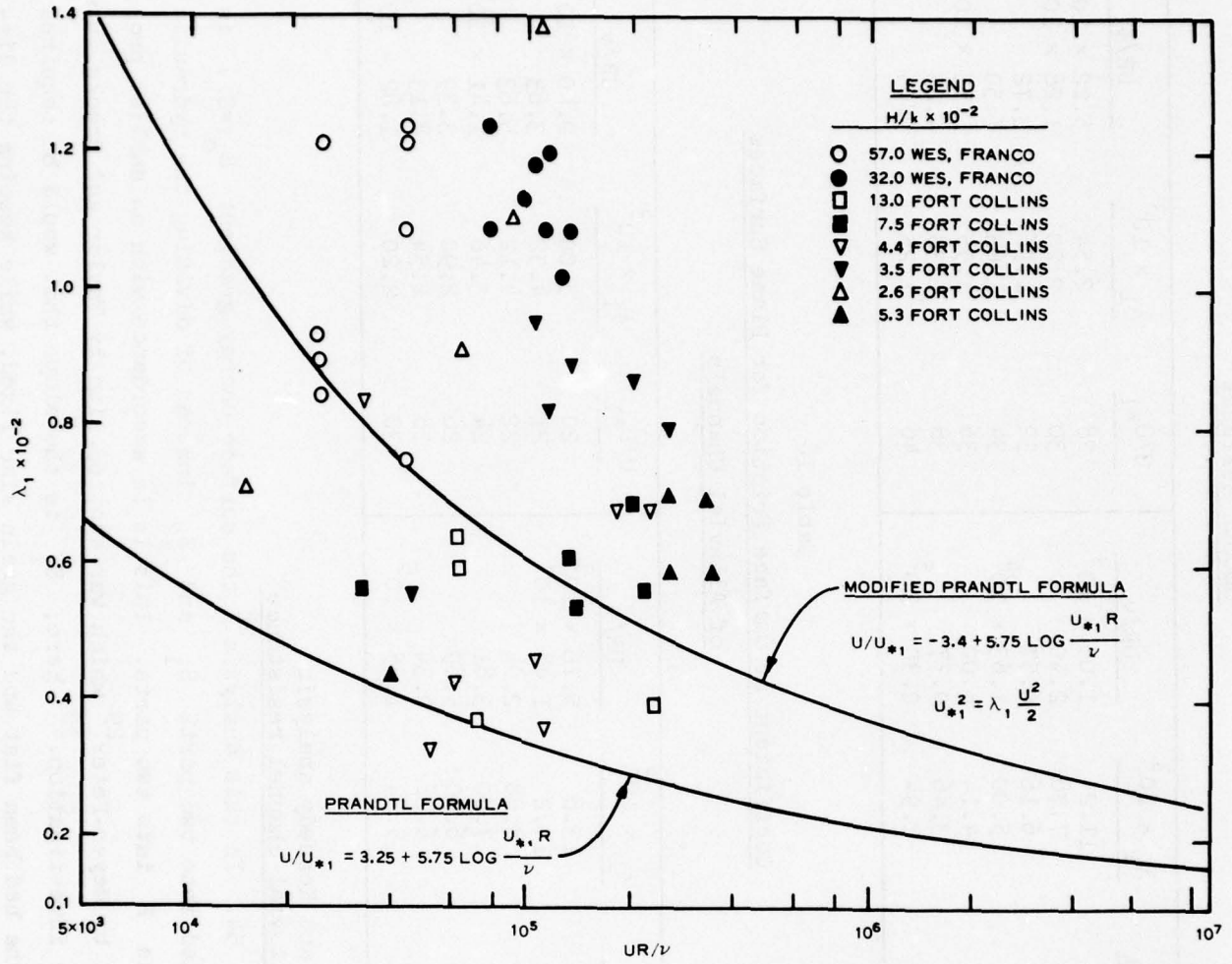

Figure 21. Coefficient of friction of plane granular surfaces in Fort Collins and WES tests

$$\tau_b = \tau_1 + \tau_2$$

and as before

$$\tau_b = \rho g R_b S_o,\ \tau_1 = \rho g R_b S_1,\ \tau_2 = \rho g R_b S_2$$

The resistance coefficients will be defined as

$$\lambda_b = \frac{2gR_bS_o}{U^2},\ \lambda_1 = \frac{2gR_bS_1}{U^2},\ \lambda_2 = \frac{2gR_bS_2}{U^2} \qquad (2.51)$$

The grain resistance coefficient λ_1 is preferably determined by the method proposed by Lovera and Kennedy.[27] With reference to λ_2, resort is made first to dimensional analysis. Following the thesis of Brooks, S_2 or its equivalent λ_2 is taken as a dependent variable

$$\lambda_2 = \lambda_2\left(\frac{U}{\sqrt{gk}},\ \frac{UR}{\nu},\ \frac{H_o}{L},\ \frac{L}{R},\ \frac{\rho_s}{\rho},\ \sigma\right) \qquad (2.52)$$

where

k = grain size d_{50}
H_o = height of dunes
L = length of dunes
ρ_s = density of sand grains
ρ = density of water
σ = geometric standard deviation of sand grains in the bed

The authors argue that the resistance of ripples and dunes is not affected by viscosity. Vanoni and Brooks have already shown that λ_2 is not affected by a change in σ. The ratio ρ_s/ρ is constant for ordinary sand, about 2.68. Thus Equation 2.52 may simplify to

$$\lambda_2 = \lambda_2\left(\frac{U}{\sqrt{gk}},\ \frac{k}{R},\ \frac{H_o}{L},\ \frac{L}{R}\right) \qquad (2.53)$$

In accordance with the Kennedy theoretical analysis[31] one may write

$$\frac{H_o}{L} = \phi\left(\frac{U}{U_c}\right) \qquad (2.54)$$

where U_c is the critical velocity for the entrainment of sand of size k. From Shields' diagram, U_{*c}^2/gk is constant for the sands commonly occurring in rivers. Since U/U_{*c} is a function of k/R, this required that

$$\frac{U_c}{\sqrt{gk}} = \phi_2\left(\frac{k}{R}\right) \tag{2.55}$$

and thus Equation 2.54 becomes

$$\frac{H_o}{L} = \phi_3\left(\frac{U}{\sqrt{gk}}, \frac{k}{R}\right) \tag{2.56}$$

Kennedy's theoretical analysis suggests also that the length of dune be given as

$$L = 2\pi \frac{U^2}{g} \tag{2.57}$$

and hence

$$\frac{L}{R} = 2\pi \frac{U^2}{gk}\frac{k}{R} \tag{2.58}$$

Using Equations 2.54 and 2.57, the relation for the resistance coefficient from Equation 2.53 is simply

$$\lambda_2 = \lambda_2\left(\frac{U}{\sqrt{gk}}, \frac{k}{R}\right) \tag{2.59}$$

The sufficiency and the applicability of the last relation was examined by Alam and Kennedy, taking a large number of data from laboratory channels and from natural rivers. The curves of Figure 22 summarize the dependence of $4\lambda_2 = f_2$ on the relative depth R/k for varying Froude numbers $U/\sqrt{gk}$. These curves reveal that when the flow Froude number $U/\sqrt{gR}$ is smaller than 0.5 the resistance coefficient of the bed features is independent of R/k and is essentially a function of $U/\sqrt{gk}$

$$\lambda_2 = \lambda_2\left(\frac{U}{\sqrt{gk}}\right) \tag{2.60}$$

Alam and Kennedy bring out the point that the parameter ψ' of the Einstein-Barbarossa analysis Equation 2.42 virtually yields the relation

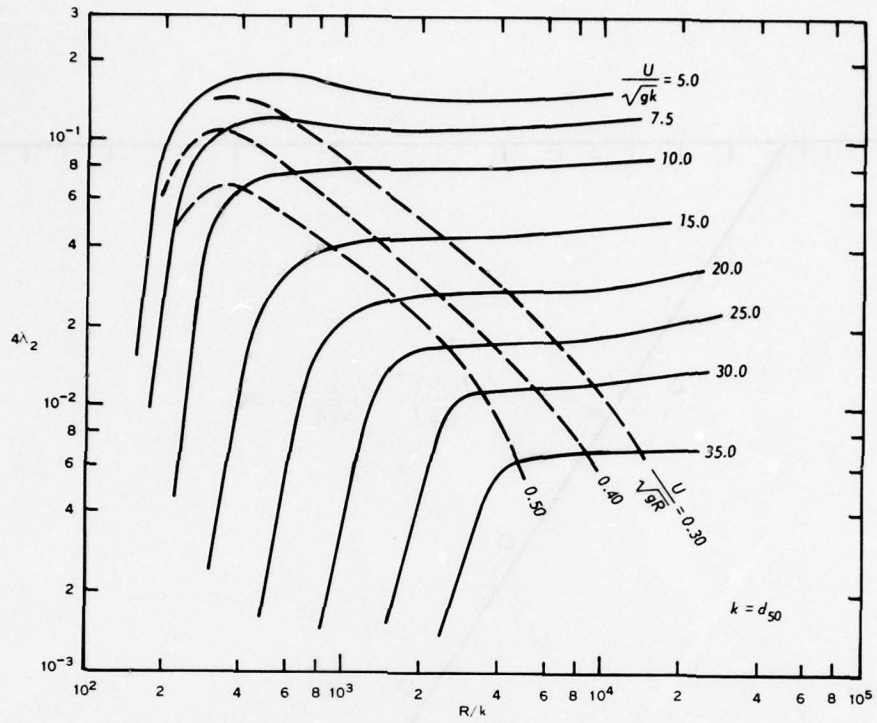

Figure 22. Form resistance in alluvial channels according to Alam and Kennedy

$$\psi' = 1.68 \frac{2}{\lambda_1} \frac{gk}{U^2} , \quad k = d_{35} \tag{2.61}$$

As λ_1 does not vary widely among different alluvial channels, there is not much variation of the granulometric distribution of the natural sand so that d_{35} is proportional to d_{50}. Accordingly the two determinations of λ_2, one by the Einstein-Barbarossa method and the other by the Alam-Kennedy method, would be close to each other for the cases where Froude numbers are less than 0.5.

55. For reference it may be desirable to have an expression from the Alam-Kennedy study for λ_2 when Froude number is less than 0.5. The averaged values of λ_2 over the horizontal portions of the curves in Figure 22 are plotted against $U/\sqrt{gk}$ in Figure 23. Representing the alignment of the points by a straight line, one now has

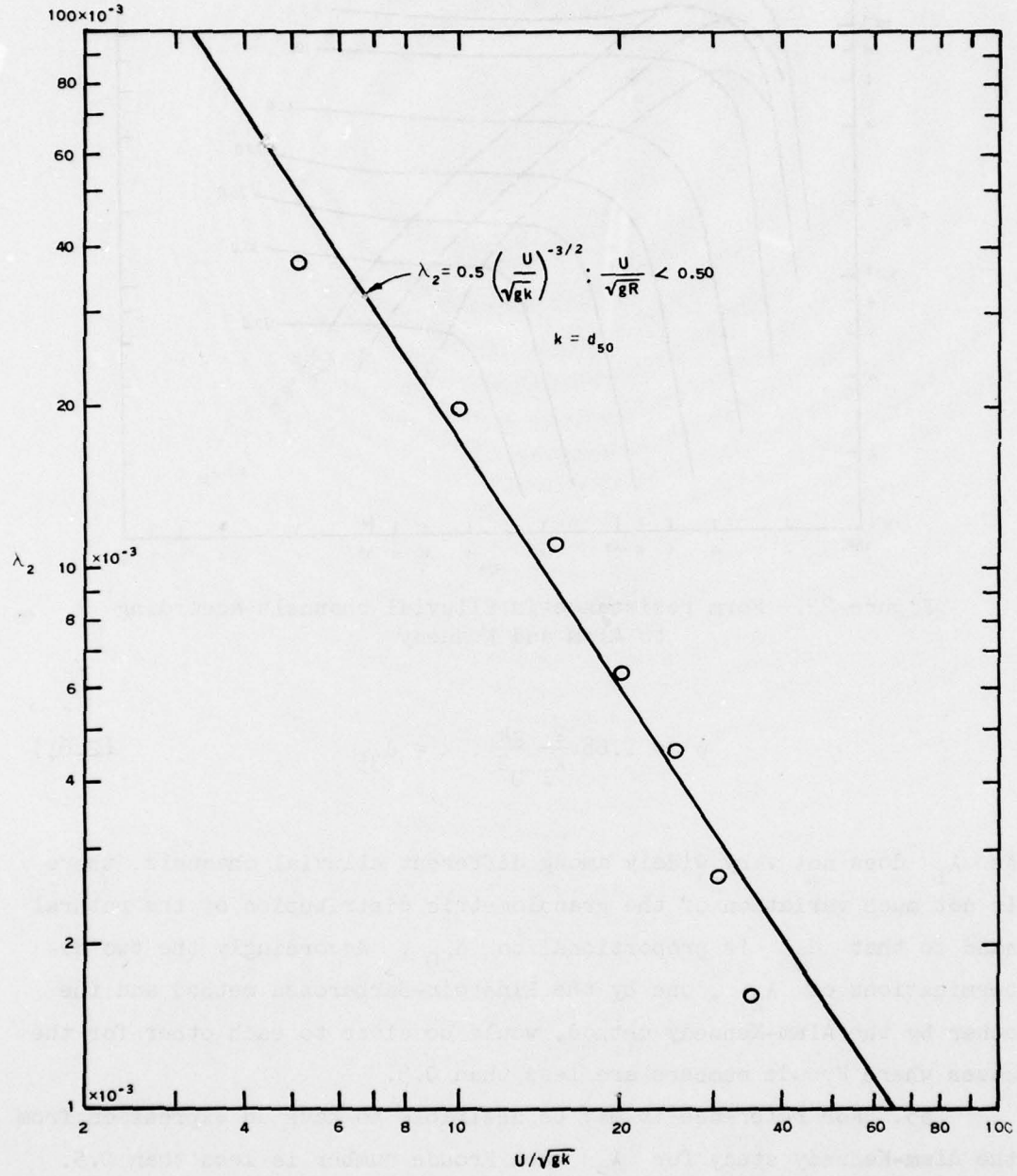

Figure 23. Form resistance coefficient of bed features for small Froude number (based on Alam and Kennedy analysis)

$$\lambda_2 = 0.5 \left(\frac{U}{\sqrt{gk}} \right)^{-3/2} \tag{2.62}$$

If we introduce the relative density of the grains, $s = 2.68$, the expression becomes

$$\lambda_2 = 0.34 \left[\frac{U}{\sqrt{(s-1)gk}} \right]^{-3/2} \tag{2.63}$$

Application of Alluvial Channel Resistance Formulae to Channels Charged with Atlantic Muck

56. Kalinske and Hsia[32] performed experiments with a bed of very finely ground silica with a specific gravity of 2.67. The gradation of the sand, shown in Figure 24, is similar to Atlantic muck. The purpose of the experiments, carried out in a steel channel 2.25 ft wide, 1.096 ft deep, and 80 ft long, was to study the transportation of such a fine sediment and to distinguish between bed load and suspended load. For our purpose we note that a range of flow conditions were tested and the Manning's n was calculated for each flow. Data associated with ripples in the bed are shown in Table 19. The entries of the column for R_o, the hydraulic radius, are our own evaluations. The energy gradient is inferred from the shear velocity given in the last column. We shall consider this data, first to see if the friction of the ripples computed by the Einstein-Barbarrosa method is in agreement with the curve derived by these investigators for the American rivers, and secondly to inquire if the values obtained are in agreement with the Alam-Kennedy formula, Equation 2.62.

57. Assuming that the kinematic viscosity of the water during the Kalinske and Hsia experiments was close to $\nu = 1 \times 10^{-5}$ ft^2/sec and the smallest value of the friction velocity was about 0.05 ft/sec, the boundary layer δ would then equal 0.0024 ft. Identify k with d_{65}, that is, $k = 0.012$ mm. The ratio of the boundary layer thickness to the grain size, δ/k, is 54. Hence, we are dealing with

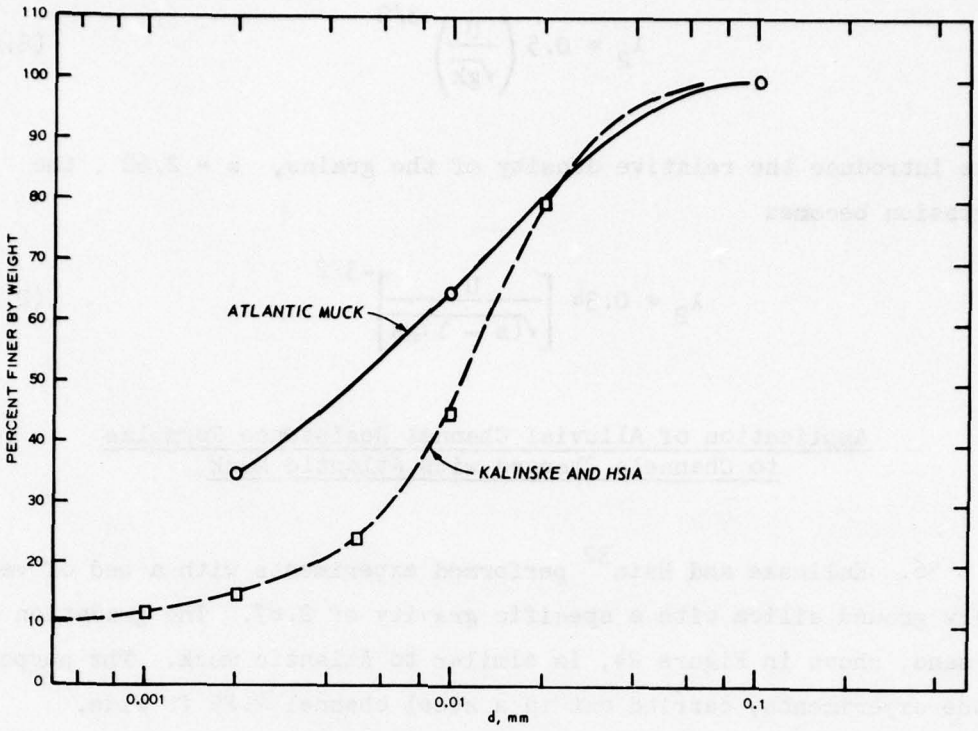

Figure 24. Size distribution in Atlantic muck and Kalinske sand

Table 19

Summary of the Kalinske and Hsia Test Data

No.	$S \times 10^4$	H , ft	U , ft/sec	R_o , ft	C	n	τ_o/ρ ft/sec
3	2.5	0.37	0.84	0.278	0.64	0.0119	0.046
4	2.5	0.49	1.14	0.342	1.29	0.0106	0.054
5	2.5	0.66	1.31	0.416	1.67	0.0105	0.061
6	5.0	0.36	1.25	0.272	1.95	0.0117	0.069
7	5.0	0.52	1.54	0.354	2.24	0.0112	0.080
8	5.0	0.64	1.81	0.410	2.27	0.0101	0.084
9	10.0	0.35	1.68	0.267	3.36	0.0119	0.096
10	10.0	0.56	2.14	0.372	6.81	0.0114	0.125

Note: S = channel slope, C = average sediment concentration in percent.

hydrodynamically smooth surfaces and Δ to be inserted in Equation 2.38 is of the value

$$\Delta = 3.3 \frac{\nu}{U_{*1}}$$

The resulting equation may be readily transformed to

$$\frac{U}{\sqrt{gR_1S}} = A + 8.65 \log (gR_1S) \tag{2.64}$$

with

$$A = 3.26 - 5.75 \log (g\nu S)$$

This determines the hydraulic radius R_1 associated with the surface friction when U_{*1}, S, and ν are known. The determinations are made by trial. Once R_1 is known

$$R_2 = R_b - R_1 \tag{2.65}$$

$$\frac{U}{U_{*2}} = \sqrt{gR_2S} \tag{2.66}$$

and

$$\psi' = \frac{1.67\, d_{35}}{R_1S} \tag{2.67}$$

58. The symbol R_b appearing in Equation 2.65 denotes the hydraulic radius of the channel bottom and is not to be confused with the channel hydraulic radius R_o. In channels where the depth H is negligible in comparison with the channel width and the asperities of the sidewalls are smaller than those of the bottom, R_b would equal R_o; otherwise, R_b would be greater than R_o. The matter of the sidewall corrections was discussed before. As

$$\frac{\tau_b}{\tau_o} = \frac{R_b}{R_o}$$

from Equation 2.24 in a rectangular channel

$$\frac{R_b}{R_o} = 1 + \frac{2H}{B}\left(1 - \frac{\lambda_w}{\lambda_o}\right)$$

and in view of Equation 1.20 and as $\lambda \sim n^2 R^{-1/3}$

$$\frac{\lambda_w}{\lambda} = \left(\frac{n_w}{n_o}\right)^{3/2}$$

where n_w is the Manning's n of the roughness of the sidewalls, n, the Manning's n of the channel

$$R_b = 1 + \frac{2H}{B}\left[1 - \left(\frac{n_w}{n_o}\right)^{3/2}\right] \tag{2.68}$$

Kalinske and Hsia note that n_w of the still channel is 0.0092. The Manning's n's of the channel with the ripples present are shown in Table 19. Determinations of the procedures in Equations 2.64 to 2.66 are shown in Table 20. Values of the parameters appearing in the last two columns of the table are plotted in Figure 18. Ignoring the scatter,

Table 20

Determination of the Einstein and Barbarossa Variables in the Kalinske and Hsia Data (Assumed: $\nu = 1 \times 10^{-5}$ ft^2/sec)

Run No.	$S \times 10^4$	U, ft/sec	R_b, ft	R_1, ft	R_2, ft	U/U_{*2}	ϕ'
3	2.36	0.84	0.306	0.226	0.080	34.0	0.77
4	2.64	1.14	0.369	0.323	0.046	58.0	0.48
5	2.97	1.31	0.461	0.385	0.076	50.2	0.38
6	5.56	1.25	0.300	0.199	0.101	29.3	0.37
7	5.61	1.54	0.386	0.267	0.119	33.2	0.27
8	5.30	1.81	0.443	0.361	0.082	48.4	0.21
9	11.98	1.68	0.272	0.201	0.071	32.2	0.17
10	13.00	2.14	0.421	0.218	0.203	26.6	0.15

Note: S = surface energy gradient computed using the entries of the last column in Table 19, $\tau_o = \rho g R S$.

the average values fall on the curve from the Einstein-Barbarossa equation

$$\frac{U}{U_{*2}} = 30(\phi')^{-1/2} \qquad (2.43 \text{ bis})$$

The scatter of the plotted points is very severe. Probably this may be due to the difficulties in measuring the energy gradient of the flows. Computations made on the basis of the experimental channel slope show a lesser degree of scattering. The method is also very sensitive to slight inaccuracies in the determination of the current mean velocities.

59. Since all the Froude numbers of the flows in the Kalinske and Hsia tests are less than 0.5, the coefficient λ_2 of the features, consisting essentially of ripples, may be also obtained by the formula

$$\lambda_2 = 0.5\left(\frac{U}{\sqrt{gk}}\right)^{-3/2} \qquad (2.62 \text{ bis})$$

where k, the median grain size, has the value of 0.010 mm. It will be recalled that the expression was based on the Alam-Kennedy analysis curves giving the dependence of λ_2 on H/k and $U\sqrt{gk}$. The determinations of λ_2 on this basis is shown in Table 21. In the same table are given also the corresponding values in accordance with the Einstein-Barbarossa method. The formula used was

$$\lambda_2 = 2\left(\frac{U}{U_{*2}}\right)^2$$

and the appropriate values were taken from the seventh column in Table 20. Although the agreement of the values for the individual runs determined by the two methods is not always satisfactory, the agreement of the means is good. We now conclude that either method would be satisfactory for the determination of λ_2 of the bed features consisting of ripples or dunes of flows with a Froude number less than 0.5.

60. The determination of the resistance of a deep and wide channel charged with Atlantic muck may be made using the principles discussed in the above sections. At this point, however, it would be useful to remark that the Einstein-Barbarossa method would be equally applicable if the surface energy gradient S is broken into two parts,

Table 21

Comparison of λ_2 for the Kalinske and Hsia Tests Determined by Alam-Kennedy and Einstein-Barbarossa Method

Run No.	Einstein-Barbarossa λ_2	Alam-Kennedy λ_2
3	1.72×10^{-3}	3.78×10^{-3}
4	0.60	1.73
5	0.80	1.95
6	2.72	2.08
7	1.82	1.52
8	0.85	1.19
9	1.93	1.33
10	2.82	0.93
Mean	1.61×10^{-3}	1.81×10^{-3}

S_1 , and S_2 , the first associated with the surface friction and the second with the form resistance of the bed features in the form of ripples and dunes. We note that $R = R_b$

$$R_1 S = R S_1$$

and

$$R_2 S = R_1 S_2$$

considering a hydrodynamically smooth surface from Equations 2.38 and 2.45

$$\frac{U}{U_{*1}} = \sqrt{\frac{2}{\lambda_1}} = 3.25 + 5.75 \log \frac{U_{*1}}{U} + 5.75 \log \frac{UR}{\nu} \qquad (2.38 \text{ bis})$$

where

$$U_{*1} = \sqrt{gRS_1}$$

Thus U/U_{*1} is a function of UR/ν and the relation of the function

was shown in Table 17. After specifying the values of U_{*1}, R, and ν the value of S_1 is determined by means of the above relation. The gradient S_2 is obtained from

$$S_2 = S_o - S_1$$

now,

$$U_{*2} = \sqrt{gS_2R}$$

$$U_{*2} = \sqrt{\frac{2}{\lambda_2}}$$

and

$$\phi' = \frac{1.76d_{35}}{S_1R} \tag{2.69}$$

Reductions from laboratory and alluvial river data made on this basis would not change the results already shown in Figure 18 since $RS_1 = SR_1$

$$\frac{U}{U_{*2}} = 30\left[(s - 1)\frac{k_s}{RS_1}\right]^{-1/2} \tag{2.70}$$

For the present, however, it would be easier to revert to Alam-Kennedy procedure to determine the form resistance of a deep channel. In the channel previously considered in paragraph 31, $R = 50.6$ ft and $\nu = 1 \times 10^{-5}$ ft^2/sec. Now n can be computed from

$$n_1 = 1.486R^{1/6}\sqrt{\frac{\lambda_1}{2g}}$$

after determining λ_1 from Equation 2.38 or using Table 17. The resulting values agree with n given in paragraph 31. As regards n_2

$$n_2 = 1.486R^{1/2}\sqrt{\frac{\lambda_2}{2g}}$$

and λ_2 may be computed from

$$\lambda_2 = 0.5\left(\frac{U}{\sqrt{gk}}\right)^{3/2} \qquad (2.62 \text{ bis})$$

for $U/\sqrt{gR}$ less than 0.5. For Atlantic muck $k = 0.005$ mm. The combined n for this channel is as follows:

U , ft/sec	n_1	n_2	n
0.5	0.0159	0.0262	0.0421
1.5	0.0152	0.0146	0.0298
2.0	0.0146	0.0088	0.0234
4.0	0.0139	0.0052	0.0191
6.0	0.0136	0.0039	0.0175
8.0	0.0131	0.0031	0.0162
10.0	0.0130	0.0026	0.0152

The Manning's n of the channel considered decreases when the current velocity is increased. In the above, λ_1 was calculated on the assumption that the surface friction is that of a hydrodynamically smooth surface. If we had used the method of Lovera-Kennedy for establishing λ_1, these would have recalled n values larger than those shown in the above. Judging from the curves shown in Figure 21, for moving particles λ_1 is almost twice as large as if the particles had been fixed. This would increase the above shown values of n by 1.4 times.

PART III: ANALYSIS OF FORM RESISTANCE IN LABORATORY CHANNELS

Form Resistance of Ripples and Dunes

61. A second method for obtaining the resistance of alluvial channels would be to relate the form resistance of the bed features present to the dimensions of the latter. Probably this will be possible more readily to features consisting of ripples and dunes. In principle, then, a formula needs to be developed relating the resistance coefficient λ_2 to the height and length of the dunes or the ripples. In addition, formulae need to be developed relating the size and the length of the features to grain size and channel stress or channel current velocity.

62. Let F_r be the resistive force of the ripples or dunes per unit width of channel and H_o the height of the dunes or ripples. Using the formula of Sadron[8]

$$F_r = C_D H_o \frac{\rho}{2} U_o^2$$

where

C_D = the coefficient of drag force

ρ = the density of the flowing liquid

U_o = the current at the crests of the bed features

Introducing τ_2 the stress arising from the bed features and L the length of the ripples on the dunes

$$\tau_2 = \frac{F_r}{L} = C_D U_o^2 \frac{\rho}{2} \frac{H_o}{L}$$

or

$$U_{*2}^2 = \frac{1}{2} C_D \frac{H_o}{L} U_o^2$$

Dividing by U^2, the channel current velocity squared,

$$\left(\frac{U_{*2}}{U}\right)^2 = \frac{1}{2} C_D \frac{H_o}{L} \left(\frac{U_o}{U}\right)^2 \qquad (3.1)$$

Expressing the local velocity u by the power formula

$$u = Cy^m \tag{3.2}$$

then expressing the water depth by H

$$\frac{U_o}{U} = (m + 1)\left(\frac{H_o}{H}\right)^m$$

Substituting this in Equation 3.1 and arranging terms

$$C_D = \left(\frac{U_{*2}}{U}\right)^2 \Bigg/ \left[(m + 1)^2 \left(\frac{H_o}{H}\right)^{2m} \frac{H_o}{2L}\right] \tag{3.3}$$

Thus C_D may be established from observed values of H_o, H, and L provided m, the exponent in the velocity law (Equation 3.2), is known.

Observed velocities
in Fort Collins tests

63. In the Fort Collins tests,[18] the observed velocities are approximated by the form

$$u = C + B \log y$$

where C is the velocity at a point 1 ft from the bottom of flume. This expression can be changed to power law

$$u = Cy^m$$

Comparing these expressions with each other

$$y^m = 1 + \frac{B}{C} \log y$$

This is satisfied for $y = 1$. Assume that it is satisfied also for $y = 0.1$ ft. Accordingly

$$m = -\log\left(1 - \frac{B}{C}\right)$$

The constants C and B are given in the appropriate tables of reference.[18] Through the latter relation, n was evaluated for ripples and also for dunes. It was noted that m did not show much variation from test to test. Averaged values are shown in Table 22, where the

Table 22

Exponent m of Velocity Distribution in Fort Collins Data

($u = Cy^m$)

Grain Size d_{50}	Ripple m	Dune m	Average m
0.19 mm	0.196	0.151	0.173
0.27 and 28	0.266	0.116	0.191
0.45	0.164	0.133	0.148
0.47	0.183	0.158	0.170
0.93	--	0.137	0.137
		Average	0.164

entries are distinguished both as grain size and feature forms. The exponent m is practically independent of grain size. Its value is somewhat greater for the ripples. Ignoring this difference we adopt the average

$$m = 0.166$$

As an example, the distribution of velocities over a ripple and also over a dune is shown in Figure 25. In a cross section, the velocities were measured at the midpoint and at points close to the two walls. Using this value of m, Equation 3.3 becomes

$$C_D = \frac{(U_{*2})^2}{U} \Bigg/ \left[\frac{49}{36}\left(\frac{H_o}{H}\right)^{1/3} \frac{H_o}{2L}\right] \qquad (3.4)$$

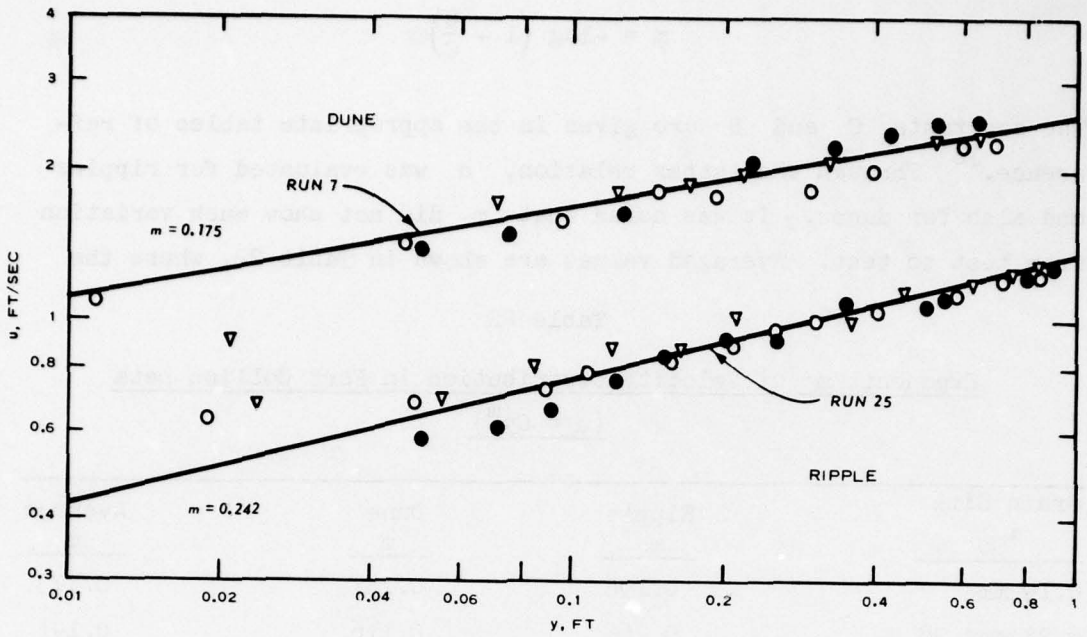

Figure 25. Velocity distribution over a ripple and a dune (8-ft channel, d_{50} = 0.19 mm)

Determination of C_D
for Fort Collins data

64. The energy gradient S is divided into two parts, S_1 balancing the resistance due to granular bottom surface and S_2 balancing the form resistance of the ripples or of the dunes. Thus

$$\tau_b = \tau_1 + \tau_2$$

with the usual definitions

$$\tau_b = \rho g S R_b;\ \tau_1 = \rho g S_1 R_b,\ \tau_2 = \rho g S_2 R_b$$

or

$$U_*^2 = gSR_b;\ U_{*1}^2 = gS_1R_b;\ U_{*2}^2 = gS_2R_b$$

and now since $S = S_1 + S_2$
Dividing by U^2 and rearranging terms

AD-A058 706 ARMY ENGINEER WATERWAYS EXPERIMENT STATION VICKSBURG MISS F/G 13/2
AN ESTIMATE OF CHANNEL ROUGHNESS OF INTEROCEANIC CANALS.(U)
JUL 78 G H KEULEGAN

UNCLASSIFIED WES-TR-H-78-13 NL

2 OF 2
AD
A058706

END
DATE
FILMED
11-78
DDC

$$\frac{(U_{*2})^2}{U} = \frac{(U_*)^2}{U} - \frac{(U_{*1})^2}{U} \qquad (3.5)$$

of the terms on the right-hand side the first is taken from the observation of the Fort Collins data[18] after sidewall corrections. As regards the second, this was determined in two ways using first, the ordinary asperities formulas, putting H equal to R_b

$$\frac{U}{U_{*1}} = 5.75 \log 12.8 \frac{H}{k_s} \qquad (2.38 \text{ bis})$$

where k_s stands for the grain median diameter d and secondly,

$$\frac{U}{U_{*1}} = -3.4 + 5.75 \log \frac{U_{*1}H}{\nu} \qquad (2.50 \text{ bis})$$

It will be recalled referring to Figure 21 that the latter expression represents on the average the granular skin friction found from the Fort Collins tests.[18] After evaluating $(U_{*2})^2/U$ for each run and noting the quantities H_o/H and H_o/L, these are entered into Equation 3.4 to obtain C_D. The computed C_D's by these two methods are plotted against L/H_o in Figures 26 and 27 in order to find if there is dependence on the relative lengths of the bed features. The data are differentiated as to the grain size and bed feature form. No dependence on the grain size is indicated. The ordinates represent the averages of C_D corresponding to L/H_o constant or very close to each other. There is much scatter which is expected owing to the difficulties in measuring H_o and the fact that U_{*2} represents a difference of terms, each open to error. It is also possible that L and H_o alone by themselves are not sufficient to formulate the stresses of the bed features. This problem has been discussed by Nordin.[33] Owing to the scatter of the points, it is difficult to give an exact graphics to define the dependence of C_D on L/H_o. Tentatively, the horizontal lines are drawn in the two figures implying that C_D is independent of L/H_o. From Figure 26, which is the case in which the granular surface resistance is computed by Equation 2.38, the roughness formula,

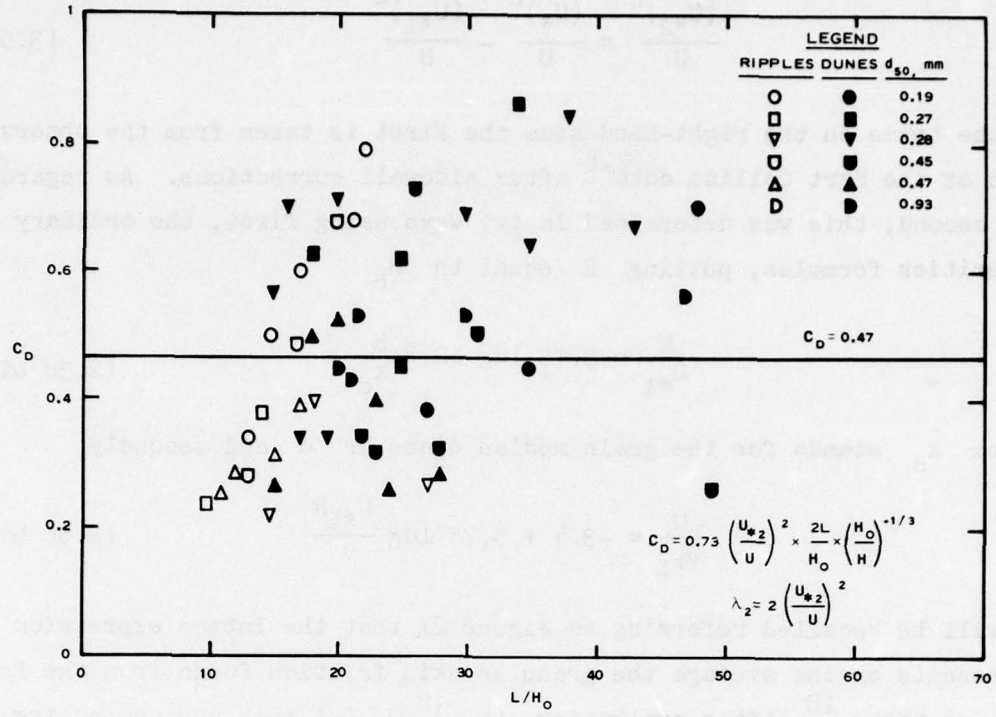

Figure 26. Dependence of the coefficient of form resistance on feature sizes and water depth in Fort Collins 8-ft flume tests. Granular surface friction computed by ordinary formula (Equation 2.38)

$$C_D = 0.47$$

and introducing into Equation 3.4 we find

$$\left(\frac{U_{*2}}{U}\right)^2 = 0.313 \frac{H_o}{L}\left(\frac{H_o}{H}\right)^{1/3}$$

and

$$\lambda_2 = 0.63 \frac{H_o}{L}\left(\frac{H_o}{H}\right)^{1/3} \qquad f_2 = 4\lambda_2 \tag{3.6}$$

From Figure 26, which is the case in which the granular surface resistance is computed by Equation 2.50, modified Prandtl formula,

$$C_D = 0.33$$

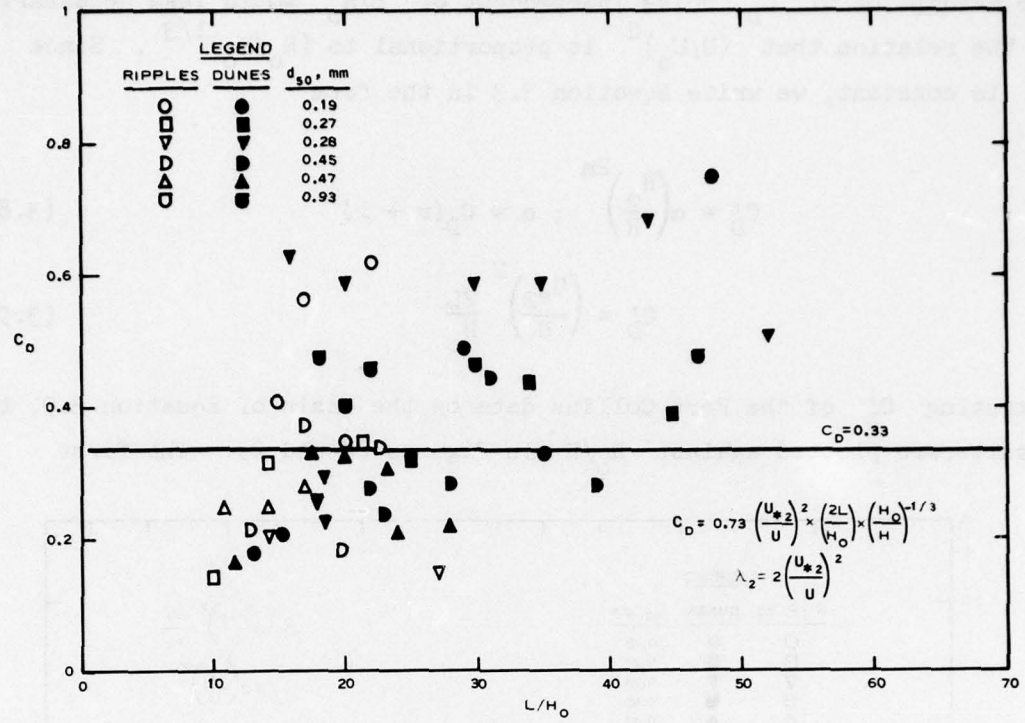

Figure 27. Dependence of the coefficient of form resistance on feature sizes and water depth in Fort Collins 8-ft flume tests. Granular surface friction computed by modified Prandtl formula (Equation 2.50)

and introducing into Equation 3.4 we find

$$\left(\frac{U_{*2}}{U}\right)^2 = 0.255 \frac{H_o}{L}\left(\frac{H_o}{H}\right)^{1/3}$$

and

$$\lambda_2 = 0.45 \frac{H_o}{L}\left(\frac{H_o}{H}\right)^{1/3} \qquad f_2 = 4\lambda_2 \tag{3.7}$$

Here in Equations 3.6 and 3.7 we have two different expressions for the resistance coefficients of bed features in terms of H_o/H and H_o/L which illustrate the importance of the law of the granular surface friction for the determination of the coefficient.

65. The above conclusion that C_D is independent of L/H_o in the Fort Collins data is based on the premise of $(U/U_o)^2$ being proportional to $(H_o/H)^{1/3}$. Conversely, it would be important to find if

the assumption of C_D being independent of L/H_o would lead necessarily to the relation that $(U/U_o)^2$ is proportional to $(H_o/H_o)^{1/3}$. Since C_D is constant, we write Equation 3.3 in the form

$$C_D' = \alpha\left(\frac{H_o}{H}\right)^{2m} \quad ; \quad \alpha = C_D(m+1)^2 \tag{3.8}$$

$$C_D' = \left(\frac{U_{*2}}{U}\right)^2 \frac{2L}{H_o} \tag{3.9}$$

Computing C_D' of the Fort Collins data on the basis of Equation 3.9, the results are plotted against H_o/H in Figures 28 and 29. The first

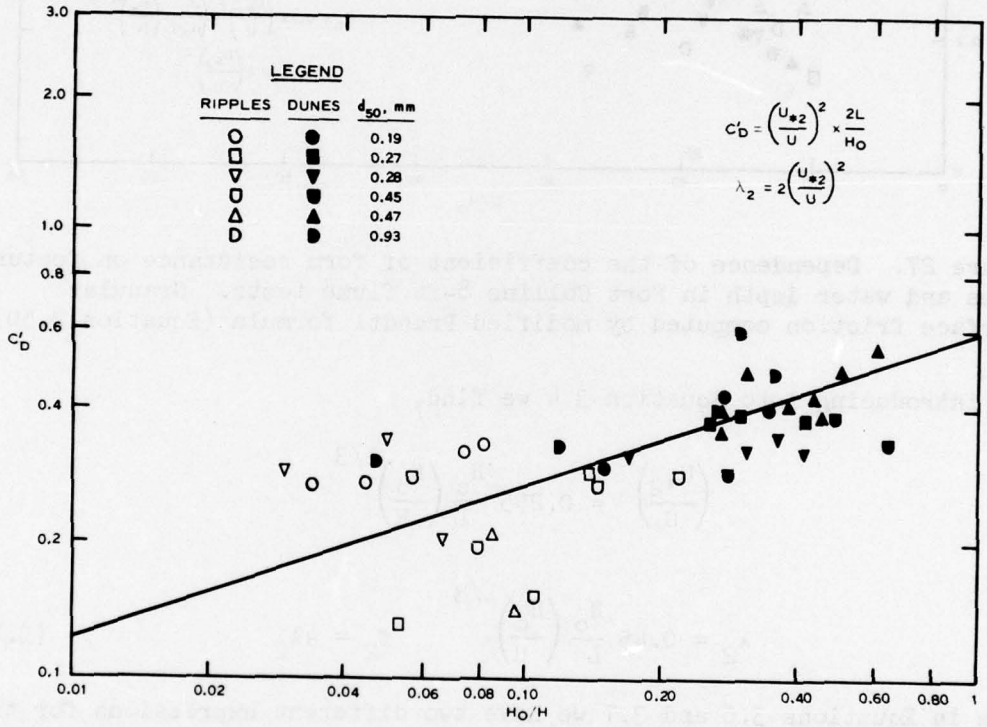

Figure 28. Dependence of the coefficient of form resistance on water depth in Fort Collins 8-ft flume tests. Granular surface friction computed by roughness formula (Equation 2.38)

represents the case in which the granular surface friction is computed by Equation 2.38 and the second where the granular surface friction is computed by Equation 2.50. The data are differentiated as to the grain

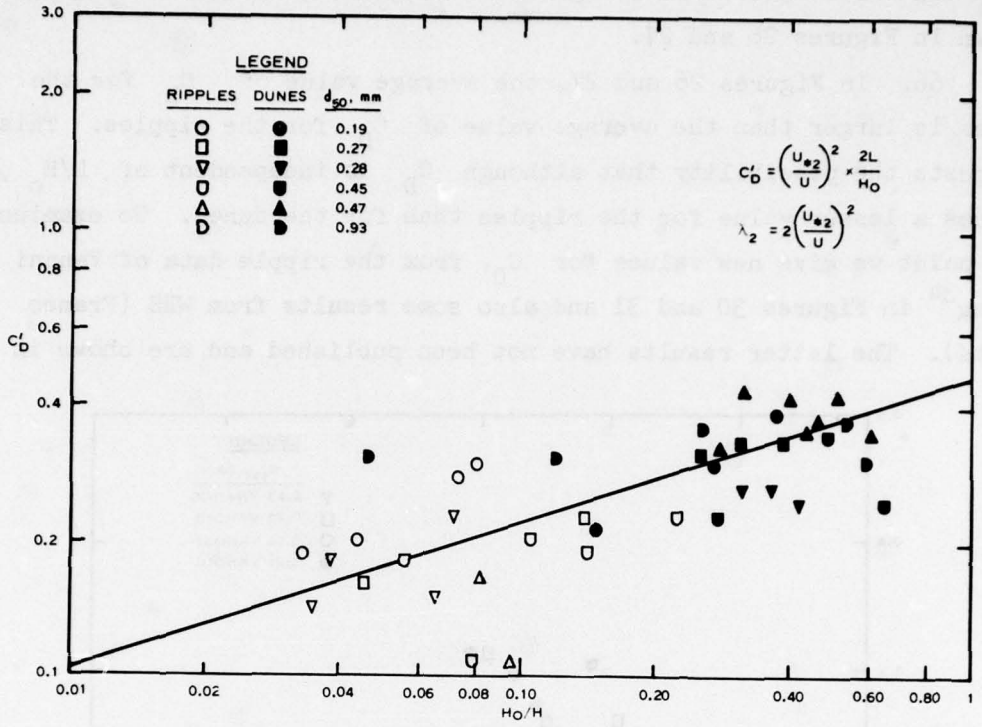

Figure 29. The dependence of the coefficient of form resistance on water depth in Fort Collins 8-ft flume tests. Granular surface friction computed by modified Prandtl formula (Equation 2.50)

size and bed feature form. No dependence on grain size is indicated. Points represent the average value C_D' in initial data of H_o/H being constant or close to each other. Although there is scatter of points, the scatter is not as severe as that in Figures 26 and 27. The lines of the figures are drawn such that the number of the points lying above the line is the same as those lying below. The lines yield

$$C_D' = 0.60\left(\frac{H_o}{H}\right)^{1/3}$$

and

$$C_D' = 0.47\left(\frac{H_o}{H}\right)^{1/3}$$

and from Equation 3.8 we find that the corresponding values of C_D are

0.44 and 0.34. These are in agreement with the ordinates of the lines shown in Figures 26 and 27.

66. In Figures 26 and 27, the average value of C_D for the dunes is larger than the average value of C_D for the ripples. This suggests the possibility that although C_D is independent of L/H_o, it has a lesser value for the ripples than for the dunes. To examine the point we give new values for C_D from the ripple data of Vanoni and Hwang[34] in Figures 30 and 31 and also some results from WES (Franco tests). The latter results have not been published and are shown in

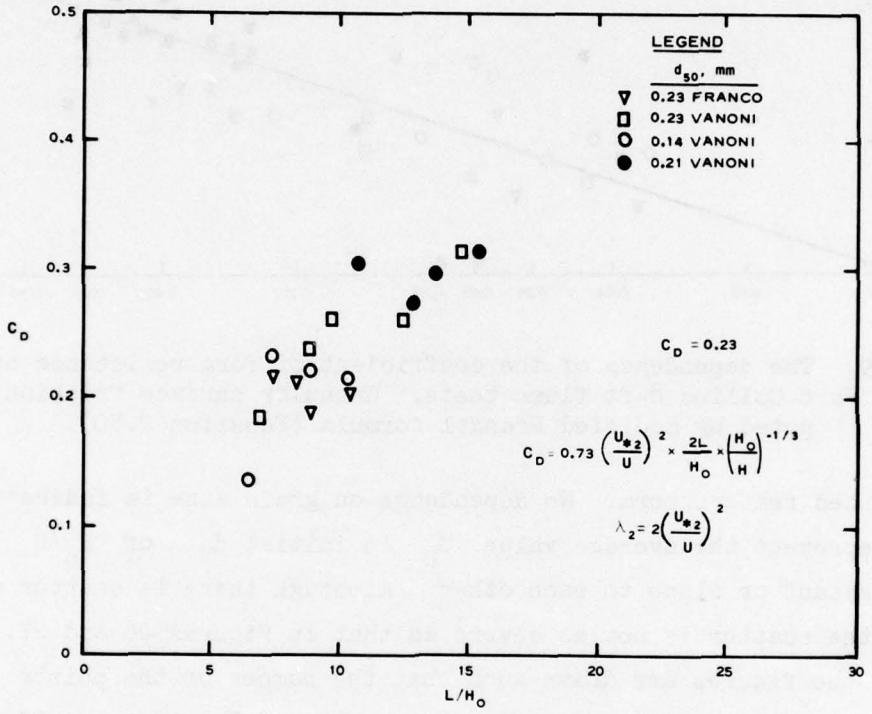

Figure 30. Dependence of the coefficient of form resistance on ripple size and water depth. Granular surface friction computed by ordinary formula (Equation 2.38)

Table 23 with the kind permission of Mr. Franco. The geometry of the ripples had been examined for a possible dependence of the size on water temperature. The surface displacement of the bottom sand had been surveyed from one end of the flume to the other. The height and the length of the ripples were deduced from the extremes in the

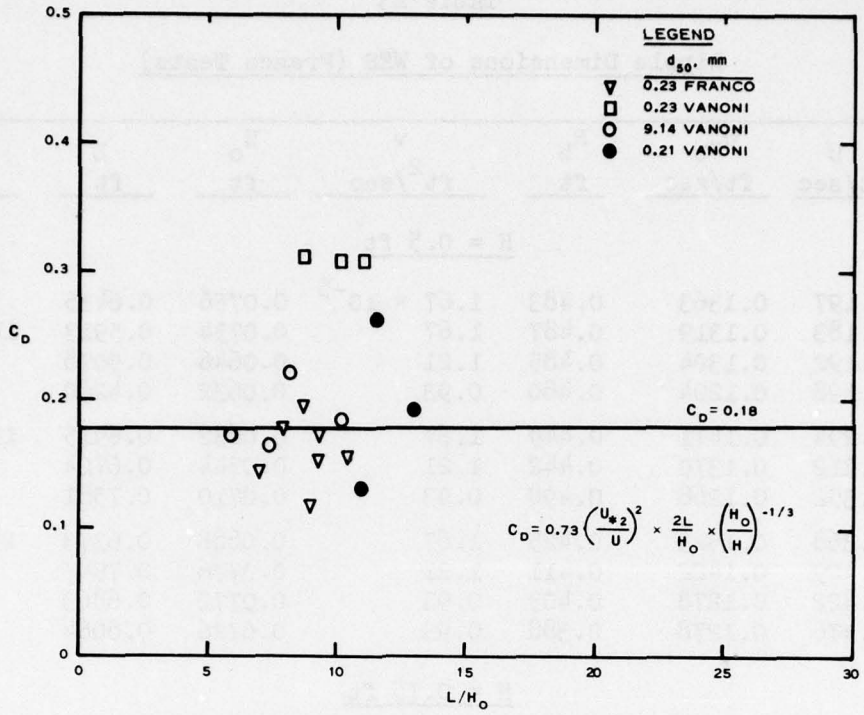

Figure 31. Dependence of the coefficient of form resistance on ripple size and water depth. Granular surface friction computed by modified Prandtl formula (Equation 2.50)

variation and the mean. Horizontal lines are drawn in both Figures 30 and 31. The suggestion is that C_D is independent of L/H_o. The lines are drawn such that the number of points above the line is equal to the number of points below the line. These give

$$C_D = 0.23$$

if the surface granular friction is computed by Equation 2.38 roughness formula, and

$$C_D = 0.18$$

if computed by Equation 2.50, modified Prandtl formula. Accordingly, in place of Equation 3.6

Table 23

Ripple Dimensions of WES (Franco Tests)

No.	U ft/sec	U_{*b} ft/sec	R_b ft	ν ft^2/sec	H_o ft	L ft	Q_s
				H = 0.5 ft			
21	1.197	0.1363	0.483	1.67×10^{-5}	0.0756	0.6435	5.6
4	1.183	0.1319	0.487	1.67	0.0754	0.5913	lb/hr/ft
6	1.192	0.1304	0.485	1.21	0.0646	0.5078	
5	1.198	0.1204	0.480	0.93	0.0632	0.4280	
15	1.294	0.1471	0.449	1.67	0.0832	0.6915	13.3
10	1.312	0.1370	0.442	1.21	0.0744	0.6724	
14	1.352	0.1268	0.498	0.93	0.0710	0.7581	
11	1.368	0.1523	0.425	1.67	0.0888	0.6373	23.3
12	1.409	0.1422	0.411	1.21	0.0776	0.7547	
10	1.422	0.1278	0.403	0.93	0.0772	0.6863	
17	1.476	0.1278	0.388	0.93	0.0726	0.8064	
				H = 0.75 ft			
30	1.513	0.1526	0.540	1.67×10^{-5}	0.0748	0.6309	23.3
31	1.640	0.1332	0.489	0.93	0.0706	0.6644	
32	1.345	0.1331	0.598	1.67	0.0684	0.6031	5.6
34	1.345	0.1198	0.594	0.93	0.0644	0.5530	
33	1.354	0.1248	0.591	1.21	0.0652	0.5518	

$$\lambda_2 = 0.31 \frac{H_o}{L}\left(\frac{H_o}{H}\right)^{1/3} \qquad 4\lambda_2 = f_2 \tag{3.10}$$

and in place of Equation 3.7

$$\lambda_2 = 0.24 \frac{H_o}{L}\left(\frac{H_o}{H}\right)^{1/3} \qquad 4\lambda_2 = f_2 \tag{3.11}$$

These apply to ripples. Interestingly enough, the last expansion is very close to the Kronoz formula

$$\lambda_2 = 0.21 \frac{H_o}{L}\left(\frac{H_o}{H}\right)^{0.25} \tag{3.12}$$

cited by Jensen and Lebreton.[35]

Dependence of Ripple and Dune Size on Current Mean Velocity

67. It is natural, intrigued by the Alam and Kennedy simple results on the resistance of alluvial streams, to inquire if similar results could be obtained applicable also to laboratory flumes. According to Alam and Kennedy, when the Froude number is less than 0.5 the form resistance coefficient λ_2 in alluvial rivers depends solely on $U/\sqrt{gk}$ where k is the median sand diameter d_{50}. For the desired examination we shall make use of that part of the Fort Collins data[18] that relates to ripples and dunes. These were observed for flows with a Froude number less than 0.5. In the preceding analysis λ_2 is expressed in terms of H_o/L and H_o/H. Hence, it is required that the dependence of these on $U^2/(s - 1)gd$ be established.

68. The dependence of H_o/d on $U^2/(s - 1)gd$ in the Fort Collins data is indicated in Figure 32. The points are differentiated as to grain size and bed feature form. The ordinates in some cases represent the average for the points having a constant or close abscissa. The dependence of H_o/d on $U^2/(s - 1)gd$ for the dunes differs considerably from that of the ripples. For the dunes

$$\frac{H_o}{d} = 40\left[U^2/(s - 1)gd\right]^{0.45} \tag{3.13}$$

and for the ripples

$$\frac{H_o}{d} = 10.3\left[U^2/(s - 1)gd\right]^{0.45} \tag{3.14}$$

if some of the points of the tests with 0.4-mm sand are disregarded. For the dunes these lead to the expression

$$\frac{H_o}{H} = 40\left[U^2/(s - 1)gd\right]^{0.45}\frac{d}{H} \tag{3.15}$$

and for the ripples

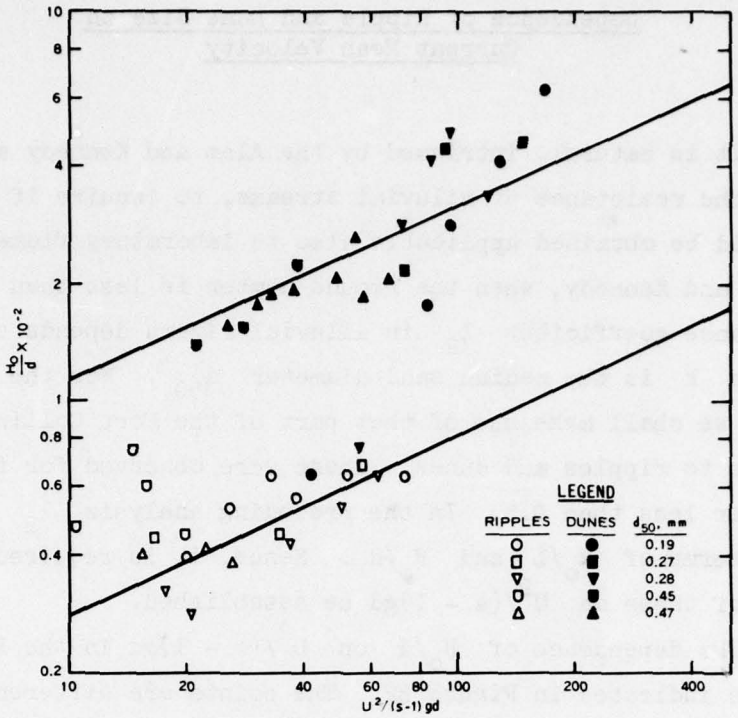

Figure 32. Dependence of bed feature heights on current velocity in Fort Collins tests (8-ft flume)

$$\frac{H_o}{H} = 10.3 \left[U^2/(s - 1)gd\right]^{0.45} \frac{d}{H} \tag{3.16}$$

The last relation furnishes the explanation why in the models of watercourses the ripple sizes are exaggerated. The relation can be written as

$$\frac{H_o}{H} = 10.3 \left[U^2/(s - 1)gH\right]^{1/2} \left(\frac{d}{H}\right)^{1/2} \tag{3.17}$$

The model currents being determined by Froudian relation, the ratio of the ripple heights in the model and in the prototype are

$$\frac{H_{om}}{H_{op}} = \left(\frac{d_m}{d_p}\right)^{1/2} \left(\frac{H_m}{H_p}\right)^{1/2} \tag{3.18}$$

69. Next the dependence of L/H_o on $U^2/(s - 1)gd$ in the Fort Collins data is indicated in Figure 33. The points are differentiated

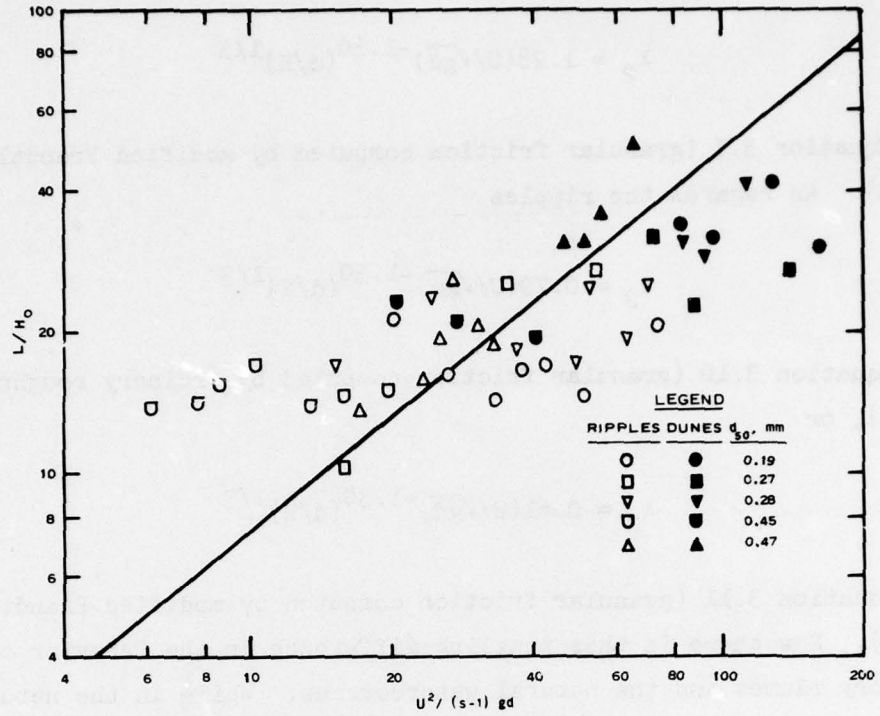

Figure 33. Dependence of the length-to-depth ratio of bed features on current velocity in Fort Collins tests (8-ft flume)

as to grain size and the bed feature form. In some cases, the ordinate values represent the averages for the points having a constant or close abscissa. Apparently, the dependence of L/H_o on $U^2/(s - 1)gd$ is the same for the ripples and for the dunes. The relation seems to be practically independent of the grain size. Accordingly

$$\frac{L}{H_o} = 1.2 \left[\frac{U^2}{(s - 1)gd}\right]^{4/5} \tag{3.19}$$

if some of the points of the tests with 0.45-mm sand are disregarded.

70. The substitution of H_o/H from Equation 3.15 or 3.16 and of L/H_o from Equation 3.19 in Equation 3.6 or 3.7 should yield the expressions of the form resistance coefficient λ_2 for dunes. Thus for the dunes, putting $S = 2.68$,

$$\lambda_2 = 1.80(U/\sqrt{gd})^{-1.30} (d/H)^{1/3} , \quad \lambda_2 = 4f_2 \tag{3.20}$$

using Equation 3.6 (granular friction computed by roughness formula), on

$$\lambda_2 = 1.28(U/\sqrt{gd})^{-1.30}(d/H)^{1/3} \tag{3.21}$$

using Equation 3.7 (granular friction computed by modified Prandtl formula). As regards the ripples

$$\lambda_2 = 0.79(U/\sqrt{gd})^{-1.30}(d/H)^{1/3} \tag{3.22}$$

using Equation 3.10 (granular friction computed by ordinary roughness formula), or

$$\lambda_2 = 0.61(U/\sqrt{gd})^{-1.30}(d/H)^{1/3} \tag{3.23}$$

using Equation 3.11 (granular friction computed by modified Prandtl formula). Now there is this puzzling difference in the behavior of laboratory flumes and the natural watercourses. While in the natural rivers the resistance coefficient λ_2 is practically independent of the ratio d/H and depends solely on $U/\sqrt{gd}$ for flows with a Froude number less than 0.5, in flumes there is also dependence on the ratio of d/H even though the Froude number of currents is below 0.5. The graphs of Equation 3.20 for the $H/d = 1 \times 10^3$ and $H/d = 0.5 \times 10^3$ are shown in Figure 34 and the points shown between the two curves are for rivers according to the Alam and Kennedy analysis.

71. The expression of L/H_o by Equation 3.19 can be obtained in another way. Values of the ratio L/d computed from the Fort Collins data[18] are shown in Figure 35. The data are identified as to grain size and bed feature form. The ordinates of some represent the average for the points having constant or very close abscissa values. The alignments of the points for the dunes and the ripples differ from each other. For the dunes

$$\frac{L}{d} = 45.0\left[U^2/(s-1)gd\right]^{5/4} \tag{3.24}$$

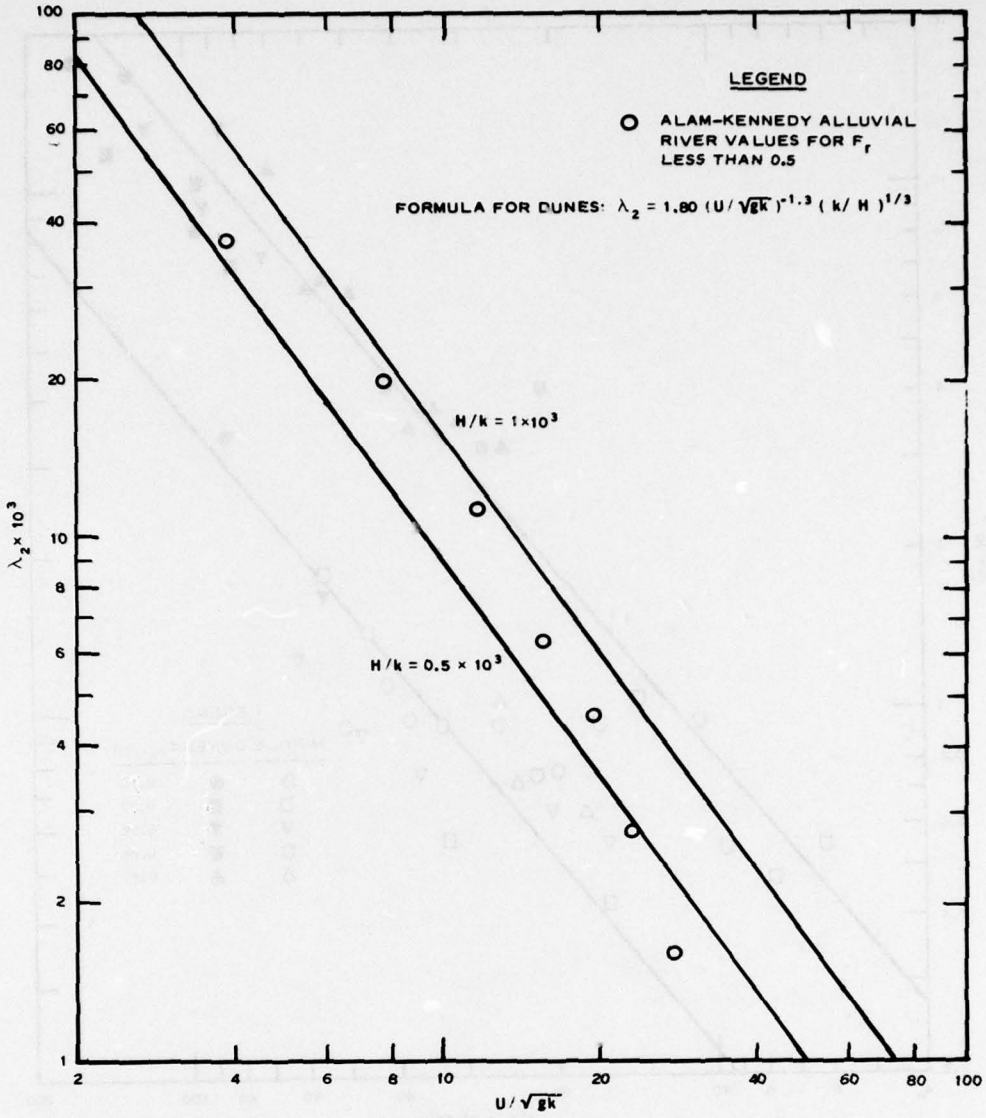

Figure 34. Comparison of form resistance coefficient based on Fort Collins tests, 8-ft flume, with Alam-Kennedy river values

and for the ripples

$$\frac{L}{d} = 12.4\left[U^2/(s-1)gd\right]^{5/4} \tag{3.25}$$

if some of the points of the tests with the 0.45-mm sand are disregarded. These equations, in conjunction with Equations 3.13 and 3.14, lead nearly to Equation 3.19.

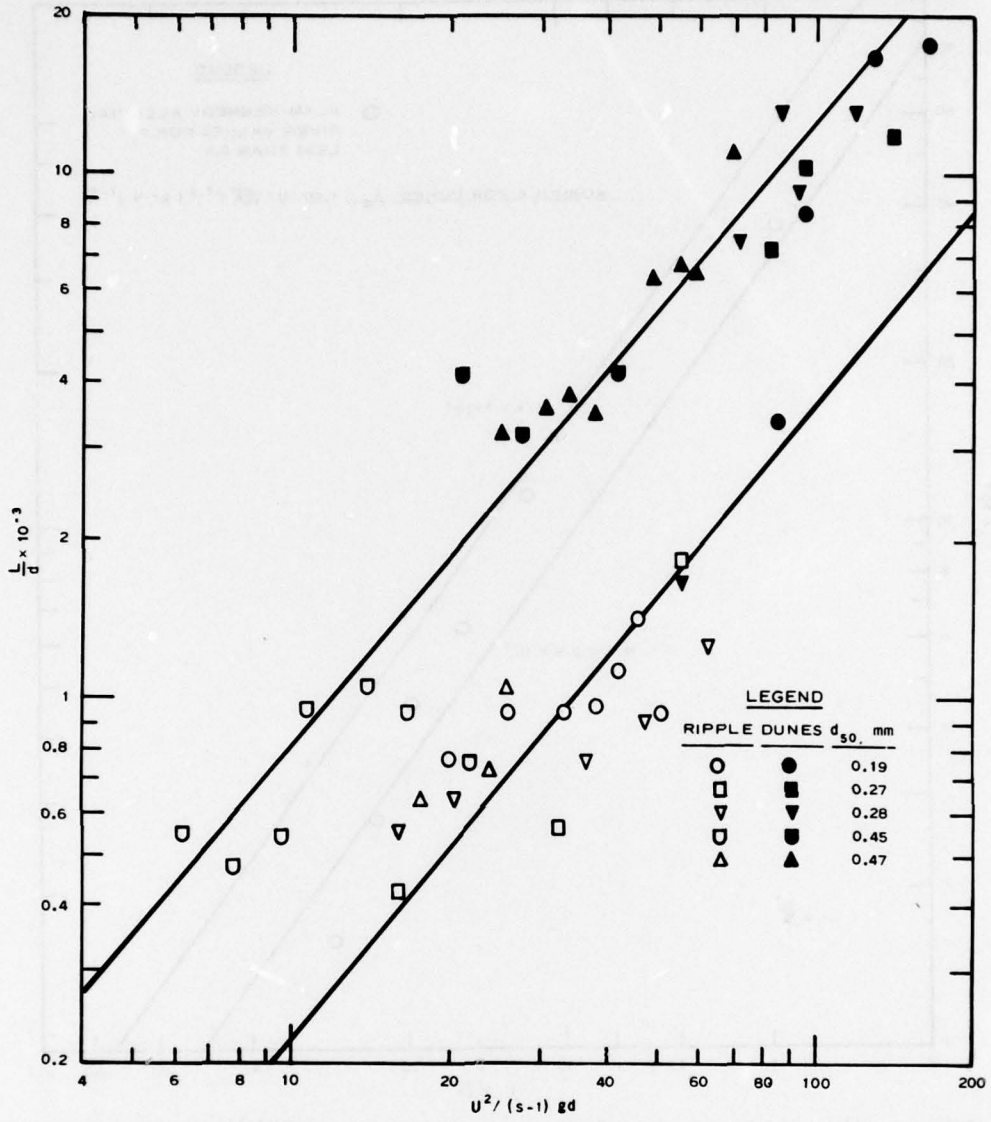

Figure 35. Dependence of bed feature lengths on current velocity in Fort Collins tests (8-ft flume)

72. The literature dealing with sediment problems was examined to see if there have been studies that have dealt with the question of dependence of the ratio of feature lengths to the size of grains on Froude number. Most combinations on the geometry of bed features have ignored this question, except one given by Jensen and Lebreton.[35] According to these authors, based on tests with sediments of varying

densities and with coarse materials satisfying the condition $d_* > 16$, the relation is

$$\frac{L}{d} = 193(s - 1)^{0.48}(U/\sqrt{gH})^{-1}$$

This can be written after replacing 0.48 with 0.50 as

$$\frac{L}{d} = 193\left[U^2/(s - 1)gH\right]^{-1/2}$$

or

$$\frac{L}{d} = 193\left[U^2/(s - 1)gd\right]^{-1/2}(d/H)^{1/2} \qquad (3.26)$$

a result which is so markedly different from the relation expressed by Equation 3.24. In the Fort Collins experiments, the L/d of dunes increases with increasing Froude numbers. In great contrast with this, in the Chatou tests L/d decreases with increasing Froude number. As in the Fort Collins tests, d_* is smaller than 16 and in the Chatou tests it is larger than 16; then the question arises if these conditions do have a bearing on the above difference noted.

A Discussion on the Formulas of Form Resistance and Feature Geometry

73. We certainly wish to consider a reputed formula of form resistance for ripples given by Vanoni and Hwang[34]

$$\frac{1}{\sqrt{4\lambda_2}} = 3.5 \log \frac{R_b}{eH_o} - 2.3 \qquad (3.27)$$

where

R_b = hydraulic radius of the bed

e = exposure ratio $A_s A$

A_s = horizontal projection of the lee forces of the ripples

A = total area under which A_s is measured

H_o = mean height of the ripples

As the heights of the ripples are controlled by the angle of repose of

the grain particles, A_s is proportional to L, the spacing between the crests of ripples. One may then take e to be proportional to H_o/L and write

$$e = \alpha \frac{H_o}{L}$$

In the data considered by Vanoni and Hwang, α is close to unity and subject to variation from one flume to another. In the data of a 40-ft channel, the mean value of α is 1.11; of a 60-ft channel, 0.96; and of a 130-ft channel, 1.36. The average is $\alpha = 1.14$. Again in the same ratio H/R_b also varies slightly from flume to flume with an average of $H/R_b = 1.09$. Inserting these quantities, the resistance formula reduces to

$$\frac{1}{\sqrt{4\lambda_2}} = 3.5 \log \frac{LH}{H_o^2} - 2.0 \qquad (3.28)$$

This may be expressed as a power law

$$\lambda_2 = 0.415 \left(\frac{H_o}{L}\right)^{0.75} \left(\frac{H_o}{H}\right)^{0.75} \qquad (3.29)$$

valid for the range of $H_o/L \times H_o/H$ from 20 to 150, the range covered by the data considered by Vanoni and Hwang. In arriving at the formula, these authors have computed the granular skin friction coefficient λ_1 using the ordinary roughness laws. Therefore, the above expression should be compared with λ_2 given by Equation 3.10; that is

$$\lambda_2 = 0.31 \frac{H_o}{L} \left(\frac{H_o}{H}\right)^{0.33} \qquad (3.10 \text{ bis})$$

a formula of the similar form but with different exponents of the corresponding quantities. The larger difference is in the exponent of H_o/H. It will be recalled that the latter was developed assuming that the velocity over the forms varies as y_m with $m = 0.166$ in the data of Fort Collins tests. Equation 3.29 suggests that for the ripples considered by Vanoni-Hwang, m can be as high as 0.38. To examine this matter, the dependence of the quantity $\lambda_2/(H_o/L)$ on H_o/H both for

the Franco data and also of the data considered by Vanoni-Hwang, Figure 36 was prepared. Individual points represent averages from the original data with close abscissa values taking two or three at a time. Despite the scatter, it is possible to represent the alignment of values from the Vanoni-Hwang data by a line drawn in the figure leading to

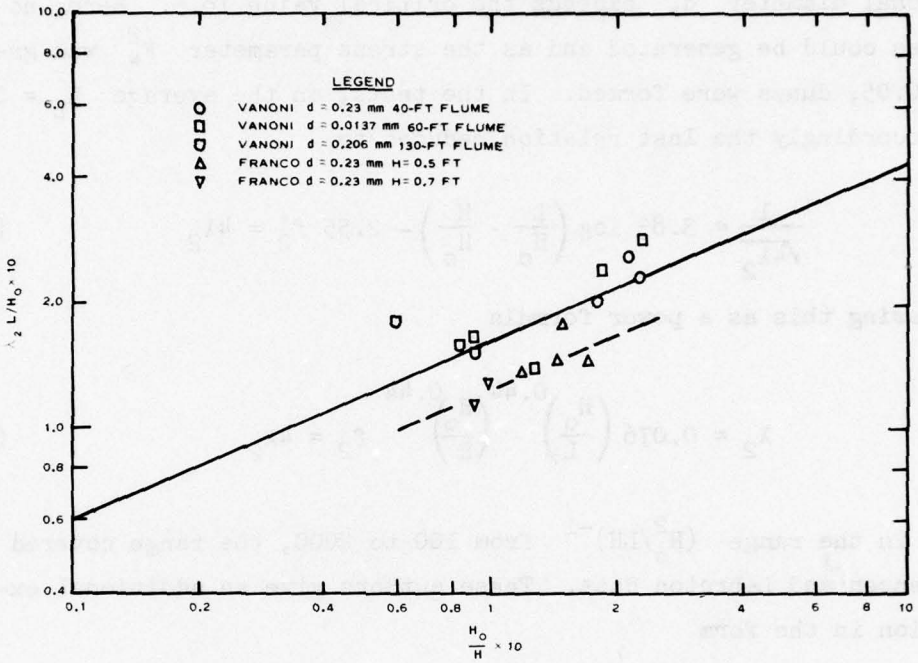

Figure 36. Dependence of coefficient of form resistance of ripples on feature dimensions

$$\lambda_2 = 0.45 \frac{H_o}{L} \left(\frac{H_o}{H}\right)^{0.45} \qquad (3.30)$$

This is, in a way, closer to Equation 3.10 and suggests that for the ripples considered, m amounts to 0.23. The data from Franco tests indicate a parallel alignment. The implication of the present results is that there is a difference in the form resistances of ripples and dunes, a matter that we shall be considering on another occasion.

74. Jensen and Lebreton[35] state that the Vanoni formula applies equally well to their experimental results. The formula they give is

$$\frac{1}{\sqrt{4\lambda_2}} = 3.83 \log\left(\frac{L}{H_o} \cdot \frac{R_b}{H_o}\right) - 2.76 \qquad (3.31)$$

which is based on experiments carried out in an inclined channel 50 cm deep, 80 cm wide, and 21 m long. The grains used were of different densities and sizes, the latter varying from 1.2 to 2.4 mm. The nondimensional diameter d_* exceeds the critical value 16.5. Here, no ripples could be generated and as the stress parameter F_*^2 was greater than 0.05, dunes were formed. In the tests, on the average $R_b = 0.88H$ and accordingly the last relation reduces to

$$\frac{1}{\sqrt{4\lambda_2}} = 3.83 \log\left(\frac{L}{H_o} \cdot \frac{H}{H_o}\right) - 2.55 \quad f_2 = 4\lambda_2 \qquad (3.32)$$

Expressing this as a power formula

$$\lambda_2 = 0.076 \left(\frac{H_o}{L}\right)^{0.44} \left(\frac{H_o}{H}\right)^{0.44} \quad f_2 = 4\lambda_2 \qquad (3.33)$$

valid in the range $(H_o^2/LH)^{-1}$ from 100 to 2000, the range covered by the Jensen and Lebreton data. These authors give an additional expression in the form

$$\frac{1}{\sqrt{4\lambda_2}} = A\left(\frac{H_o}{L}\right)^n \left(\frac{H_o}{R_b}\right)^m \quad f_2 = 4\lambda_2 \qquad (3.34)$$

The constants A_1, n, and m are determined by the method of least squares. Results of the Jensen-Lebreton data may be changed to

$$\lambda_2 = 0.107 \left(\frac{H_o}{L}\right)^{0.40} \left(\frac{H_o}{H}\right)^{0.66} \quad f_2 = 4\lambda_2 \qquad (3.35)$$

Equations 3.32 and 3.35 as applying to the same experimental data should have been identical, having the same factor A and the same exponents m and n. Owing to the scatter in the data, this condition is not realized.

75. A criticism generally expressed regarding the usual formula of resistance of alluvial streams and of the geometry of features is that factors expressing the influence of viscosity are lacking. The criticism is on the grounds that a change in the temperature of waters affects the resistance of alluvial streams. The problem of the influence of the effect of viscosity is well documented by Vanoni[36] by examining the importance of the $\sqrt{gd} \cdot d/\nu$ for the prediction of the bed features. Simons and others[37] find that the Barekyan formula is quite applicable to the determination of dune heights in the Fort Collins data, yet in this formula an appropriate viscosity parameter is missing. In the presentation we now give in Figure 37 this defect is remedied by

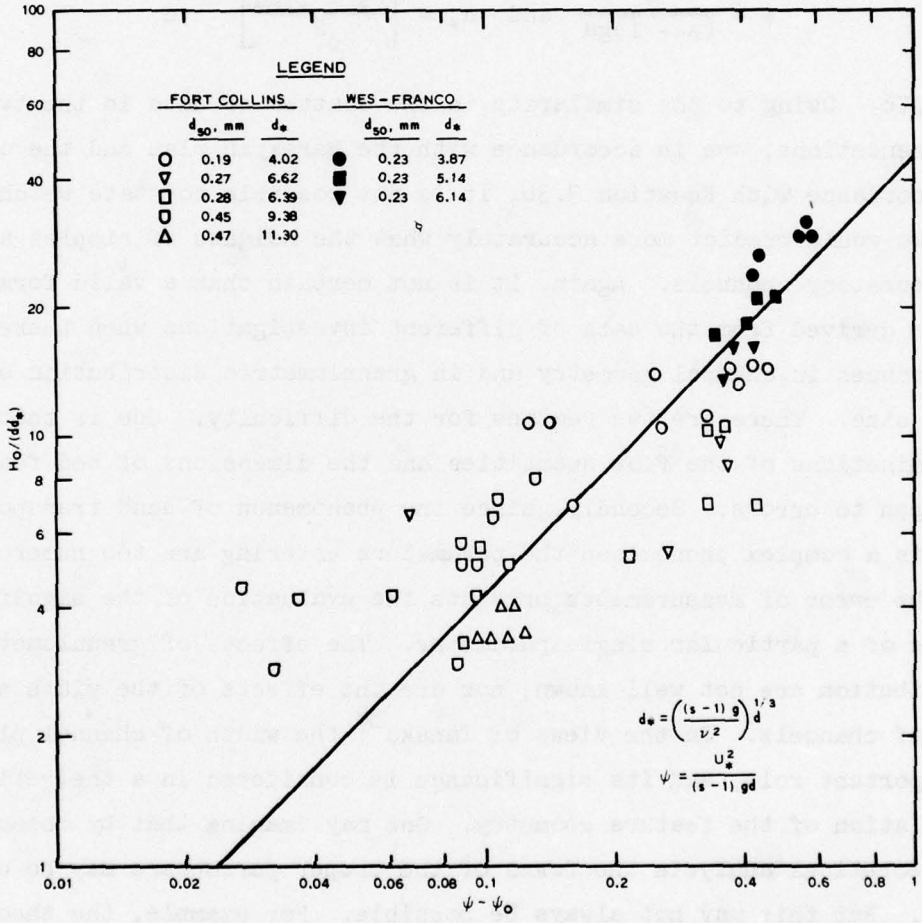

Figure 37. Ripple height relative to grain median diameter in Fort Collins and WES tests

introducing the grain parameter d_* which involves the kinematic viscosity ν. In the figure, $H_o/(dd_*)$ is plotted against $\psi - \psi_o$ where ψ_o is the Shields' parameter for the initiation of sand entrainment. Included also in the figure are points from the WES-Franco data which are in good agreement with the Fort Collins data. On the present basis, the expression for the ripple height is

$$H_o = 45(\psi - \psi_o)dd_* \tag{3.36}$$

where

$$\psi = \frac{U_*^2}{(s - 1)gd} \quad \text{and} \quad d_* = \left[\frac{(s - 1)gd}{\nu^2}\right]^{1/3} d$$

76. Owing to the similarity in the scatter of data in the two representations, one in accordance with the Barekyan plan and the other in accordance with Equation 3.36, it is not possible to state which of the two would predict more accurately what the heights of ripples are in laboratory channels. Again, it is not certain that a valid formula can be derived from the data of different investigations when there are differences in channel geometry and in granulometric distribution of grain size. There are two reasons for the difficulty. One is that the determinations of the flow quantities and the dimensions of bed features are open to errors. Secondly, since the phenomenon of sand transportation is a complex phenomenon the parameters entering are too numerous and the error of measurements prevents the evaluation of the significance of a particular single parameter. The effects of granulometric distribution are not well known, nor are the effects of the width and form of channels. In the views of Tanaka[38] the width of channel plays an important role, and its significance is considered in a theoretical formulation of the feature geometry. One may imagine that by resorting to theoretical analysis the forms of the proper parameters may be defined. But this may not always be possible. For example, the theory of Kennedy[39] predicts that L/H should decrease with $(U/U_o)/U$. This is verified in the Fort Collins data obtained with sand of

d_{50} = 0.93 mm. In the same data, on the other hand, with the sand of the lesser size just the opposite is observed; that is, L/H_o increased with $(U - U_o)/U$. Should this anomaly be explained on the grounds that d_* of the sands lesser than d_{50} = 0.93 is below the critical d_* = 16.5? Even when tests are made with sands of dimensionless size parameter d_* less than 16, we sometimes notice differences in the behavior of the size parameters as reported by different authors. For example, in the Shinohara and Tsubaki[40] results with sand d_{50} = 0.21 mm we find that both L/d and H_o/d decrease with $U^2/(s - 1)gd$, whereas the opposite was true in the Fort Collins results.

77. In the present analysis, it was not possible to derive the resistance coefficients of alluvial streams in the form established by Alam and Kennedy from the data obtained from laboratory channels. In rivers when the Froude number is less than 0.5, λ_2 is independent of d/H and depends on U^2/gd solely. When the flow Froude number is less than 0.5 the associated bed forms consist of ripples or dunes. In contrast with the above, deductions from laboratory testing show that λ_2 depends also on d/H in addition to being dependent on U^2/gd. The analysis involved two steps. First, it was sought to express λ_2 in the parameters H_o/L and H_o/H and secondly, to relate H_o/H and H_o/L separately to U^2/gd. It may be of interest to reexamine the steps, making use of the dimensionless sand size d_* in the reductions. For time being it should be adequate to use the Alam-Kennedy or Einstein-Barbarossa procedure in establishing the resistance of natural rivers.

The Dune Initiation Criteria in Terms of Channel Current

78. In the previous development, the criteria for the initiation of ripples and dunes were expressed in terms of the shear velocity. For the ripples

$$U_* = 0.72 \left[(s - 1)g\nu\right]^{1/3} \qquad (2.31 \text{ bis})$$

and for the dunes

$$U_* = 3.06[(s - 1)gd]^{1/5} \left(\frac{\nu}{d}\right)^{3/5} \qquad (2.32 \text{ bis})$$

with the restriction that d_* is larger than 3.2 but smaller than 16.5. In the Fort Collins data, this restriction is fulfilled for all the tests except those carried out with sand of $d_{50} = 0.93$ mm. These criteria can be readily changed to new relations containing U , the current velocity, instead of U_* . For the reduction, it is sufficient to obtain the ratio U/U_* applicable to Fort Collins data. An explanatory examination showed that U/U_* would vary as the one-sixth power of H/k . To find if the ratio is further affected by the Froude number, the graph of Figure 38 was prepared. The quantity $U/U_* \div (H/k)^{1/6}$ is

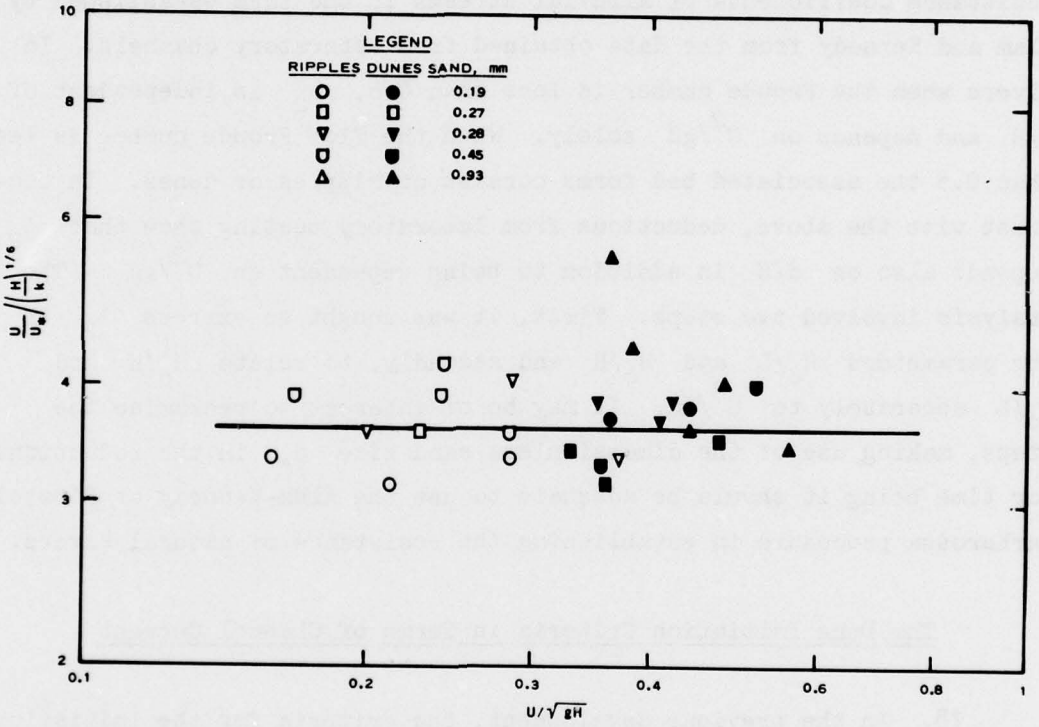

Figure 38. Dependence of the ratio of the current velocity to shear velocity on channel depth in Fort Collins tests (8-ft flume)

plotted against Froude number $U/\sqrt{gH}$. Data are differentiated to grain size and bed features. The ordinate of each point represents the average of three or four like points with abscissa values very close to each other. It is obvious that the graph can be represented as

$$\frac{U}{U_*} = 3.6\left(\frac{H}{k}\right)^{1/6}$$

independent of bed form feature and Froude number. Substituting in Equations 2.31 and 2.32, the criterion for the initiation of the ripples in terms of current velocity is

$$U = 2.59[(s - 1)g\nu]^{1/3}\left(\frac{H}{d}\right)^{1/6} \tag{3.37}$$

and for the initiation of dunes

$$U = 11.0\ [(s - 1)gd]^{1/5}\ \left(\frac{\nu}{d}\right)^{3/5}\ \left(\frac{H}{d}\right)^{1/6} \tag{3.38}$$

Transitions occur at

$$U = 3.1\ [(s - 1)]^{1/2}\left(\frac{H}{d}\right)^{1/6} \tag{3.39}$$

a relation that follows from Equation 2.33. By dividing the two sides of Equation 3.38 by $\sqrt{gH}$ and putting $s = 2.67$, we have

$$\frac{U}{\sqrt{9H}} = 12.1\left(\frac{gd^3}{\nu}\right)^{-3/10}\left(\frac{H}{d}\right)^{-1/3} \tag{3.40}$$

This allows comparison with the Vanoni graphics on the question of bed forms.[36] The above relation for the initiation of the dunes is valid in the range of d_* greater than 3.2 and less than 16.5. The connection between the Vanoni symbol R_g and d_* is

$$(s - 1)R_g^2 = d_*^3 \tag{3.41}$$

Thus, the relation in Equation 3.40 for the initiation of dunes should be valid for R_g less than 0.50 but greater than 4.45. Equation 3.40 requires that within this range $U/\sqrt{gH}$ should vary as the minus one-third power of H/d. This is comparable with the data shown in

Figures 2-5, inclusive, in the paper by Vanoni.[36] Although in these figures the paths of the curves separating the dunes from the ripples are somewhat irregular, on the average $U/\sqrt{gH}$ would vary as the minus one-third power of H/d .

79. Again, in the similar manner, Equation 2.32 after d is divided by $\sqrt{gd}$ and s is put equal to 2.67, for ordinary sands, the critical relation for the initiation of dunes would be

$$\frac{U_*}{\sqrt{gd}} = 3.4\left(\sqrt{gd} \cdot \frac{d}{\nu}\right)^{-0.60} \tag{3.42}$$

This is also comparable with the results of Vanoni[36] in Figure 7 of his paper. The equation of the line in the figure separating the dunes from the ripples is

$$\frac{U_*}{\sqrt{gd}} = 3.8\left(\sqrt{gd} \cdot \frac{d}{\nu}\right)^{-0.75} \tag{3.43}$$

The agreement between these two results is close. This is an important matter, since these equations would predict what the effect of temperature would be on bed forms. It is to be remembered that the validity of these relations is for the range of d_* greater than 3.2 but less than 16.5 or for the range of R_g greater than 4.45 but less than 50, for the case of ordinary sand, $s = 2.67$. For another comparison of the results, see Figure 39 where $U_*^2/(s - 1)gd$ is plotted against d_* . The diamonds (∇) are reductions from the straight line in Figure 7 of Vanoni's paper[36] separating the dunes from the ripples; the full circles are reductions from the Chabert and Chauvin curve in Figure 17 of the present study separating the dunes from the ripples; and the open circles are the reductions from the Fort Collins data. As expected, the points from the Vanoni study align themselves on a straight line, whereas the alignment of the points from the Chabert and Chauvin curve and those from the Fort Collins tests is curvilinear. The curve that is drawn through the latter points, although close to the straight line drawn, suggests that the effect of temperature is more significant for sands with d_* values less than 16.5 but not differing much from it. Further research in this problem would be desirable.

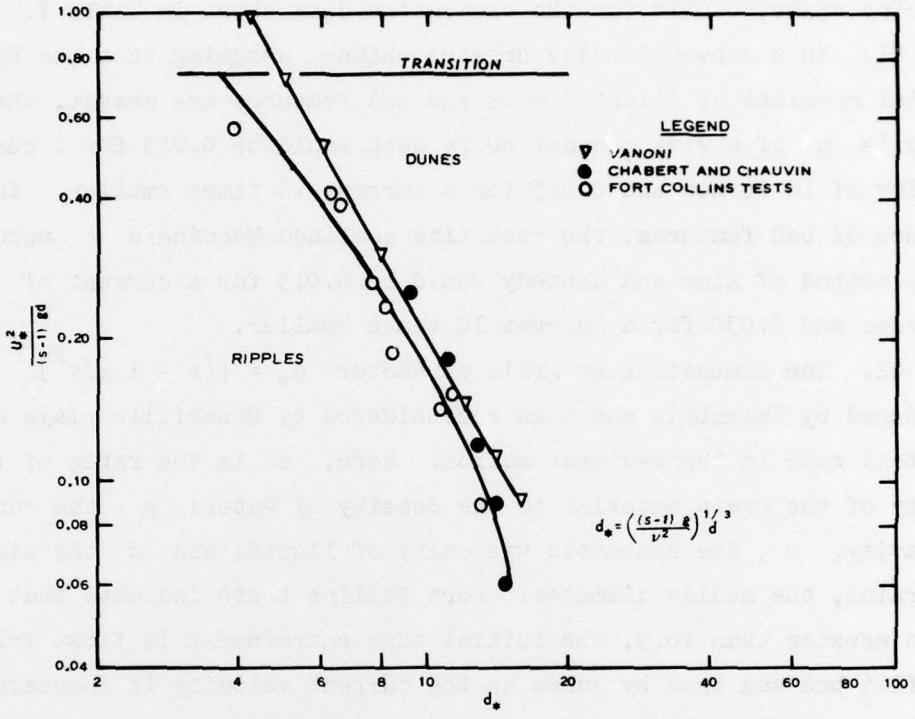

Figure 39. The criteria of dune formation after Vanoni, Chabert and Chauvin, and Fort Collins tests

PART IV: CONCLUSIONS

80. The Manning's n_e of nuclear-created channels may be supposed to consist of two parts, one due to the asperities of the ejecta and the other due to the expansions and the contractions in the channel caused by the disperse explosions. In the channels of basalt ejecta, the combined n_e is estimated to be 0.0762; with rhyolite, 0.0609 and with clay shale, 0.0514 for the excavation data shown in Table 7.

81. In a conventionally created channel assuming that the bed material consists of Atlantic muck and bed features are absent, the Manning's n of a wide channel 60 ft deep would be 0.013 for a current velocity of 10 ft/sec and 0.015 for a current 10 times smaller. In the presence of bed features, the resulting combined Manning's n according to the method of Alam and Kennedy would be 0.015 for a current of 10 ft/sec and 0.030 for a current 10 times smaller.

82. The dimensionless grain parameter $d_* = [(s - 1)g/\nu^2]^{1/3} d$ introduced by Valembois and then reconsidered by Bonnefille plays an important role in the sediment motion. Here, s is the ratio of the density of the grain material to the density of water; g, the constant of gravity; ν, the kinematic viscosity of liquid; and d the size of the grains, the median diameter. Fort Collins tests indicate that when d_* is greater than 16.5, the initial sand entrainment is first followed by a flat bed and then by dunes as the current velocity is increased without the intermediate ripple formation. Where d_* is less than 3.2, ripples are followed by transitions without the intermediate formation of dunes. In the range $3.2 < d_* < 16.5$ the criterion for the formation of dunes is

$$\frac{U_*}{\sqrt{(s - 1)gd}} = 3.06\, d_*^{-0.9}$$

where

U_* = the critical shear velocity

d = the median grain diameter

This is an approximation and the actual fraction showed marked deviations from the above. Since the criterion is predictive of the changes produced by temperature, these deviations need to be studied further. Putting in the above $s = 2.67$, the resulting expression of the criterion agrees reasonably well with the findings of Vanoni.

83. For the study of the form resistance of bed features in terms of their characteristic dimensions, the Sadron formula is adopted. In the formula, the resistance is related to the velocity U_k prevailing at the apices of the bed forms, ripple or dune. Assuming that the local velocities in terms of distance from the bed are proportional to y_m, the Sadron formula allows for the form resistance coefficient the expression

$$\lambda_2 = A \left(\frac{L}{H_o}\right)^{\alpha} \left(\frac{H}{H_o}\right)^{2m}$$

where A is a constant and the effect of B/H is neglected.

84. Fort Collins data on velocities indicate that the velocity index m is somewhat higher for the ripples than for the dunes. There are also variations with the grain size. Taking averages, m is equal to 0.202 for the ripples and to 0.139 for the dunes. For the studies made, m is taken as 1.66, an average from all the determinations--ripples and dunes alike. As regards the exponent α, the data suggest that it is permissible to take α equal to unity. Owing to scatter, this selection may not be positive. Adopting α equal to unity, factor A is somewhat larger for the dunes than for the ripples.

85. When the crest height H_o and the length L of the bed features are expressed in terms of d, the grain median diameter, the resulting ratios are functions of $(s - 1)U^2/gd$ unaffected by the grain size and water depth ratio d/H. The functional dependencies are not the same for ripples and for dunes. These are the findings from the Fort Collins data. There is an indication that the ratio H_o/d is affected by viscosity. Owing to the scatter of data, the resolution is not definite and for the analysis made this possibility is ignored.

86. Introducing the depth and the length values of bed features

in terms of the current velocity in the formula of resistance involving the length and the depth of the features, it is found that for laboratory flumes the coefficient λ_2 depends both on H/d and $(s - 1)U^2/gd$. In rivers as found by Alam and Kennedy, the coefficient is a function of $(s - 1)U^2/gd$ only when the Froude number $U/\sqrt{gH}$ is less than 0.5. As the Froude number of the laboratory flume considered was also under 0.5, it is seen that the resistance processes are different for laboratory flumes and natural rivers.

87. Because of this difference in the behavior of laboratory channels and natural rivers, it is preferable that the form resistance of deep channels carrying fine sediments be evaluated by the Alam-Kennedy method.

REFERENCES

1. Keulegan, G. H., "Laws of Turbulent Flow in Open Channels," U. S. Bureau of Standards Journal of Research, Vol 21, No. 6, Dec 1938, pp 707-741.

2. Schlichting, H., "Experimental Investigation of Roughness Problem" (abridged translation), Proceedings, American Society of Civil Engineers, Vol 63, No. 9, 1937, pp 1-74.

3. Koloseus, H. J. and Davidian, J., "Roughness-Concentration Effects on Flow over Hydrodynamically Smooth Surfaces," Water Supply Paper 1592-D, 1966, U. S. Geological Survey.

4. O'Loughlin, E. M. and MacDonald, E. G., "Some Roughness Concentration Effects on Boundary Resistance," LaHouille Blanche, Vol 7, 1964.

5. Miller, I. E. and Petersen, M. S., "Roughness Standards for Hydraulic Models; Study of Finite Boundary Roughness in Rectangular Flumes," Technical Memorandum No. 2-364, Report 1, Jun 1953, U. S. Army Engineer Waterways Experiment Station, CE, Vicksburg, Miss.

6. Brown, B. J. and Chu, Y. H., "Boundary Effects in Uniform Size Roughness Elements in Two-Dimensional Flow in Open Channels," Miscellaneous Paper H-68-5, Dec 1968, U. S. Army Engineer Waterways experiment Station, CE, Vicksburg, Miss.

7. Fage, A., "Fluid Flow in Rough Pipes," Aeronautical Research Committee Reports and Memoranda No. 1585, Oct 1933, Great Britian Air Ministry.

8. Sadon, C. H., C. R. Acad. Sci. Paris, Vol 200, 1935, p 292.

9. Brown, B. J., "Boundary Effects of Graded Roughness Elements in Two-Dimensional Flow in Open Channels," Miscellaneous Paper H-70-6, May 1970, U. S. Army Engineer Waterways Experiment Station, CE, Vicksburg, Miss.

10. Tollmien, W., "The Calculation of Turbulent Expansion Processes" (in German), Translated by J. Vanier, National Advisory Committee for Aeronautics Technical Memorandum 1085, 1945.

11. Sager, R. A., McNair, E. C., Jr., and Keulegan, G. H., "Hydraulic Characteristics of Nuclear Excavated Channels," Miscellaneous Paper H-69-5, May 1969, U. S. Army Engineer Waterways Experiment Station, CE, Vicksburg, Miss.

12. Shields, A., "Aanwendung der Achnlichkeitgmechanik und der Turbulensforschung auf die geschiebe Bewegung (Application of Similarity Principles and Turbulence Research to Bedload Movement)" (in German), Berlin 1936, California Institute of Technology, U. S. Soil Conservation Service.

13. Vanoni, V. A., "Measurements of Critical Shear Stress for Entraining Fine Sediments in a Boundary Layer," Report No. KH-R-7, May 1964, Division of Engineering and Applied Science, California Institute of Technology, Pasadena, Calif.

14. Rouse, H., "An Analysis of Sediment Transportation in the Light of Fluid Turbulence," SCS-TP-25, Jan 1939, Soil Conservation Service, Washington, D. C.

15. White, C. M., "The Equilibrium of Grains on the Bed of a Stream," Proceedings, Royal Society of London, Vol 174, No. 958, Feb 1940, pp 322-338.

16. Valembois, J., "Model Study of Littoral Transport, Similarity Conditions," Proceedings, 7th Conference on Coastal Engineering, The Hague, Netherlands, Aug 1960, Vol I, J. W. Johnson, ed., pp 307-317.

17. Bonnefille, R., "Essais de synthèse des lois de début d'entrainement des sédiments sous l'action d'un currant en régime continu," Bulletin de Centre de Recherches et d'Essais de Chatou, No. 5, Oct 1963, pp 67-72.

18. Guy, H. P., Simons, D. B., and Richardson, E. V., "Summary of Alluvial Channel Data from Flume Experiments, 1956-1961," Professional Paper 462-I, 1966, U. S. Geological Survey.

19. Liu, H.-K., "Mechanics of Sediment-Ripple Formation," Journal, Hydraulics Division, American Society of Civil Engineers, Vol 83, No. HY2, Paper No. 1197, 1957.

20. Chabert, J. and Chauvin, J. L., "Formation des dunes et des rides dans les modéles fluviaux," Bulletin du Centre de Recherches et d'Essais de Chatou, No. 4, Jun 1963, pp 31-51.

21. Einstein, H. A. and Barbarossa, N. L., "River Channel Roughness," Transactions, American Society of Civil Engineers, Vol 117, Paper No. 2528, 1952, pp 1121-1146.

22. Franco, J. J., "Effects of Water Temperature on Bed-Load Movement," Journal, Waterways and Harbors Division, American Society of Civil Engineers, Vol 94, No. WW3, Proceedings Paper 6083, Aug 1968, pp 343-352.

23. Vanoni, V. A. and Brooks, N. H., "Laboratory Studies of the Roughness and Suspended Load of Alluvial Streams," Report No. E-68, Dec 1957, Hydrodynamics Laboratory, California Institute of Technology, Pasadena, Calif.

24. Smith, K. V. H., "The Einstein-Barbarossa Diagram for Computing Bed-Form Resistance in Alluvial Channels," Proceedings, The Institution of Civil Engineers, Vol 46, Paper 7291, Jun 1970, pp 164-184.

25. Vanoni, V. A. and Nomicos, G. N., "Resistance Properties of Sediment-Laden Streams," Transactions, American Society of Civil Engineers, Vol 125, Paper 3055, pp 1140-1176.

26. Engelund, F., "Hydraulic Resistance of Alluvial Streams," Journal, Hydraulics Division, American Society of Civil Engineers, Vol 92, No. HY2, Proceedings Paper 4739, 1966, pp 315-326.

27. Lovera, F. and Kennedy, J. F., "Friction-Factors for Flat-Bed Flows in Sand Channels," Journal, Hydraulics Division, American Society of Civil Engineers, Vol 95, No HY4, Jul 1969, pp 1227-1234.

28. Alam, A. M. Z. and Kennedy, J. F., "Friction Factors for Flow in Sand-Bed Channels," Journal, Hydraulics Division, American Society of Civil Engineers, Vol 95, No HY6, Nov 1969, pp 1973-1993.

29. Meyer-Peter, E. and Muller, R., "Formulas for Bed-Load Transport," Proceedings, Second Meeting, International Association for Hydraulic Structures Research, Stockholm, Feb 1948, pp 39-64.

30. Taylor, R. H. and Brooks, N. H., Discussion of "Resistance of Flow in Alluvial Channels," by D. B. Simons and E. V. Richardson, Transactions, American Society of Civil Engineers, Vol 127, Part I, 1962, pp 982-992.

31. Kennedy, J. F., "The Mechanics of Dunes and Antidunes in Erodible-Bed Channels," Journal, Fluid Mechanics, Vol 16, Part 4, Aug 1963, pp 521-544.

32. Kalinske, A. A. and Hsia, C. H., "Study of Transportation of Fine Sediments by Flowing Water," Studies in Engineering Bulletin No. 29, pp 1-30, 1945, University of Iowa, Iowa City, Iowa.

33. Nordin, C. F. and Richardson, E. V., "Statistical Descriptions of Sand Waves from Stream Bed Profiles," Bulletin, International Association of Scientific Hydrology, Bulletin 13, No. 3, Sep 1968.

34. Vanoni, V. A. and Hwang, L.-S., "Relation Between Bed Forms and Friction in Streams," Journal, Hydraulics Division, American Society of Civil Engineers, Vol 93, No. HY3, May 1967, pp 121-144.

35. Jensen, P. and Lebreton, J. T., "Quelques résultats expérimentaux concernant les caractéristiques des dunes et leur representation sur les modèles à fonds mobiles," Bulletin de la Direction des Etudes et Recherches, Scrie A, No. 4, 1969, p 15.

36. Vanoni, V. A., "Factors Determining Bed Forms of Alluvial Streams," Journal, Hydraulics Division, American Society of Civil Engineers, Vol 100, No. HY3, Mar 1974, pp 363-378.

37. Simons, D. B., Richardson, E. V., and Nordin, C. F., Jr., "Bedload Equation for Ripples and Dunes," Professional Paper 462-H, 1965, U. S. Geological Survey.

38. Tanaka, Y., "On the Geometrical Characteristics of Sand Waves," 13th Congress, International Association for Hydraulic Research, 31 Aug-5 Sep 1969, Vol 5-1, pp 249-256.

39. Kennedy, J. F., "The Formulation of Sediment Ripples, Dunes, and Antidunes," Annual Review of Fluid Mechanics, Vol 1, 1969.

40. Shinohara, K. and Tsubaki, T., "On the Characteristics of Sand Waves of the Open Channels and Rivers," Report of Research Institute for Applied Mechanics, Kyushu University, Vol VII, No. 25, 1959.

APPENDIX A: NOTATION

A_b	Domain of influence of the frictional action of the bottom, $A_o = A_w + A_b$
A_o	Channel cross section
A_r	Total value of projected area of all the asperities over an area A
A_s	Horizontal projection of lee faces the ripples
A_w	Domain of influence of the frictional section of the two walls
A_x	Contact area between current and isostatic flow
A, A_1	Area, wetted wall surface in a crater segment; area of separation surface
A_1, A_2, A_3	The extreme and the mid-cross sections in a crater segment
$\bar{A}_i$	The average cross section of the i^{th} crater
B	Channel width
C	Drag coefficient; velocity at a point 1 ft from bottom of the flume
C_D	A coefficient defining λ_2 in terms of H_o/L and H_o/H, Equation 3.3
C'_D	A coefficient defining λ_2 in terms of L/H_o, Equation 3.10
C_1	A function of placement of the shape of sands, and Reynolds number $U_r d/v$
d	Median diameter of sand grains, pebbles or rocks
d_*	Bonnefille modification of Valembois sand parameter $d_*^3 = G$
e	Exposure ratio
E, E_1, E_2, E_L	Jet dissipation due to free turbulence in a nuclear segment
f	Darcy-Weisbach resistance coefficient, $f = 4\lambda$
f_1	Darcy-Weisbach resistance coefficient for granular surfaces of bed features, $f_1 = 4\lambda_1$
f_2	Darcy-Weisbach resistance coefficient for form resistance of bed features, $f_2 = 4\lambda_2$
F_p	Resistive force of a ripple or a dune or sand. Also Froude number $U/\sqrt{gH}$
F_r	Resistive force

F_*	Stress Froude number $F_* = u^*/\sqrt{(s-1)gd}$
g	Gravitational constant
G	Valembois grain parameter $G = s - 1/\nu^2 g d^3$, $s = p_s/p$
H	Depth of water in channel; also range of tide
H_o	Crest height of ripples or dunes measured from bottom
k	Height of asperities; Karman constant
k_s	Equivalent sand roughness
K	A coefficient in the resistance equation in power form for granular surfaces, hydraulically smooth
l_i	Depths of channel bottom areas of uniform asperities k_i and of Manning's n_i ; $i = 1,2,\ldots, n$
L	Length of ripples and dunes; usually a length of channel segment
L_1, L_2	Length of converging and diverging parts of a crater segment of length L . $L = L_1 + L_2$.
m	Constant close to unity; exponent in the law of variation of separation length ℓ ; exponent in the power loss of velocity distribution
n	Manning's roughness coefficient
n_e	Effective Manning's n for a cratered segment due to granular surfaces and contractions and expansions in the segment
n_o, n_w, n_b	Manning's n for composite channel, for sidewalls and for bottom
p_b	Wetted perimenter of bottom, $p_w = B$
p_o	Wetted perimeter of a complete channel, $p_o = B + 2H$
p_w	Wetted perimeter of sidewall, $p_w = 2H$
q_s, q_t	Mass rate of flow of sand material expressed as pounds per hour per foot
q_s^*	Volume rate of flow of sand material expressed as cubic feet per hour per foot
Q	Discharge through a nuclear segment
r	Hydraulic radius
R	Hydraulic radius in general
R_b	Hydraulic radius corresponding to the bottom of channel
R_o	Hydraulic radius of a composite channel
R_w	Hydraulic radius corresponding to the sidewalls

R_*	Grain Reynolds' number U_*d/ν
R_1	Hydraulic radius in Einstein's theory associated with the granular surfaces in a wide channel
R_2	Hydraulic radius in Einstein's theory associated with the form resistance of bed features in a wide channel, $R = R_1 + R_2$
R_1, R_2, R_3	The extreme and the midhydraulic radii in a crater segment
$\overline{R}_i$	The average hydraulic radius of the i^{th} crater
s	Ratio of densities of grain to density of water, $s = \rho_s/\rho$; arc length measured from the lowest point in the section
S, S_o, S_b	Energy gradient; energy gradient in a composite channel; energy gradient in wide channel
S_1	Energy gradient in Meyer-Peters' theory associated with granular surface resistance in wide channels
S_2	Energy gradient in Meyer-Peters' theory associated with form resistance of bed features in a wide channel
u	Local velocity at distance y from bottom
U	Mean current velocity in channel
U_c	Sand entrainment critical velocity
U_k	Current velocity at the apices asperities
U_o	Current at crests of bed features
U_r	Velocity of current at the apices of sands
U_1	Velocity of current at the start of a nuclear segment
U_*	Shear velocity, $U_* = \sqrt{\tau/\rho}$
U_{*1}	Shear velocity of granular surfaces, $U_{*1} = \sqrt{\tau_1/\rho}$
U_{*2}	Shear velocity of bed features, $U_{*2} = \sqrt{\tau_2/\rho}$, $\tau = \tau_1 + \tau_2$
W	Fall velocity of grains
x	Horizontal distance
y	Vertical distance from channel bottom
y_m	Depth of water in channel
ℓ_1	Average length of separated area in the direction of flow in a segment
ℓ_{1m}	Length of separation area in the direction of flow observed at the water surface in an expanding segment

α	Angle of inclination
δ	Boundary layer thickness, $\delta = 11.6\nu/U_*$
Δ	Einstein's symbol for effective asperity, Equations 2.38 and 2.44
ΔH	Fall of energy line
λ	Resistance coefficient; $2\lambda = U_*^2/U^2$, $4\lambda = f$
$\lambda_o, \lambda_w, \lambda_b$	Resistance coefficients of composite channel, of channel walls, and of channel bottom
λ_1	Resistance coefficient of granular surfaces, $2\lambda_1 = (U_{*1}/U)^2$
λ_2	Force resistance coefficient of bed features, $2\lambda_2 = (U_{*2}/U)^2$
ν	Kinematic viscosity of water
ρ	Density of water
ρ_s	Density of granular material
σ	Gradation number $2\sigma = d_{50}/d_{16} + d_{84}/d_{50}$
τ	Channel stress
τ_b	Average shear of bottom surface, $\tau_b = \rho g R_b S$
τ_o	Channel average stress in composite channels
τ_w	Average shear of sidewalls, $\tau_w = \rho g R_w S$
τ_1	Stress due to granular surfaces, $\tau_1 = \rho g R_b S_1$
τ_2	Stress due to bed features, $\tau_2 = \rho g R_b S_2$, $S_b = S_1 + S_2$, $S_b = S_o R_o$
ϕ, ϕ_o, ϕ_1, etc.	Functional symbols
χ	Average wetted parameter in a crater expansion segment
ψ	Shields' parameter
ψ'	Einstein's transport function $\psi' = 1.67 d_{35}/R_1 S$

In accordance with letter from DAEN-RDC, DAEN-ASI dated 22 July 1977, Subject: Facsimile Catalog Cards for Laboratory Technical Publications, a facsimile catalog card in Library of Congress MARC format is reproduced below.

Keulegan, Garbis Hovannes
An estimate of channel roughness of interoceanic canals / by Garbis H. Keulegan. Vicksburg, Miss. : U. S. Waterways Experiment Station ; Springfield, Va. : available from National Technical Information Service, 1978.
124, 4 p. : ill. ; 27 cm. (Technical report - U. S. Army Engineer Waterways Experiment Station ; H-78-13)
Prepared for U. S. Army Engineer District, Jacksonville, Jacksonville, Florida.
References: p. 121-124.

1. Canal construction. 2. Canals. 3. Excavated channels. 4. Hydraulic roughness. 5. Interoceanic canals. I. United States. Army. Corps of Engineers. Jacksonville District. II. Series: United States. Waterways Experiment Station, Vicksburg, Miss. Technical report ; H-78-13.
TA7.W34 no.H-78-13